Observations of atmospheric Cerenkov light produced in high energy cosmic ray showers

Wellby, D. W.

OBSERVATIONS OF ATMOSPHERIC CERENKOV LIGHT PRODUCED IN HIGH ENERGY COSMIC RAY SHOWERS

by

D.W. Wellby, B.Sc.

A thesis submitted to the University of Durham in accordance with the regulations for admittance to the Degree of Doctor of Philosophy.

Department of Physics
University of Durham

October 1977

CONTENTS

ABSTRACT

An experiment to observe the atmospheric Cerenkov light produced in extensive air showers, has been under development at the British Universities' Joint Air Shower Array at Haverah Park, since 1972. This thesis is concerned with the Cerenkov light measurements made at Haverah Park during the U.K. winter of 1975/76, when the experimental equipment was first improved to its present specification.

An introduction to extensive air showers and the relevance of Cerenkov light studies, is followed by an account of the theoretical aspects of Cerenkov radiation. The most recent computer simulations of the features of Cerenkov light in extensive air showers are briefly described. A detailed account of the design and performance of the current Cerenkov light detection equipment is given, and the measurements made are reported. Very detailed measurements of the Cerenkov light in air showers can be made with the equipment.

The average characteristics of the Cerenkov light in showers of energies around 5×10^{17} eV are established. Measurements of both the photon density and the details of the light pulse shape are made at core distances up to about 600 m. The curvature of the Cerenkov light front in air showers is also determined, from measurements of the arrival times of the light. A Cerenkov light measure of primary particle energy is identified. The dependences of the Cerenkov light parameters on shower energy and zenith angle are quantified, and are used to estimate the sensitivities of the parameters to depth of shower cascade maximum. The data measured here agree well with earlier measurements, where such comparison may be made.

The measured average characteristics of the Cerenkov light in air showers are found to be in good agreement with predictions from the recent computer simulations. Comparison of the experimental

and theoretical data, leads to an estimate of the average atmospheric depth at which showers reach cascade maxima. It is not possible, however, to interpret this estimate in terms of primary particle mass.

Finally, the fluctuations in Cerenkov light signals are examined, by studying the light measurements made in a small sample of individual showers. It is shown that fluctuation values of Cerenkov light parameters, contain information about shower development, which is additional to that derived from the average characteristics of the light parameters. An upper limit for the range of atmospheric depths over which showers reach cascade development maxima, as a result of variations in the nucleon interactions in their cascades, is derived.

It is concluded that future Cerenkov light measurements in a large sample of showers, may contribute significantly towards the identification of the masses of the primary cosmic ray particles.

PREFACE

This thesis is an account of experimental work carried out at the British Universities' Joint Air Shower Array at Haverah Park, in Yorkshire. An experiment to observe the Cerenkov light in extensive air showers has been under development there, since 1972. In the period from 1974 to 1975, the experimental equipment was completely rebuilt in order to make the improved measurements, which are reported in this work.

The author played a major part in the design, construction and commissioning of the improved Cerenkov light detection apparatus, which is described in Chapter 3. He was wholly responsible for the routine operation and maintenance of the experiment during its first period of operation, in the U.K. winter of 1975/76. Together with his colleagues, he shared the work of measuring the film records gathered in this period.

The information on the shower arrival directions, core positions and energies, which is used for the results presented in this thesis, was obtained from analyses of the Haverah Park particle detector data, provided by the University of Leeds. Using this information, the author was wholly responsible for the experimental results presented in Chapters 4, 5 and 6, with the exception of the determination of the light front radii of curvature described in Chapter 4.

None of the material in this thesis has previously been submitted by the author to Durham, or any other university, for admittance to a degree.

CHAPTER ONE

INTRODUCTION

1.1 The Cosmic Radiation

The presence of an ionizing radiation at the surface of the Earth, was first suggested to account for observations by C.T.R. Wilson (the originator of the Wilson Cloud Chamber). In 1900, he observed that an insulated gold leaf electroscope lost its charge even when the greatest care was taken with its insulation. The radiation ionized the gas in the electroscope and resulted in its discharge (Wilson (1901)). A series of balloon flights by Hess (1912) and Kolhorster (1914) carried electroscopes to altitudes up to 9200 m and showed that the intensity of the radiation increased to ten times its sea-level value at this height, thus establishing that the radiation was extra-terrestrial in origin. It has become known as cosmic radiation and its investigation has led to important discoveries in physics, including the discovery of the positron in 1932 by Anderson, and later, the discoveries of the μ-meson and π-meson.

The majority of the known primary cosmic radiation incident at the top of the atmosphere consists of atomic nuclei; mainly protons and light nuclei but with a small proportion of heavier nuclei; together with some electrons and gamma-rays. Its most remarkable property is its wide range of energies which extends from less than 10^9 to at least 10^{20}eV per nucleus. The energy spectrum of the primary cosmic radiation is now relatively well known, and a synopsis of the spectrum by Watson (1974) is shown in fig.1.1. The integral energy spectrum can be represented by a simple power law:-

$$N(>E) \propto E^{-\gamma} \quad \text{... equ.1.1}$$

with the exponent, γ, varying slowly with energy. In the energy range 10^{11} to 10^{15}eV γ has values of 1.6 to 1.7 (see, for example, Grigorov et

Figure 1.1. Summary of measurements of the energy spectrum of the primary cosmic radiation. (From Watson (1974).)

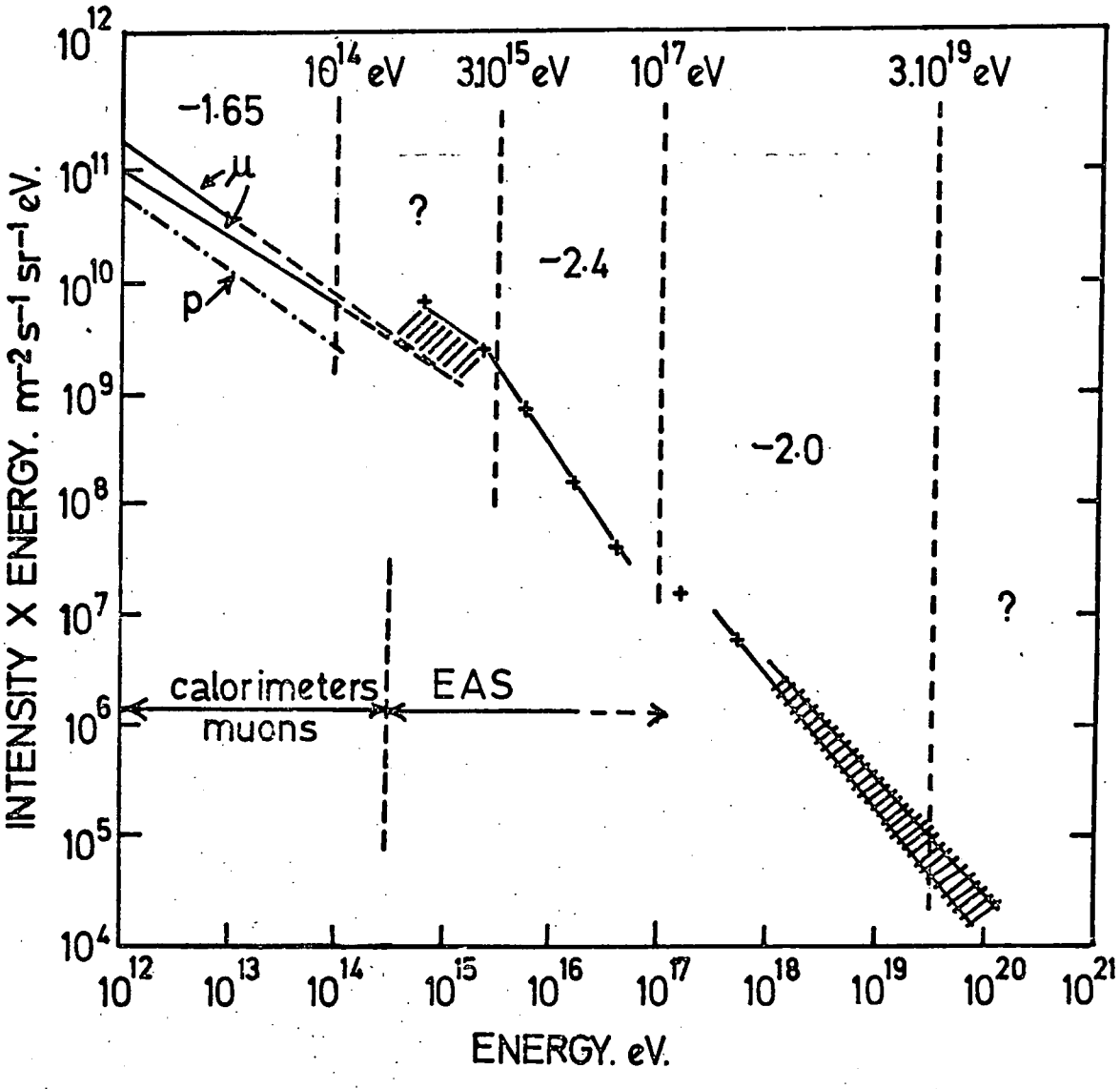
10^{14} eV
3.10^{15} eV
10^{17} eV
3.10^{19} eV
−1.65
μ
p
?
−2.4
−2.0
?
calorimeters
muons
EAS
INTENSITY X ENERGY. $m^{-2} s^{-1} sr^{-1}$ eV.
ENERGY. eV.
10^{12}
10^{11}
10^{10}
10^{9}
10^{8}
10^{7}
10^{6}
10^{5}
10^{4}
10^{12} 10^{13} 10^{14} 10^{15} 10^{16} 10^{17} 10^{18} 10^{19} 10^{20} 10^{21}

al. (1971)). Between 3×10^{15} and 10^{17}eV the spectrum is steeper with $\gamma = 2.4$, and at the highest energies the slope is $\gamma \simeq 2$ (see Edge (1974)). At the highest energies little is known of the mass of the primary cosmic ray particles.

1.2. Extensive Air Showers

Direct observations of primary cosmic ray particles have been made at energies up to about 10^{14}eV, notably with nuclear emulsion stacks or spark chambers. These have been either flown at the top of the atmosphere by balloons or rockets (e.g. Fowler et al. (1967)), or placed on satellites (Grigorov et al. (1967)).

At primary energies greater than 10^{14}eV the decreasing particle flux makes direct observation of the cosmic radiation impossible (for example, at energies greater than 10^{16}eV, the flux of primary cosmic ray particles is less than one particle m^{-2} yr^{-1} at the top of the atmosphere). Studies of these high energy particles can be made only indirectly by observing at ground level the laterally extensive cascades of secondary particles produced in interactions of the primary particles with nuclei of atoms of the upper atmosphere. The atmosphere effectively acts as a particle amplifier and spreads the cascade of particles over an area that may be as large as tens of square kilometers at sea-level, so very much increasing the chance of detecting the arrival of a primary particle. Known as "extensive air showers", (EAS), these cascades of particles were first observed in 1938 by Auger et al. and by Kolhorster et al. who found that Geiger-Müller counters separated by up to 150 m, detected the arrival of radiation in coincidence.

1.2.i The Formation of an Air Shower

A primary particle incident at the top of the atmosphere interacts strongly with nuclei of atmospheric atoms. It undergoes several inter-

actions while traversing the 1030 g cm^{-2} of atmosphere before reaching sea-level. At each interaction it is thought that about half the energy of the primary particle is lost in producing a range of secondary particles; mostly pions together with kaons, nucleons, anti-nucleons and other strange particles. These nuclear-active particles form a compact shower core.

Some of the charged pions produced in the nuclear interactions interact catastrophically with other air nuclei and produce more pions (the interaction length of pions in air is often taken as 120 g cm^{-2}). Others decay by the reaction $\pi^{\pm} \rightarrow \mu^{\pm} + \nu$ (lifetime of a charged pion is 2.6×10^{-8} s) and form the muon component of a shower. This component is highly penetrating and many of the muons survive until they reach ground level. The transverse momentum with which the pions are produced causes the cascades of particles to spread laterally.

The neutral pions produced in the nuclear cascade decay almost instantaneously (lifetime of π^{o} is 10^{-16} s) into two gamma-rays, each of which initiates a photon-electron cascade. This propagates primarily by the processes of positron-electron pair production, Compton scattering, bremsstrahlung and ionization. The electron-photon component of an air shower grows by the superposition of many of these individual cascades, with energy being continuously fed from the nuclear component as more neutral pions are produced. The electrons are considerably affected by Coulomb scattering, and so the electron-photon component of an air shower is also laterally spread out.

Averaged over a whole shower, the electrons are by far the most abundant particles, although most of the energy of a shower is carried by the nuclear and muonic components. Typically 80% of the total energy is carried by 10% of the total particles.

As an air shower develops in the atmosphere, the total number of particles in the shower cascade first increases to a maximum and then, as the energy of the shower is expended, the particle number starts to decrease. On average, therefore, showers initiated by primary particles of higher energies, penetrate deeper into the atmosphere before reaching their cascade development maxima, than do showers initiated by lower energy primary particles. The details of the cascade developments of individual showers will also depend on variations in the nuclear reactions taking place in the showers, as well as on the primary particle energy. It is reasonable that the mass of the primary particle will considerably influence the first reactions in a shower and may thus affect the overall development of the shower, too.

1.2.ii The Mass of the Primary Particle

Considerable interest in the mass composition of primary cosmic rays of the highest energies has been stimulated by the possibility of determining their place of origin. The radius of gyration in the galactic magnetic field of protons of energies about 10^{16}eV is comparable with the extent of the magnetic field. Protons of greater energies are thus expected to escape from our galaxy, and a protonic flux of highest energy primary cosmic rays would suggest that these particles are of extra-galactic origin. In contrast, iron nuclei, with their greater charge, are less magnetically rigid and are expected to be contained in the galaxy. A high energy primary cosmic ray flux of iron nuclei would indicate galactic origin.

Perhaps more realistically, the magnetic cut-off rigidity of the galaxy may progressively exclude protons, then light nuclei, leaving only heavy nuclei in the primary cosmic ray flux at the highest energies. It

has been suggested that changes in the slope of the primary energy spectrum indicate changes in the mass composition of the primary particles.

At the low energies where direct detection is possible, the mass composition of the primary cosmic radiation has been determined with good resolution from nuclear emulsion data. The relative abundances of the elements are shown in fig.1.2. There have been isolated cases of the direct identification of higher energy primary particles - protons, and oxygen and calcium nuclei of energies between 10^{14} and 10^{15}eV have been found - but the number of observations is too small to indicate relative abundances.

The chemical composition of the primary particles in the air shower region of the energy spectrum is uncertain. Because of the very indirect nature of the measurements, the resolution in composition is poor, but it may be possible to differentiate between a mainly protonic, mixed, or mainly heavy nuclei primary particle flux. A review of the available data on primary composition in the energy range 10^{10} to 10^{19}eV, together with the interpretations with which they were presented, has been given by Sreekantan (1972) but the implications, however, are inconclusive.

1.2.iii Fluctuations in Air Shower Longitudinal Development

The details involved in estimating the primary particle mass composition at air shower energies depend to some extent on the particular parameter (or parameters) which is investigated. However, there is a general approach which is applicable to several observed shower parameters. Computer simulations show that the average characteristics of air showers do not vary strongly with primary particle mass (Dixon (1974)). In fact, the average values of observed shower parameters vary as much between two different (but plausible) models, as they do between a heavy (say iron nucleus) primary particle and a proton primary particle. For composition

Figure 1.2. The relative abundances of the elements in the primary cosmic radiation at energies less than 10^{12}eV. (From Wild (1975).)

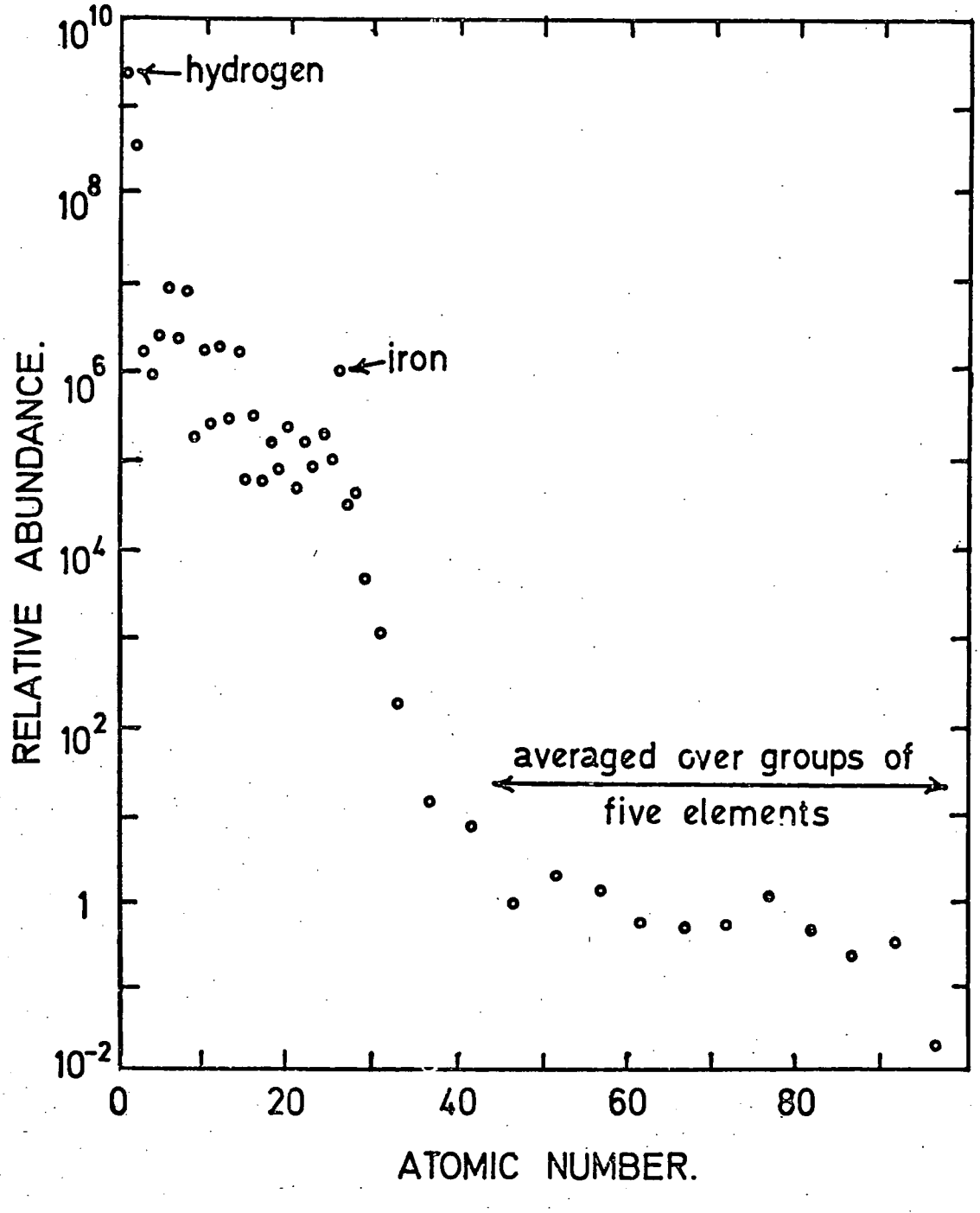
10^{10}
hydrogen
10^{8}
10^{6}
iron
10^{4}
10^{2}
averaged over groups of
five elements
1
10^{-2}
0
20
40
60
80
RELATIVE ABUNDANCE.
ATOMIC NUMBER.

determination, parameters which are relatively model independent but which still vary with primary mass need to be found. The models suggest that the study of the fluctuations in the values of various parameters measured in individual showers, may help to identify protons in the primary cosmic ray flux.

The nuclear cascade, which is the backbone of a shower, is dominated by a very few high energy interactions - perhaps sometimes only the first interaction of the primary particle. It is reasonable that a primary proton will not completely lose its identity on interacting, but that it will continue with a significant fraction of its incident energy. The proton will deposit this energy in "lumps" distributed at random along its path through the atmosphere. Variations in the way the energy is distributed will be reflected by variations in the values of observed shower parameters.

In contrast, a heavy primary particle can be expected to disintegrate into a large number of separate nuclei at its first interaction. Each would then continue independently, and the superposition of the "sub-showers" so formed would lead to much reduced fluctuations in the values of measured parameters of the complete shower.

The above situation will be enhanced by the longer mean free path for collision with an air nucleus of a proton ($\sim$80 g cm^{-2}), compared with that of a heavy particle ($\sim$14 g cm^{-2} for an iron nucleus). Only proton primary particles can be expected to occasionally penetrate deeply into the atmosphere before initially interacting, and the very low depth of cascade maximum expected in the resulting shower should lead to unique extreme fluctuations in the values of observed shower parameters.

The model calculations by Dixon (1974) have simulated the longitudinal developments of showers initiated by protons and iron nuclei of

energy 10^{17}eV. Fig.1.3 summarizes how the developments of individual showers in each group vary. The two curves shown for each primary particle mass represent the extreme cases of early and late cascade developments in the atmosphere, which are exceeded by about 5% of all showers. It is seen that the spread in the depths at which individual proton initiated showers reach their cascade development maxima, is much greater than the spread in the depths of the cascade development maxima of individual iron nucleus initiated showers. The model shows that this is reflected by the fluctuations in the values of many shower parameters observed at ground level. The fluctuations are about five times greater for proton initiated showers, than for iron nucleus initiated showers, according to the model.

1.3 Cerenkov Light in Extensive Air Showers

Following the suggestion by Blackett in 1948, that Cerenkov light is emitted on the passage of cosmic ray particles through the atmosphere, Galbraith and Jelley (1953) first detected Cerenkov light from the night sky. They observed light pulses in coincidence with extensive air showers, which provided the high local electron concentrations necessary to produce enough Cerenkov light to be visible above the background light of the night sky.

Many of the electrons in extensive air showers are sufficiently energetic to radiate visible Cerenkov light. The detection of the light provides an alternative method to the more usual one of particle detection for investigating shower properties. Perhaps the most distinguishing feature of this method is that, whereas all other extensive air shower measurements yield information mainly about the lateral distribution of particle energies and densities; and then only for the particular atmospheric level at which the equipment is situated; the

Figure 1.3. Variations in the longitudinal developments of the electron cascades of individual cosmic ray showers of energy 10^{17}eV (5% limits). (From the simulations by Dixon (1974).)

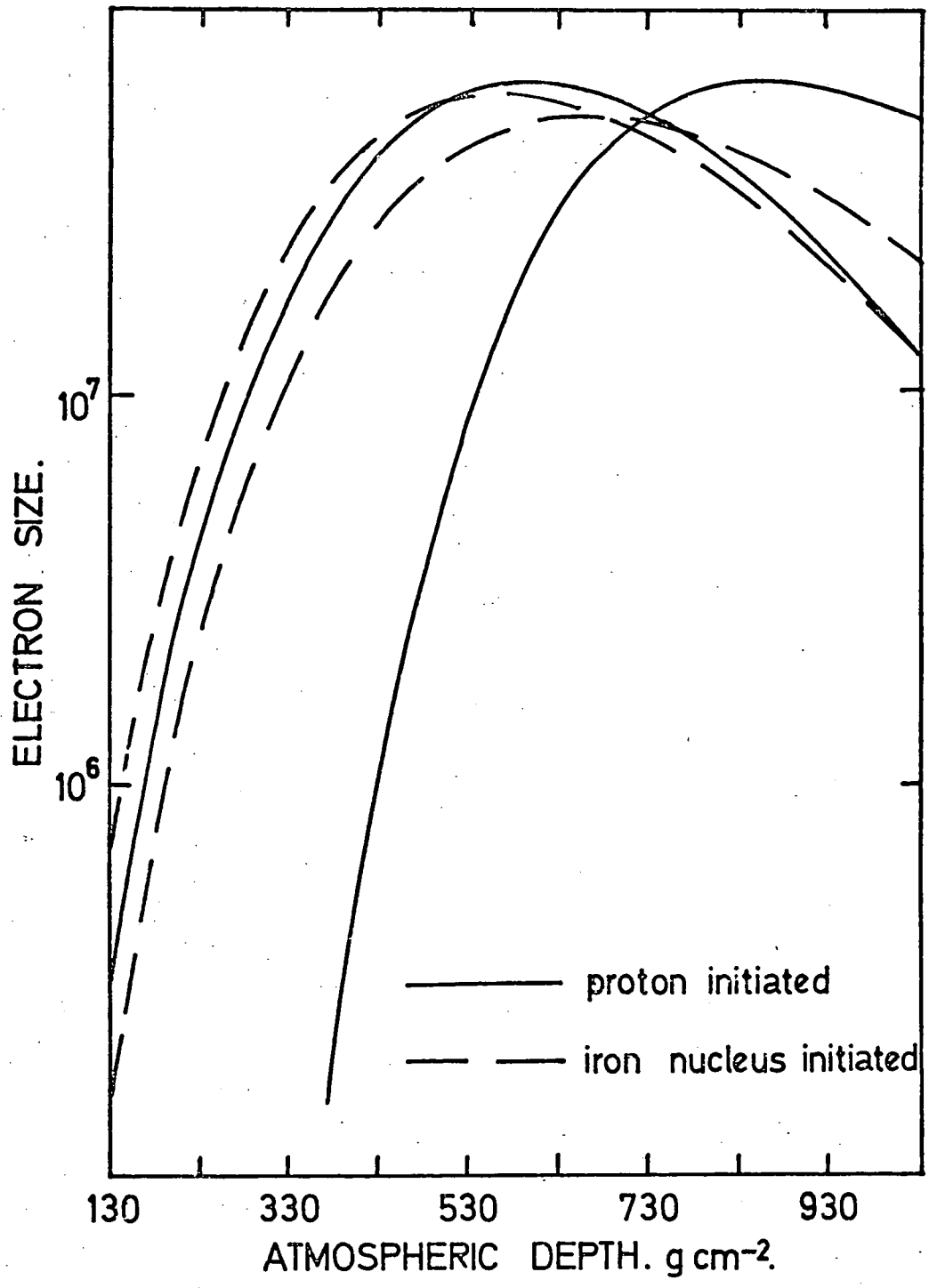
ELECTRON SIZE.
10^7
10^6
130
330
530
730
930
ATMOSPHERIC DEPTH. g cm^{-2}.
proton initiated
iron nucleus initiated

Cerenkov light technique in principle yields information on shower longitudinal history. The light reaching the observation level is not proportional to the local particle density, but to the path length of all those particles, which, at some time during shower development and decay, were energetic enough to radiate Cerenkov light.

Cerenkov light measurements, then, would seem a good place to start a search for parameters exhibiting fluctuations sensitive to shower longitudinal development and primary particle mass.

As is discussed more fully in Chapter 2, the Cerenkov photons in an extensive air shower are very numerous and so are easily and reliably detected. However, experiments can be carried out only during clear, moonless nights and so have a low duty cycle.

The first exploratory measurements of the lateral distribution of Cerenkov light in extensive air showers were made by Jelley and co-workers (see, for example, Jelley (1958)). These were followed by the work of Chudakov et al. (1960), who operated light receivers in conjunction with an extensive air shower particle detector array at an altitude of 3860 m, and made measurements of the distribution of the Cerenkov light at core distances between 10 and 250 m in showers of energies around 10^{15}eV.

Kreiger and Bradt (1969) used an array of Cerenkov light detectors at the Chacaltaya air shower array to measure the ratio of Cerenkov photon density to particle density. Showers of energies between 10^{16} and 10^{17}eV, which are near to cascade development maximum at the array altitude of 5200 m, were studied. Using model calculations similar to those of La Pointe et al. (1968), a small number of showers rich in Cerenkov light were interpreted as an indication of a primary cosmic ray flux of mixed chemical composition, much as it is at 10^{12}eV.

More recently, observations of the Cerenkov light in showers of energies up to about 5×10^{17}eV have been made at the Yakutsk air shower array, which is at sea-level. These observations have been reported by Efimov et al. (1973) and by Dyakanov et al. (1973). Some measurements of the width of the observed light pulses are given by these authors as well as measurements of the lateral distribution of the light.

1.4 The Scope of this Thesis

An experiment to observe the Cerenkov light produced in extensive air showers of energies between about 10^{17} and 10^{18}eV has been developing at the Haverah Park extensive air shower array since 1972. This thesis is concerned with those Cerenkov light measurements made there during the winter of 1975/76, when the experimental equipment was first improved to its present specification.

A description of the relevant theoretical aspects of the characteristics of Cerenkov light, and a brief account of the most recent computer simulations of its properties in extensive air showers, are given in Chapter 2.

Chapter 3 describes in detail the detection and recording equipment used for the Cerenkov light observations, and includes an account of the performance of the equipment.

The average characteristics of the Cerenkov light observed in the showers recorded are given in Chapter 4. Detailed measurements of the shapes of the observed light pulses are described, as well as measurements of the lateral distribution of the Cerenkov light. Some measurements of the relative times at which the Cerenkov light arrives at the various detector positions, are also reported.

In Chapter 5, the measured average characteristics of the Cerenkov light in extensive air showers, are compared with the results from the most recent computer simulations. The simulation results considered are those by Protheroe and Turver (1977). The experimental measurements are also compared with the results of other workers, where such comparisons may be made.

Finally, in Chapter 6, the Cerenkov light measurements made in a small number of individual showers are examined. Evidence that independent Cerenkov light parameters show correlated fluctuations that arise from variations in shower cascade development, is found.

The overall aim of the program of Cerenkov light measurements at Haverah Park, is to determine how the measurements can be used to investigate the mass composition of the most energetic primary cosmic ray particles. The work described in this thesis is a step in that direction. The average features of the Cerenkov light are established and the parameters most suitable for further study can be identified. The studies of the Cerenkov light measurements made in individual showers, demonstrate that the measurements are sensitive to variations in shower cascade development. However, the next stage of the argument - the extension to comment on the mass of the primary particles - must await measurements of Cerenkov light in a much larger sample of showers.

CHAPTER TWO

THEORETICAL ASPECTS OF CERENKOV LIGHT IN EXTENSIVE AIR SHOWERS

The theory of the production of Cerenkov light is examined in this Chapter. Radiation from a single particle is dealt with first, and then follows a brief review of the most recent computer simulations of the characteristics of the Cerenkov light in extensive air showers. The implications of these theoretical results for the design of an experiment to detect the light produced in extensive air showers, are considered.

2.1 Cerenkov Radiation from a Single Particle

Electromagnetic radiation is produced whenever a charged particle traverses a dielectric medium with a velocity in excess of the phase velocity of light in that medium. The first experimental studies of this radiation by Cerenkov (1934,1937) were followed by a satisfactory theoretical interpretation by Frank and Tamm (1937) based on classical electromagnetic theory. For the purposes of this thesis, the accounts of the effect by Jelley (1958,1967), or that by Boley (1964) are wholly adequate.

The passage of a charged particle through a medium sets up a transient polarization of the medium around the particle track, which results in the emission of radiation. Fig.2.1(a) shows an electron passing some point S in the medium. When the electron is at point e_1, the local polarization vector at S, P_1, will be directed at the retarded position of the electron, e_1'. As the electron proceeds to point e_2, the polarization vector turns and points to the new retarded position e_2'. Fig.2.1(b) shows the time variation of the radial and axial components of the polarization vector at S. The radial components do not contribute

Figure 2.1. The transient polarization produced by the passage of a charged particle through a dielectric medium, showing:- (a) the local polarization vector, P, at a point, S, and (b) the time variation of its resolved components. (From Jelley (1958).)

Figure 2.2. (a) Huygen's construction to illustrate the coherence of Cerenkov radiation.
(b) The formation of the Cerenkov light cone. (From Jelley (1958).)

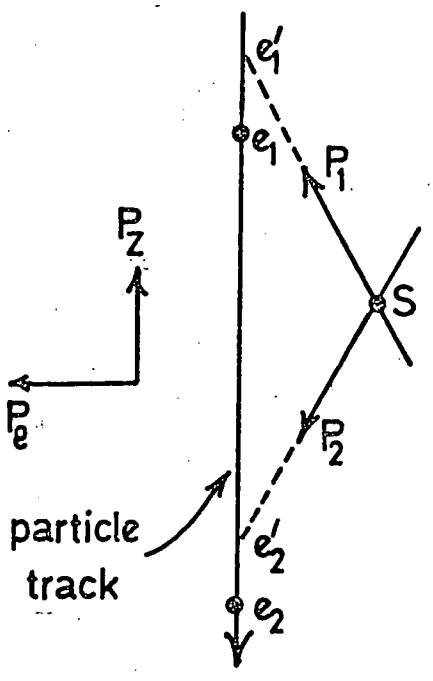
e'1
e1
P1
S
Pz
Pe
P2
particle
track
e'2
e2

(a)

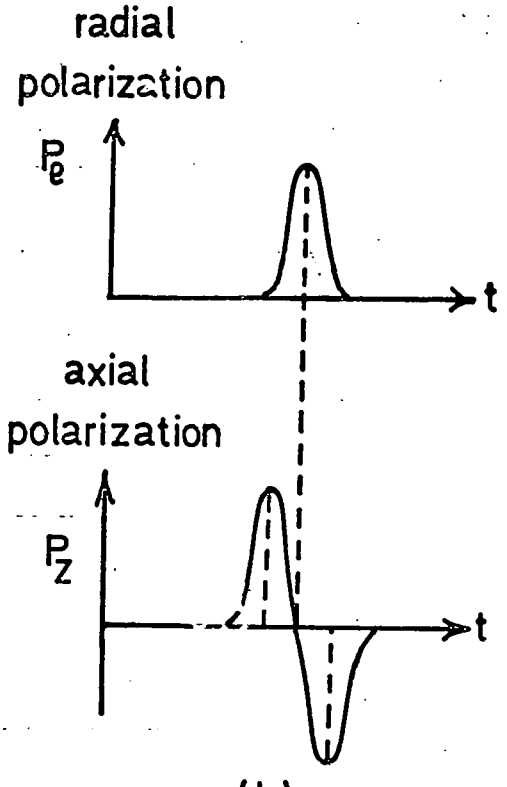
radial
polarization
Pe
t
axial
polarization
Pz
t

(b)

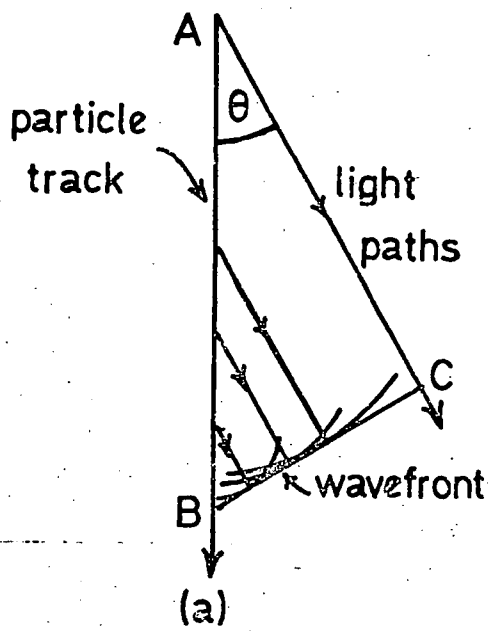
A
θ
particle
track
light
paths
C
wavefront
B

(a)

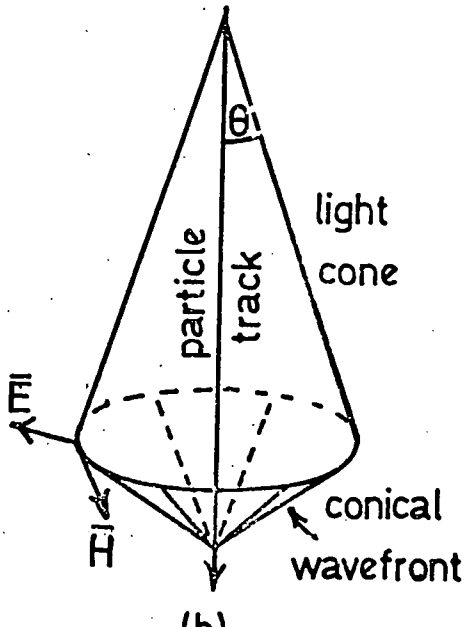
θ
light
cone
particle
track
E
H
conical
wavefront

(b)

to the radiation since they are axially symmetric and so lead to no resultant field at large distances. The axial components combine to form a resultant axial dipole field at large distances, which takes the form of the derivative of a delta-function, and it is these components which are involved in the production of Cerenkov radiation.

The discussion so far concerns only a single element of particle track, of length comparable to the wavelength of the emitted radiation. In general, the radiated wavelets from all parts of the track will interfere destructively so that there is still no resultant field at large distances. However, if the velocity of the passing particle is greater than that of light in the medium, it is possible for wavelets from different portions of the particle track to be in phase and so to produce a resultant field. The Huygen's construction shown in fig.2.2(a) shows that the radiation produced is observed only at a particular angle, θ, with respect to the particle track, at which the wavelets from all parts of the track are coherent. The coherence condition occurs if the particle traverses AB in the same time as the light propogates from A to C. If the particle velocity is βc, then in a time Δt the particle travels a distance:-

$$AB = \beta c \, \Delta t$$

and if the refractive index of the medium is n, the light travels:-

$$AC = \frac{c}{n} \Delta t$$

So from the coherence condition the fundamental Cerenkov relation is obtained:-

$$\cos\theta = \frac{1}{\beta n} \qquad \ldots \text{ equ.2.1}$$

Three conditions follow immediately from this:-

(i) Only particles for which $\beta n > 1$ can produce Cerenkov light. Thus for a given refractive index there is a threshold

particle velocity given by

$$\beta_{min} = \frac{1}{n} \qquad \text{... equ.2.2}$$

(ii) For an ultra-relativistic particle with $\beta = 1$, there is a maximum angle of emission given by

$$\theta_{max} = \cos^{-1}\left(\frac{1}{n}\right) \qquad \text{... equ.2.3}$$

(iii) Cerenkov radiation can occur only at those frequencies for which $n > 1$; in the microwave, infrared, visible and ultra-violet parts of the spectrum, but not in the x-ray and γ-ray regions.

Fig.2.2(a) has been drawn only in one plane. Because of the axial symmetry, the radiation does in fact occur over the surface of a cone of semi-apex angle θ, the axis of which is the particle track (see fig.2.2(b)). The electromagnetic field on the surface of the cone is such that the electric field vector is everywhere normal to the surface, and the magnetic field vector tangential to it.

From the results first derived by Frank and Tamm (1937) the energy dE lost to Cerenkov photons of wavelengths between λ_1 and λ_2, by a particle of charge ze, in traversing a path length dL, is:-

$$\frac{dE}{dL} = 4\pi^2 z^2 e^2 \int_{\lambda_1}^{\lambda_2} \left(1 - \frac{1}{\beta^2 n^2}\right) \frac{d\lambda}{\lambda^3} \qquad \text{... equ.2.4}$$

where n is the refractive index of the medium and βc is velocity of the particle. Two points of interest arise from this:-

(i) The rate of production of Cerenkov photons is inversely proportional to the square of the wavelength of the photons. So the spectrum of Cerenkov light is much enriched at the shortest wavelengths at which its production is possible, in the U.V. and blue regions.

(ii) The rate of production of Cerenkov photons is proportional to the square of the charge of the radiating particle.

2.2 Cerenkov Radiation in the Atmosphere

The refractive index of air at S.T.P. is n = 1.00029 and is so close to unity that the features of Cerenkov radiation in the atmosphere differ considerably from those encountered with solid and liquid media. The production threshold energies of particles are higher; the emission angles smaller; and the production rates lower than for dense media:-

(i) Equ.2.3 leads to a value of $\theta_{max} = 1.3^{o}$ for the maximum angle of emission of Cerenkov light emitted in air at S.T.P. by a particle with $\beta = 1$. Thus, in air, the radiated light is quite closely directionally related to the path of the radiating particle.

(ii) Equ.2.2 allows the threshold kinetic energies of various particles in air at S.T.P. to be found. They are 21 MeV for electrons; 4.3 GeV for muons; and 390 GeV for protons.

(iii) The production rate of Cerenkov photons by a particle of one electronic charge in air at S.T.P. can be obtained from equ.2.4. It is about 30 photons m^{-1} for emission at wavelengths in the range 3500 - 5500 Å (typical of the response of most photomultipliers).

* * *

Of course, the above results apply only at sea-level and at other altitudes must be modified to account for the differing refractive index. Jelley (1967) derives the following results by writing the refractive index of air as $n = (1 + \eta)$ and pointing out that η varies with altitude similarly to atmospheric pressure, as a first approximation:-

(i) The maximum Cerenkov angle at an altitude h, at which the pressure is p_h, is related to that at sea-level by:-

$$\theta_{p_h} = \theta_{p_o} \left(\frac{p_h}{p_o}\right)^{\frac{1}{2}} \quad \ldots \text{ equ.2.5}$$

θ_{p_o} is the maximum angle at sea-level and p_o is the sea-level pressure.

(ii) The form of the variation with altitude of the threshold kinetic energy of a particle is:-

$$E_{min,p_h} = E_{min,p_o} \left(\frac{p_o}{p_h}\right)^{\frac{1}{2}} \quad \ldots \text{ equ.2.6}$$

where E_{min,p_h} is the threshold kinetic energy at altitude h, at which the pressure is p_h, and E_{min,p_o} is the sea-level threshold kinetic energy.

(iii) For an isothermal atmosphere we have the altitude variation of refractive index contained in:-

$$\eta = 2.9 \times 10^{-4} \exp\left(-\frac{h}{h_o}\right)$$

where h_o = 7.1 km, is the scale height of the atmosphere. Jelley shows that the production rate of Cerenkov photons is proportional to η, and so for the altitude variation of the production rate we have:-

$$\left(\frac{dE}{dL}\right)_h = \left(\frac{dE}{dL}\right)_{h=o} \times \exp\left(-\frac{h}{h_o}\right) \quad \ldots \text{ equ.2.7}$$

* * *

The features of Cerenkov light in the atmosphere described so far will be considerably modified by multiple Coulomb scattering of the radiating particles. The Cerenkov angle, θ_c, in air is so low that the scattering angles, θ_s, even for the relativistic energies of particles

in extensive air showers, are often larger, so that many of the directional features of Cerenkov radiation are masked by the scattering. The mean square scattering angle has been derived by Rossi and Griesen (1941) as:-

$$\langle \theta_s^2 \rangle = \left(\frac{E_s^2}{p^2\beta^2}\right) t \quad \text{radians} \quad \ldots \text{ equ.2.8}$$

where E_s = 21 MeV, is a constant; p is the momentum of the particle; and t is the particle path length expressed in radiation lengths. For air, the radiation length is X_o = 37.7 g cm^{-2}, and from equ.2.8 we find that for p = 100 $\frac{MeV}{c}$, typical of the momentum of electrons in an extensive air shower, θ_s = 12^o, much larger than the Cerenkov emission angle.

Other processes which affect the observed characteristics of Cerenkov light produced in the atmosphere are ozone absorption, aerosol attenuation and Rayleigh scattering. Allen (1955) gives for the absolute transmission of the atmosphere in the zenith 63%, 73% and 80% for the wavelengths 4000, 4500 and 5000 $\mathring{A}$, respectively. For observations away from the zenith these figures will, of course, be reduced; atmospheric transmission varying as the secant of the zenith angle (for a source outside the atmosphere, strictly). Detailed information on aerosol attenuation and Rayleigh scattering has been given by Elterman (1968).

The processes of dispersion, diffraction and refraction do not significantly affect Cerenkov light produced in the atmosphere (Jelley (1967)).

* * *

Any experiment to observe Cerenkov light in the atmosphere must operate in the presence of the background light of the night sky. Jelley (1958) quotes a figure of $\phi_B = 6.4 \times 10^7$ photons $cm^{-2}s^{-1}sr^{-1}$ for photons

in the wavelength range 4300 - 5500 Å as the night light flux, but points out that this figure may vary greatly with site location and conditions. Commenting on the spectrum of the night sky, Allen (1955) states that the intensity of the continuum radiation rises steadily by about a factor of six between 3600 and 6500 Å. This is fortunate for the observation of Cerenkov light, the spectrum of which peaks towards the blue, as already discussed. The continuum radiation is composed of starlight, diffuse galactic light and zodiacal light. Superimposed on it are many lines and molecular bands; in the visible region the O_3 line at 5577 Å and the OH bands between 5600 and 5900 Å are, notable. (See, for example, Blackwell, Ingham and Rundle (1960).)

2.3 Cerenkov Radiation in Extensive Air Showers

The large majority of the Cerenkov light produced in extensive air showers is radiated by electrons. This is so because the Cerenkov light production threshold of an electron is much lower than that of any other particle, and because electrons are by far the most numerous particles in a shower cascade. About 85% of shower electrons arriving at sea-level have energies above the sea-level production threshold of 21 MeV.

For each shower electron reaching sea-level there are about 100 radiation lengths of electron path in the atmosphere. Equ.2.7 leads to the result that about 4×10^5 Cerenkov photons are produced for each electron arriving at sea-level (Boley (1964)). The numerical excess of Cerenkov photons over particles in an extensive air shower makes them much more easily detected. At large distances from shower cores, measurements of the Cerenkov light flux can be made without the statistical limitations inherent in the measuring of the very small particle densities that occur at these positions in showers.

The unique aspect of the Cerenkov light arriving at ground level in an extensive air shower, is that it is not proportional to the local particle number, but to its integral over the whole history of the shower. The signal registered by a particular detector will be a complex sum of the contributions of all those electrons that, at one time or another in their participation in the shower development, radiate light into the acceptance solid angle of that detector. In principle then, the characteristics of the light reflect the overall development of the shower through the atmosphere. They may relate to the depth into the atmosphere of the initial interaction of the primary particle, and hence to the mass of the primary (as outlined in Chapter 1).

2.4 Computer Simulations of Cerenkov Light in Extensive Air Showers

Simulations of the characteristics of Cerenkov light in air showers of energies similar to those detected at Haverah Park ($>10^{17}$eV) have been carried out at Durham University as part of a larger program of work involving many aspects of extensive air showers.

2.4.i The Model by Smith and Turver (1973)

The first simulations were of the Cerenkov light produced in proton initiated showers, and were carried out by Smith and Turver (1973). The model of the hadron cascade by Cocconi et al. (1961) was used to calculate the numbers of pions of various energies produced in the nuclear cascade at various heights in the atmosphere. From this pion distribution, the electrons giving rise to the majority of the Cerenkov radiation were derived. The development of the electron cascade was followed by using cascade theory under Approximation A to consider the initial higher energy particles, and then the results from the 3-D Monte-Carlo calculations by Messel and Crawford (1969) to trace the lower energy particles.

The total electron track length was evaluated and the numbers of optical Cerenkov photons reaching ground level at various core distances were calculated. Fig.2.3(a) shows the results for the average lateral distribution of the Cerenkov light (in the wavelength range 3500 - 5000 Å) produced in showers initiated by vertically incident protons of energies 10^{15}, 10^{16}, 10^{17} and 10^{18}eV. The lateral light spread is seen to be broader in the lower energy showers.

Fluctuations in the points of interaction and in the inelasticity of the nucleons, cause individual showers to reach their cascade development maxima at different depths in the atmosphere. The affect of such fluctuations on the lateral distribution of the Cerenkov light in 10^{17}eV proton initiated showers was also simulated. Fig.2.3(b) shows the results which suggest that the lateral extent of the light distribution is an indication of shower development: the distribution broadens with decreasing depth into the atmosphere of shower cascade development maximum. However, in the region of 200 m from the shower core, the photon density is seen to be independent of shower development and so should relate well to the primary particle energy.

It was largely upon the basis of these simulation data that the present program of experimental work to investigate the characteristics of Cerenkov light in high energy extensive air showers was commenced.

2.4.ii <u>The Model by Protheroe and Turver (1977)</u>

The most recent simulations undertaken at Durham are those by Protheroe and Turver (1977). They incorporate the Feynman scaling hypothesis in the model of the pion production. The production of Cerenkov photons in space and time is rigorously simulated using Monte-Carlo techniques and the effects of ozone absorption, aerosol attenuation and Rayleigh scattering on the progress of the Cerenkov

Figure 2.3. Characteristics of the lateral distribution of the Cerenkov light in vertical, proton initiated showers, according to the simulations by Smith and Turver (1973).

(a) The average light distributions in showers of four primary energies.

(b) The sensitivity to depth of shower cascade development maximum shown by the light distributions of individual showers of energy 10^{17}eV.

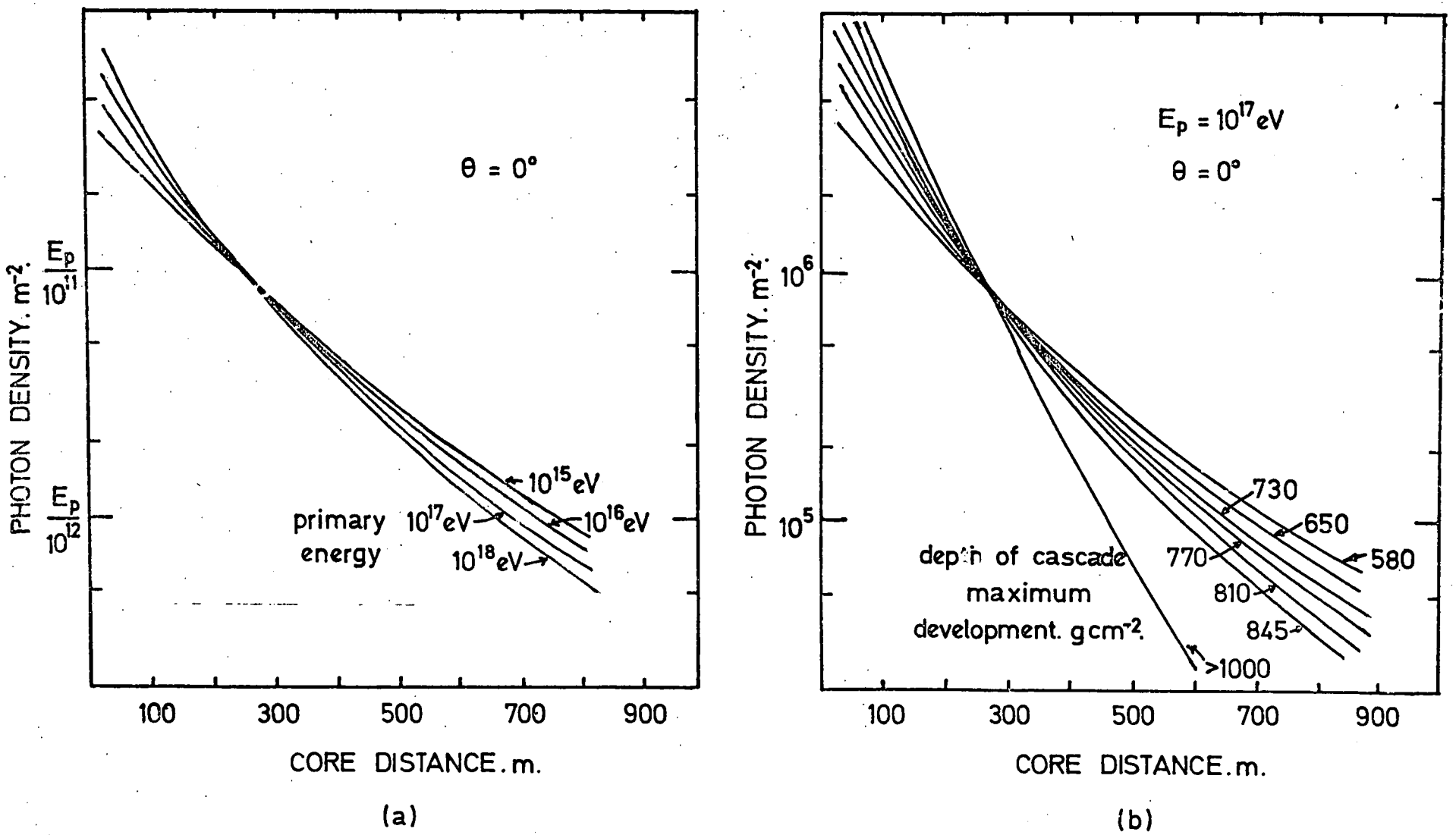
θ = 0°
PHOTON DENSITY. m⁻².
10^(11) E_p
10^(12) E_p
primary energy
10^15 eV
10^16 eV
10^17 eV
10^18 eV
100
300
500
700
900
CORE DISTANCE. m.
(a)
E_p = 10^17 eV
θ = 0°
PHOTON DENSITY. m⁻².
10^6
10^5
depth of cascade maximum development. g cm⁻².
730
650
580
770
810
845
>1000
100
300
500
700
900
CORE DISTANCE. m.
(b)

light through the atmosphere are included. Details of the light pulse shape and the arrival time of the Cerenkov light are given, as well as the lateral distribution of the light. The results of the simulations are made specific to the 1975/76 Cerenkov light detection experiment at Haverah Park (described in Chapter 3). The spectral response of the detectors used in that experiment is folded into the simulations, and the effects of the system bandwidth are accounted for by convoluting the temporal results with an appropriate response function. The average characteristics of the Cerenkov light produced in showers initiated by vertically incident protons, alpha particles and iron nuclei of energies 10^{16}, 10^{17} and 10^{18}eV are determined.

The results of the simulations suggest that the average features of the Cerenkov light do not uniquely reflect either the primary particle energy or mass, but that several parameters are well correlated with depth of shower cascade development maximum:-

(i) The lateral light spreads in showers developing higher in the atmosphere are broader than those in showers developing lower in the atmosphere, in agreement with the model by Smith and Turver (1973). The exponent of a power law description of the light distribution increases monotonically with increasing depth of shower cascade development maximum.

(ii) The shape of the Cerenkov light pulse is also sensitive to depth of shower cascade development maximum. At all core distances the rise-time (10% - 90%) and the full-width-half-maximum (50% - 50%) of the light pulse increase mononton-ically with increasing depth of cascade maximum; although the variation of the pulse rise-time is much less than that of the full-width-half-maximum. Other light pulse shape parameters - the top-time (90% - 90%) and the fall-time

(90% - 50%) - also vary with depth of shower cascade development maximum, but not in such a simple way.

(iii) The curvature of the Cerenkov light front in extensive air showers indicates depth of shower cascade development maximum, too. The light front is near-spherical and its radius decreases monotonically with increasing depth of shower cascade maximum.

The simulations also suggest that at core distances greater than about 100 m, the temporal structure of the Cerenkov light pulse mirrors the overall form of the development of the shower electron cascade. Despite the effects of the refractive index of the atmosphere, the first light reaching ground level originates highest in the atmosphere, and so on. Thus, the rise-time of the light pulse in principle reflects the growth of the electron cascade. Similarly, the top-time of the light pulse is a measure of the width of the electron cascade in the region of the cascade development maximum, and the light pulse fall-time relates to the decay of the electron cascade.

The results of the simulations by Protheroe and Turver (1977) are compared with the experimental measurements of the present work in Chapter 5. There, some of the simulation results are illustrated in the appropriate figures.

2.5 Implications for Experiment Design

The theoretical results presented in this Chapter clearly show that measurements of several Cerenkov light parameters can be made in large air showers. They give much guidance for the design of an experiment to make the measurements.

The results of the computer simulations suggest that Cerenkov photon fluxes well above the background light of the night sky occur out to core distances of about 500 m in showers of energy as low as 10^{17} eV.

An array of simple, small area light detectors should be quite adequate for observation of the light. Measurements of the light flux with an accuracy of ±5% should be precise enough to show up the predicted differences in the shapes of the lateral light distributions in showers reaching cascade development maxima at different atmospheric depths. Also, this measurement precision should be sufficient for shower core location analyses on the basis of the Cerenkov photon density measurements. It may be possible to estimate primary particle energy from the photon density at 200 m core distance.

It is also evident, from the simulations by Protheroe and Turver (1977), that with a system of 10 ns response time, useful measurements of various Cerenkov light pulse shape parameters should be obtained at core distances greater than about 200 m. (Closer to the core than this, the observed light pulses are likely to be "bandwidth limited".) The values of the Cerenkov light pulse shape parameters vary monotonically with core distance, making shower core location analyses on the basis of measurements of these parameters just as feasible as the more conventional use of signal density measurements for shower analysis.

Measurements of the relative arrival time of the Cerenkov light at spatially separated detectors would allow the curvature of the light fronts of individual showers to be determined. Good timing accuracy would be necessary: in a shower with a spherical light front of radius 8 km (typical of the light front radii predicted by the simulations by Protheroe and Turver (1977)) light would arrive at a detector situated at the shower core impact point only 47 ns before its arrival at a second detector 500 m distant. So pursuing timing accuracies as precise as ±2 ns would be worthwhile with a detector baseline of this order.

As far as the interpretation of experimental results in terms of primary particle mass is concerned, the aim of the present work is to avoid reliance on model calculations. The simulation results suggest that many Cerenkov light parameters measured at ground level are related to depth of shower cascade development maximum. However, while estimates of this depth may be obtained by comparing experimental measurements with the simulation results, subsequent identification of primary particle mass is entirely dependent on the model of the high energy nuclear physics assumed in the simulations. A possible approach to the problem of finding the primary particle mass without reliance on detailed simulation results, may be to study the fluctuations from average, of values of various Cerenkov light parameters.

CHAPTER THREE

THE ATMOSPHERIC CERENKOV LIGHT DETECTOR ARRAY AT HAVERAH PARK

Since 1972, an experiment to measure the characteristics of the Cerenkov light that is produced in large cosmic ray air showers[c] has been under development at the site of the Haverah Park air shower array, near Harrogate in Yorkshire (latitude 53^{o} 58.2' N; longitude 1^{o} 38.2' W; mean altitude above sea-level 222 m). This Chapter describes the current experimental arrangements there. A brief survey of the previous work is given first, since it is from this that the present system has been derived. Then follows a detailed description of the present equipment and a report of its performance during its first period of operation.

3.1 Previous Observations of Atmospheric Cerenkov Light at Haverah Park

The first attempt to observe Cerenkov light produced in showers detected by the Haverah Park air shower array was made by Smith and Turver during the U.K. winter of 1972/73. A single 7" diameter photo-multiplier (E.M.I. type 9623) pointing vertically upwards and without any optical system was used to obtain measurements in about 100 showers of energies in the order of 3×10^{17} eV, incident at zenith angles less than 60^{o}.

The following winter (1973/74) the same workers extended the system to an array of six light detectors, all similar to the one of the initial experiment, to make measurements of the lateral distribution of the Cerenkov light in individual showers. The light signals registered by each detector were fed along relay cable to a central recording station, suitably delayed, displayed on a multi-beam oscilloscope and recorded photgraphically. The oscilloscope was triggered by the Haverah Park 500 m particle detector array and the total bandwidth of the system was about 1 MHz. At the time of writing

the results of this experiment remain unpublished.

Neither of the experiments at Haverah Park had attempted to preserve details of the shape of the Cerenkov light pulse or to measure the time of arrival of the light, and it was the improving of the system bandwidth to try to measure these temporal parameters that gave rise to the work reported in this thesis.

During the next winter (1974/75), an array of 7 fast response light detectors was commissioned at Haverah Park. Again the type of detector - a simple E.M.I. type 9623 photomultiplier with no optical system - and the method of recording -the photography of oscilloscope displays - remained essentially the same as before, but the bandwidth of each channel was improved to about 10 MHz, chiefly by using better quality cable for the signal delays. The results of this experiment included further measurements of the lateral distribution of Cerenkov light; the observation of a curvature to the light front; and measurements of the light pulse rise-time and full-width-half-maximum as functions of core distance. The details of this experiment and the results obtained have been reported by Orford et al. (1975).

It was the findings, both scientific and technical, of the 1974/75 work that most influenced the design of the current Haverah Park Cerenkov light detection experiment. Although no specific details of the 1974/75 experiment, or of its results are given here, reference to certain aspects of that work will be made when describing the present system, as a means of highlighting some design considerations.

3.2 The Design of the Current Atmospheric Cerenkov Light Detector Array

The current experiment to detect the Cerenkov light produced in the extensive air showers selected by the Haverah Park particle detector array, was commissioned in the U.K. winter of 1975/76. It uses an array of eight light detectors spread over an area of about 1 km^2, as shown in

Figure 3.1. The layout of the array of atmospheric Cerenkov light detectors, commissioned at Haverah Park during the winter of 1975/76.

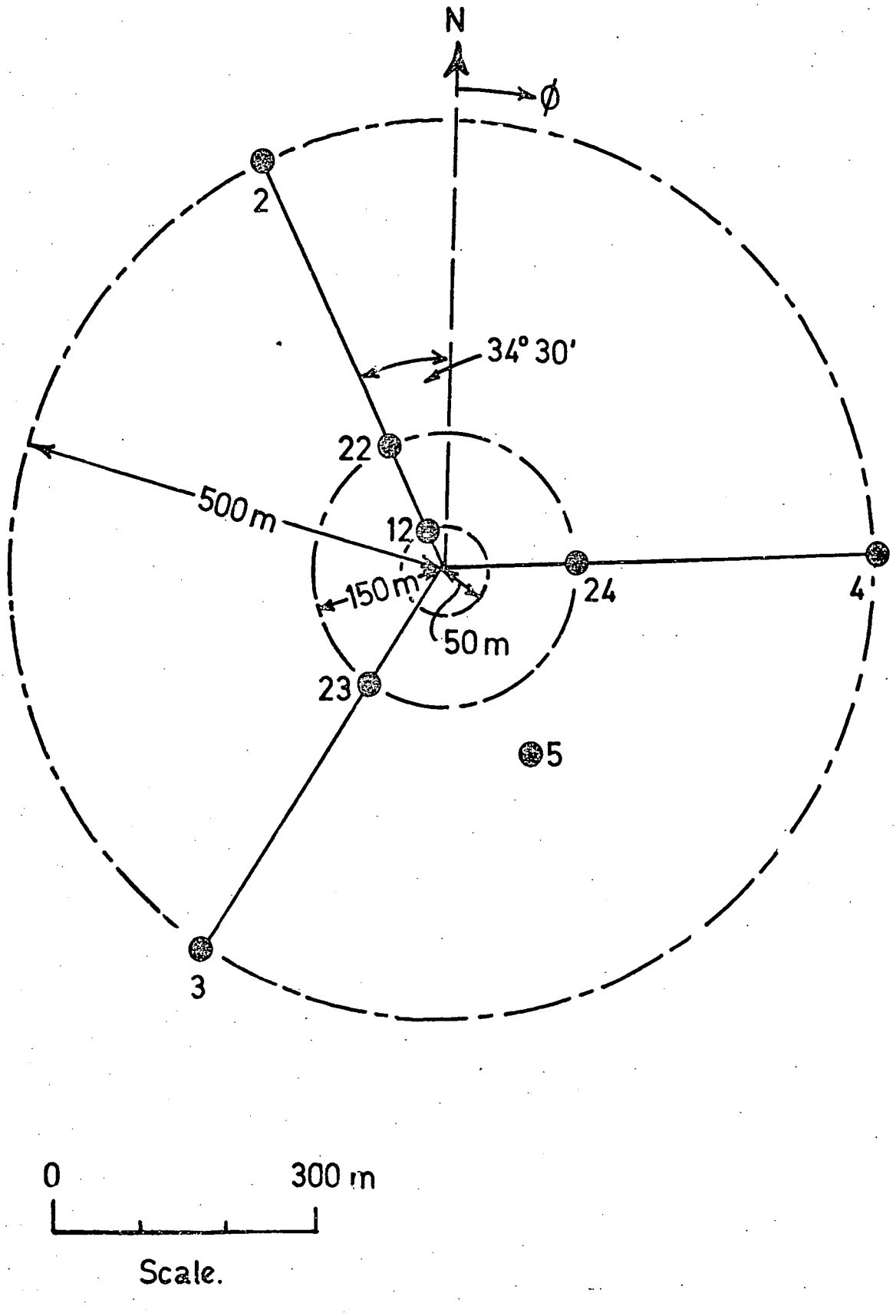
N
ϕ
2
34° 30'
22
500 m
12
150 m
50 m
24
4
23
5
3
0
300 m
Scale.

Figure 3.2. Schematic diagram of one complete channel of the atmospheric Cerenkov light detector array. (Signal paths are indicated by double arrows; single arrows represent other functions.)

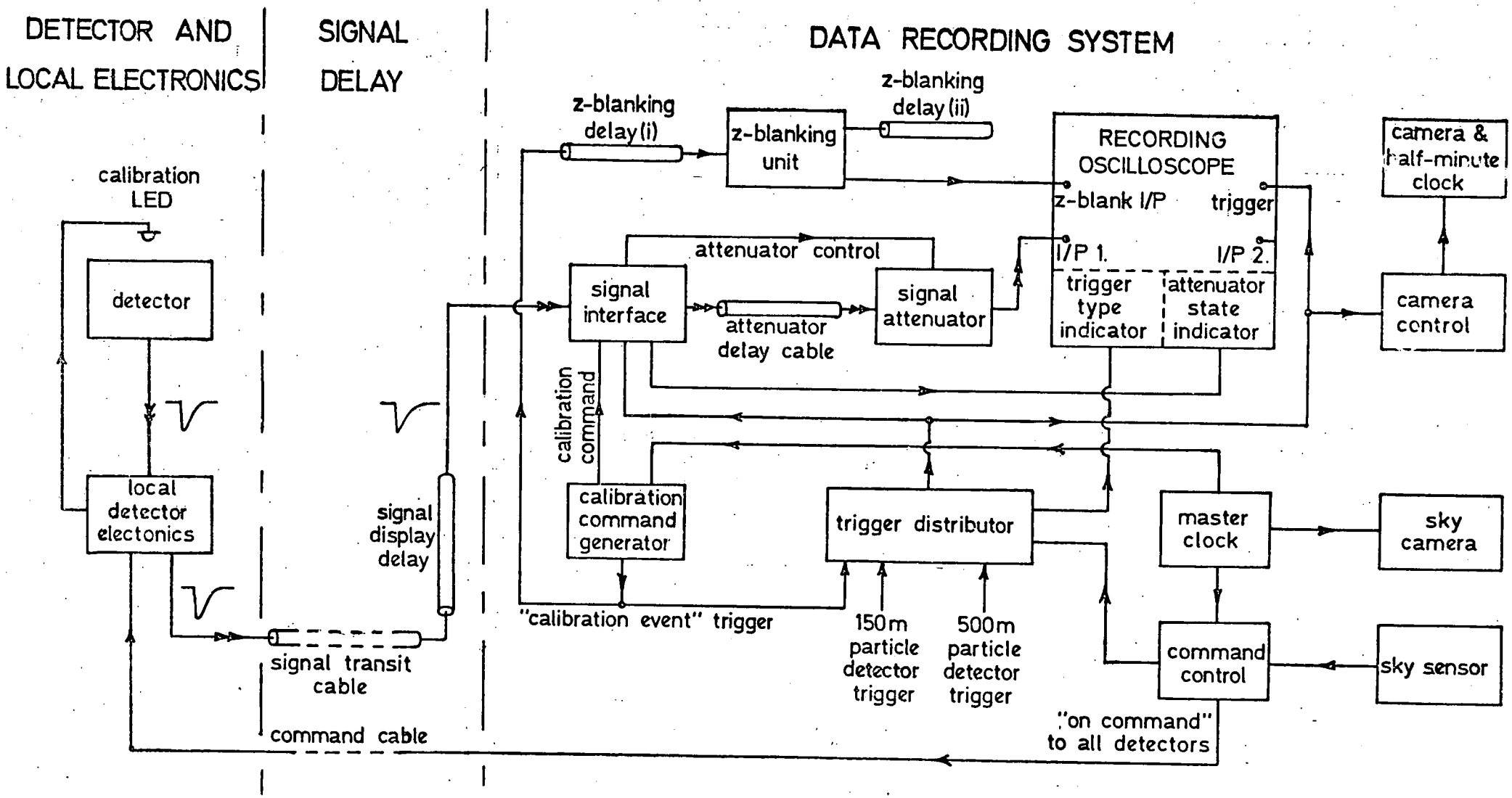
DETECTOR AND LOCAL ELECTRONICS
SIGNAL DELAY
DATA RECORDING SYSTEM
calibration LED
detector
local detector electonics
signal transit cable
command cable
signal display delay
z-blanking delay (i)
z-blanking unit
z-blanking delay (ii)
RECORDING OSCILLOSCOPE
z-blank I/P
trigger
I/P 1.
I/P 2.
trigger type indicator
attenuator state indicator
camera & half-minute clock
camera control
attenuator control
signal interface
attenuator delay cable
signal attenuator
calibration command
calibration command generator
"calibration event" trigger
trigger distributor
150m particle detector trigger
500m particle detector trigger
master clock
sky camera
command control
sky sensor
"on command" to all detectors

fig.3.1. The light detectors are mounted in the roofs of the huts at Haverah Park, and six of them (labelled 2,3,4,22,23,24, in fig.3.1) are in the same positions as the particle detectors. The light detector locations are known to within about 30 cm.

Like its forerunners, the experiment employs an analogue data recording system and this is located in the hut housing detector 12. Fig.3.2 is a schematic diagram of one complete channel of the system and it is seen that two cables connect each detector and the data recording system. Signals from each detector pass along the signal transit cable and on arrival at the recording system, are displayed on oscilloscopes and photographed. The command cable carries a command from the data recording system which causes E.H.T. to be applied to the detector photomultipliers during night running periods.

The data recording system also automatically calibrates the detectors and recording oscilloscopes, and monitors the night sky clarity.

In the detailed description of the equipment that now follows, the reader will find it useful to refer to fig.3.1 and fig.3.2.

3.2.i Triggering from the Haverah Park Particle Detector Array

The Haverah Park extensive air shower particle detector array has been described many times (see, for example, Wilson et al. (1963) or Tennent (1967)) and only a very brief account is given here, chiefly to clarify the arrangements for the triggering of the atmospheric Cerenkov light detection equipment.

The layout of the Haverah Park 500 m and 150 m particle detector arrays is shown in fig.3.3. Three water Cerenkov detectors, A2, A3, A4 are symmetrically spaced at a radius of 500 m about a fourth similar detector, A1. Each of these detectors is built up from 15 tanks of water, 120 cm deep, each viewed by a photomultiplier which detects a small

Figure 3.3. The layout of the array of particle detectors at Haverah Park.

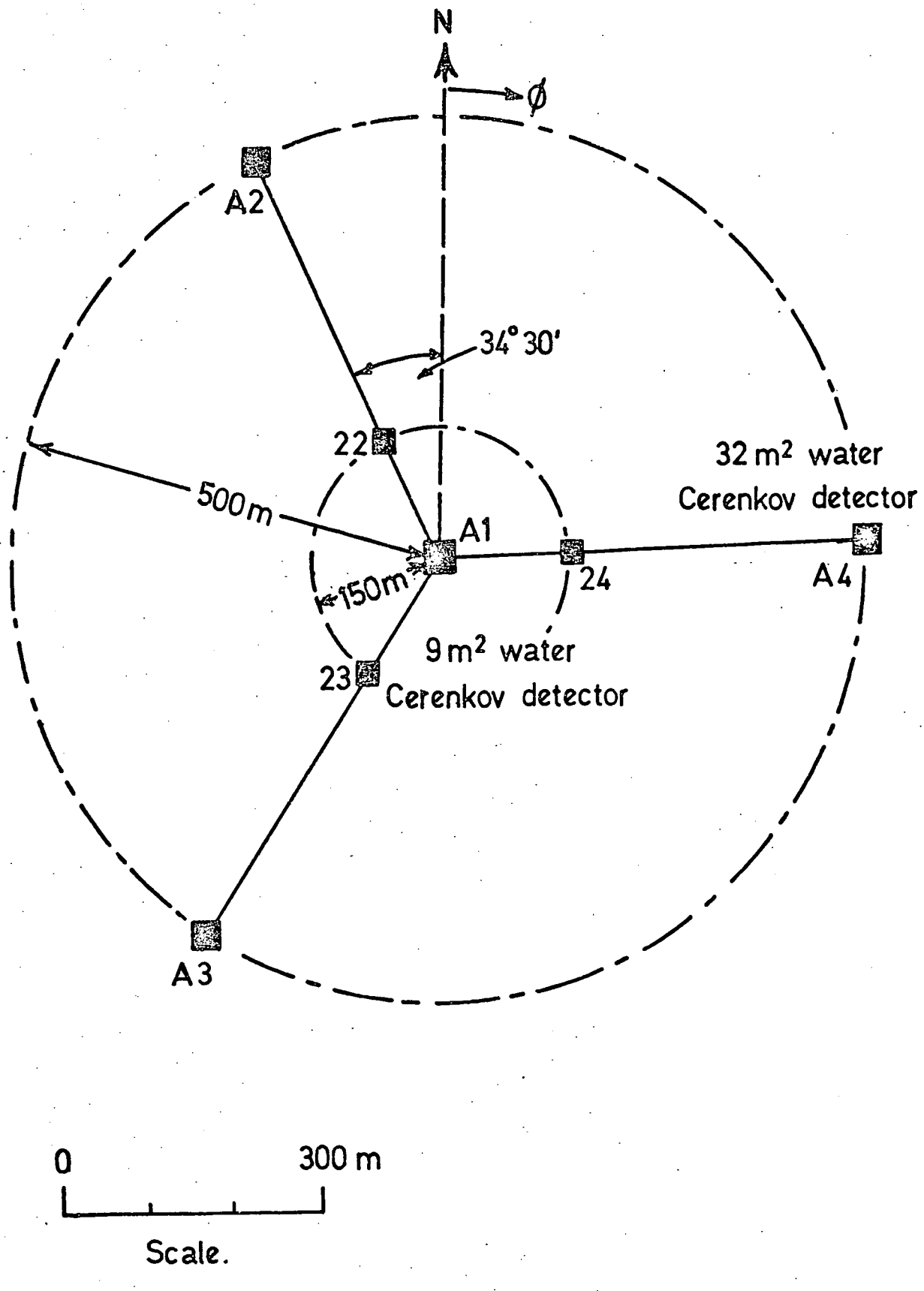
N
Ø
A2
34° 30'
22
500m
A1
150m
24
A4
32 m² water
Cerenkov detector
9 m² water
Cerenkov detector
23
A3
0
300 m
Scale.

fraction of the Cerenkov light emitted by particles traversing the water. The signals from each tank are added giving a total sensitive area of 32 m^2. Detectors, 22, 23, 24 each consist of 9 m^2 of the same water tanks and are spaced 150 m from the central detector A1.

The 500 m particle detector array records an extensive air shower when the density of particles at detector A1 and any two of detectors A2, A3, A4 give a signal corresponding to an energy loss greater than 0.3 equivalent muons m^{-2} within a 4 μs coincidence window. The trigger pulse obtained when this coincidence requirement is met, occurs no sooner than 4.0 μs after the central detector, A1, exceeds the 0.3 muons m^{-2} discrimination level. Signals from any detectors must be delayed by at least this time if they are to be displayed on an oscilloscope located at the central detector and triggered by this "500 m particle detector trigger". In practice, delays of 6.3 μs are used to allow for the time taken for a shower to traverse the array as well as the time taken to generate the coincidence pulse. (For each 500 m particle detector, about 2.3 μs of this delay is in the underground transmission cable that brings the signals to the central recording station.)

Air showers detected as a result of coincidences between 500 m particle detector signals are referred to as "500 m events" in the text and occur at a rate of about 1 hr^{-1}.

* * *

Usually, all subsidiary experiments at Haverah Park are triggered by the 500 m particle detector trigger. The 150 m particle detector array is not used to generate coincidences but only to provide additional energy loss measurements in showers selected by the 500 m particle detectors. However, for an analogue experiment to observe the temporal characteristics of atmospheric Cerenkov light, the 500 m particle detector

trigger has a distinct disadvantage. The comparatively long time (about 0.3 μs) that any light signal must be delayed before being recorded on a display triggered by it, leads to an unacceptable lowering of the system bandwidth in an application in which the response time should be as fast as possible in order not to distort the light pulse shape. (For example, the 1974/75 atmospheric Cerenkov light experiment at Haverah Park had shown that as far as 300 m from the shower core, light pulses with full-width-half-maxima as short as 40 ns are observed.)

To overcome the long generation time of the 500 m particle detector trigger, the present Cerenkov light detection experiment uses the 150 m particle detector array to select the showers recorded. In a manner similar to that of the larger array of detectors, showers are selected when coincident particle densities greater than 0.3 equivalent muons m^{-2} occur at the central detector, A1, and at any two of detectors 22, 23, 24. The smaller spatial separation of these detectors reduces the trigger generation time to 1.75 μs and also increases the rate at which showers are recorded to about 11 hr^{-1}.

This "150 m particle detector trigger" responds to all but the most distant or inclined of the showers selected by the 500 m particle detectors. (Of the 86 500 m events recorded during clear nights in the winter of 1975/76, 68 were also registered by the 150 m particle detector trigger; the remaining 18 falling outside the bounds of the 500 m array.) In addition, it also registers a much larger number of showers, of energies lower than those of 500 m events. These additional showers are referred to as "150 m events" in the text. Shower analyses on the basis of particle detector measurements are available only for 500 m events, and 150 m events must be analysed solely on the basis of the recorded Cerenkov light signals if these lower energy showers are to be studied.

3.2.ii The Cerenkov Light Detectors

Each Cerenkov light detector consists of an R.C.A. type 4522, 5" diameter photomultiplier mounted vertically upwards in a simple aluminium box, as shown in fig.3.4. There is no optical system and the photomultiplier views the sky through an almost horizontal, $\frac{1}{8}$" thick glass window in the roof of a Haverah Park hut. The dimensions of the window and detector housing are such that almost the complete sky is within the field of view of the photomultiplier. The dynode chain is constructed on two circuit boards mounted vertically at the sides of the neck of the photomultiplier. E.H.T. is applied to the photomultiplier by a relay, which is mounted in the lower part of the detector box and is activated by the "on command" fed along the command cable from the central data recording system.

A light emitting diode (L.E.D.) is mounted on the upper edge of the photomultiplier housing and is used for the regular calibration of the detector gain. The light generated when it is illuminated, is directed over the whole of the photomultiplier face by a small mirror (see fig.3.4). A green L.E.D. is used in preference to the more common red ones because its light output has a spectrum more similar to that of atmospheric Cerenkov light.

A Nuclear Enterprises type N.E. 130 radio-active light source is mounted on the face of each photomultiplier. It consists of an americium α-emitter isotropically embedded in type N.E. 102 plastic scintillator, and it provides an essentially delta-function light pulse of about 2000 photons, at a repetition rate of about 700 s^{-1}. This light source enables the gain and temporal characteristics of the detector to be checked by an alternative method at various times during the operating season.

* * *

Figure 3.4. One of the atmospheric Cerenkov light detectors. The side panel of the box has been removed to show the photomultiplier and dynode chain. The L.E.D. and small mirror at the top edge of the box are used to calibrate the gain of the detector.

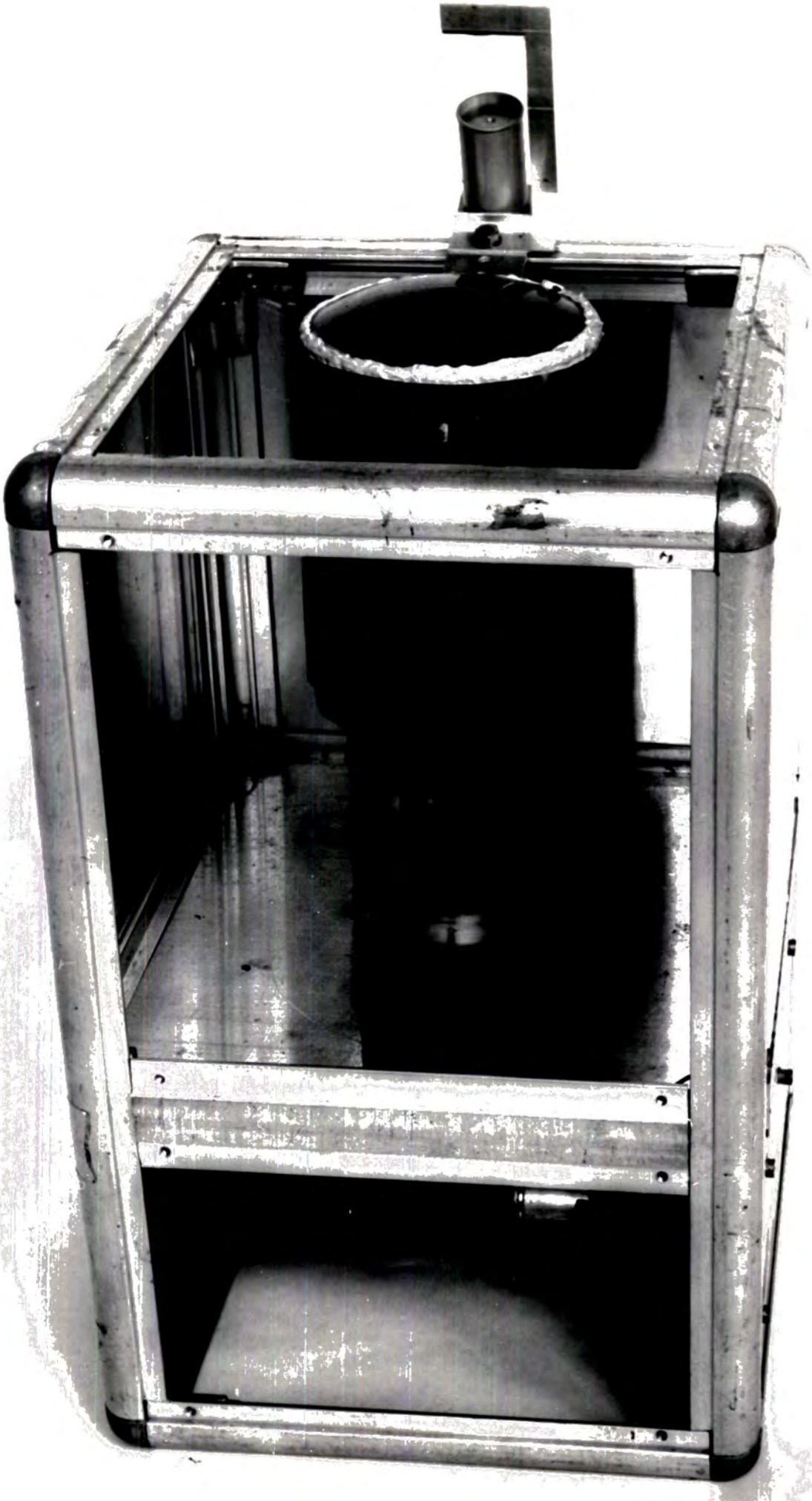

When viewing the night sky, a photomultiplier is required to operate in the presence of a background of starlight and other scattered light sources. The applied E.H.T. must, therefore, be sufficiently low that this ambient background light does not cause the maximum permissible D.C. anode current of the photomultiplier to be exceeded. Also, a dynode chain current much greater than the D.C. anode current is needed to avoid large charges in photomultiplier gain as the ambient background light varies.

The R.C.A. type 4522 photomultiplier has an absolute maximum D.C. anode current rating of 500 μA and the eight detectors were set up firstly by setting the E.H.T. applied to each, to give D.C. anode currents of about 200 μA on a clear moonless night. The E.H.T. values were then trimmed to make the complete channel gains of the more distantly located detectors (2,3,4 and 5) approximately equal and twice that of the more centrally placed detectors (12, 22, 23 and 24), the gains of which were also adjusted to be similar. The final E.H.T. values ranged from 1.90 to 1.98 kV, which with dynode chain resistances of 0.67 MΩ, resulted in dynode currents of 3 mA. These were some 15 times greater than the 200 μA D.C. anode currents and the photomultiplier gains varied little as the background light level changed. Between the brightest, cloudy and darkest, clear, night skies, the gain changes were never more than a factor of two.

In the present experiment no attempt is made to stabalize these photomultiplier gain variations, but rather, any changes in gain are taken into account by frequently calibrating the detectors. This is in contrast with the method that had been employed in the 1974/75 experiment, for which 7" diameter E.M.I. type 9623 photomultipliers had been used; again with high dynode chain currents and low applied E.H.T.s; but with an optical servo-loop to hold the phototube gains

completely constant. The anode current of each phototube had been monitored by sensing the voltage across the anode load resistor: if this dropped, four L.E.D.s in the field of view of the photomultiplier were brightened, raising the anode current once more and thus stabilizing the gain.

The disadvantage with such an optically fed back automatic gain control (A.G.C.) is its addition to the background sky noise which lowers the signal-to-noise ratio of the detectors. It was for this reason that frequent calibration to take account of gain changes, was used in preference to an optical A.G.C. in the present experiment. In fact, without the A.G.C., no detectable gain changes occurred during the course of any one acceptably clear night: the only observed gain changes were between different nights.

The delta-function light pulses of the type N.E. 130 radio-active light sources positioned on the photomultiplier faces gave signals at the phototube outputs that were ten times the background noise from a typical clear night sky. However, the signal-to-noise ratio of a complete channel was reduced from this figure, mainly by the bandwidth limit of the signal transit cable, making the smallest confidently measurable signal about 2000 photons (i.e. that given by the radio-active light sources).

* * *

Before finally commissioning the detectors, various checks of the photomultiplier performances were carried out in the laboratory using an artificial night sky background light.

The manufacturer claims that using a delta-function light input, an output pulse with a rise-time of 2.3 ns and a full-width-half-maximum of 6 ns can be obtained from a type 4522 photomultiplier operated at an E.H.T. of 3 kv, although the performance at lower E.H.T.s is

expected to be slower. Testing with the type N.E. 130 radio-active light sources achieved rise-times better than 7 ns and full-width-half-maxima of 12 ns from all the photomultipliers, when operated at their working E.H.T.s around 1.9 kV.

The linearity of each of the photomultipliers was checked by placing two polaroids between each phototube face and a green L.E.D. light source, and varying, in a way known from Malus's Law, the amount of light incident on the photocathode by adjusting the angle between the polaroids. The photomultipliers were found to be linear over a dynamic range of at least 50:1, the lower end of this range corresponding to the amplitude of the smallest signals readily distinguished from the background noise of a typical clear night sky.

Finally, a check for differences in spectral response from tube to tube was made. The detection efficiency of the photocathode and window as a function of wavelength, claimed by the manufacturer, is shown in fig.3.5. Similarity between the photomultipliers was checked by placing a range of filters from deep violet to deep red between an incandescent bulb light source and each phototube in turn. For each spectral range the photomultipliers were found to have responses similar to within $\pm$10%.

3.2.iii The Local Detector Electronics

With each light detector is a set of electronics, comprising a signal amplifier, a calibration pulse generator and a stabalized E.H.T. supply. These are mounted close to the photomultiplier housing.

The signal amplifier uses a type SN52733 video amplifier integrated circuit, the two differential outputs of which feed a double-sided emitter follower line driver. Its gain is nominally 5, its bandwidth is 70 MHz, and it is non-inverting.

Figure 3.5. The detection efficiency of the photocathode and window of an R.C.A. type 4522 photomultiplier (manufacturer's specification).

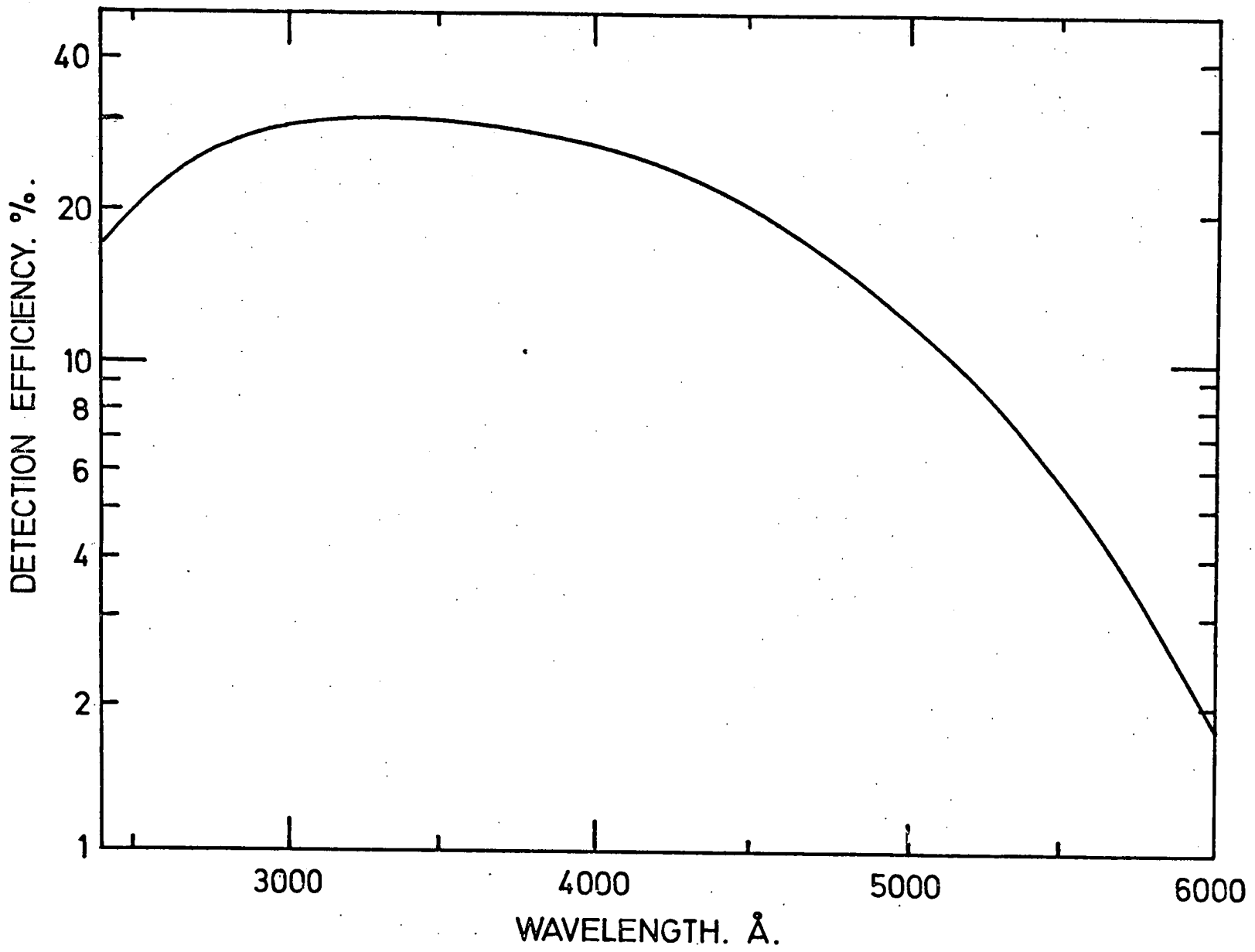
DETECTION EFFICIENCY. %.
40
20
10
8
6
4
2
1
3000
4000
5000
6000
WAVELENGTH. Å.

The calibration pulse generator illuminates the calibration L.E.D. of each detector when activated by the calibration command generator of the data recording system. A positive going calibration command signal is sent back up the signal transit cable and its arrival at the signal amplifier output is sensed by the calibration pulse generator, which then drives the calibration L.E.D. with a constant current source. Negative going Cerenkov light signals from the detector are unaffected by the calibration pulse generator. The temperature stability of both the calibration pulse generator and the L.E.D. were tested and found to be excellent over the small range of temperatures encountered in the huts in which the detectors are mounted.

The photomultipliers are powered by stabilized negative E.H.T. supplies with a current capability of 8 mA, and Harwell 95 Series L.T. units power the signal amplifiers and calibration pulse generators.

3.2.iv The Signal Delays

It is necessary to delay the signals from the Cerenkov light detectors to allow time for the 150 m particle detector trigger to be generated and relayed to the data recording station, and also to adjust the arrival time of the light signals to suit the requirements of the recording system. (These requirements are determined mainly by the recording oscilloscope timebase sweep speeds.) The length of the signal delay in each channel varies between 2.3 μs and 3.0 μs and comprises mainly the signal transit cable that conveys the signals from the detector to the data recording station, plus the additional signal display delay. For all this delay either Aerialite type 4305 or type 4303 high quality relay cable is used.

* * *

The bandwidths of the signal delays were tested by passing a series of pulses, of shape similar to that of atmospheric Cerenkov light signals, along the cables and noting the effect on various pulse shape parameters. The delay cables of all channels were found to have essentially the same bandwidth and fig.3.6 shows how the rise-time (10% - 90%), the fall-time (90% - 50%) and the full-width-half-maximum of the test pulses were affected by the cables. It is seen that even the fastest pulses achieved with the type 4522 photomultipliers will be only very slightly distorted by the signal cables.

* * *

The bandwidths of the complete signal channels could be conveniently checked with the type N.E. 130 radio-active light sources, permanently mounted on the photomultiplier faces. The delta-function light outputs produced by the light sources were passed through the complete system and observed on the recording oscilloscopes. The pulses seen all had full-width-half-maxima in the range 17 to 19 ns, and rise-times between 8 and 10 ns, indicating the fastest signals to which the system would usefully respond, and confirming that the channel bandwidths were all essentially the same.

3.2.v The Data Recording System

The data recording system records the Cerenkov light signals detected in the air showers selected by the 150 m particle detector trigger, by photographing oscilloscope displays. It also automatically calibrates the system, controls the operating periods of the equipment and monitors the night sky conditions.

Dealing first with the signal paths, a Cerenkov light pulse proceeds from the signal transit cable, through the display delay and arrives at the signal interface, where it is interrogated for dynamic

Figure 3.6. The effect of the signal delay cables on test pulses of shape similar to that of atmospheric Cerenkov light signals. The pulse shape parameters considered are:-

(a) the rise-time (10% - 90%)

(b) the fall-time (90% - 10%)

(c) the full-width-half-maximum.

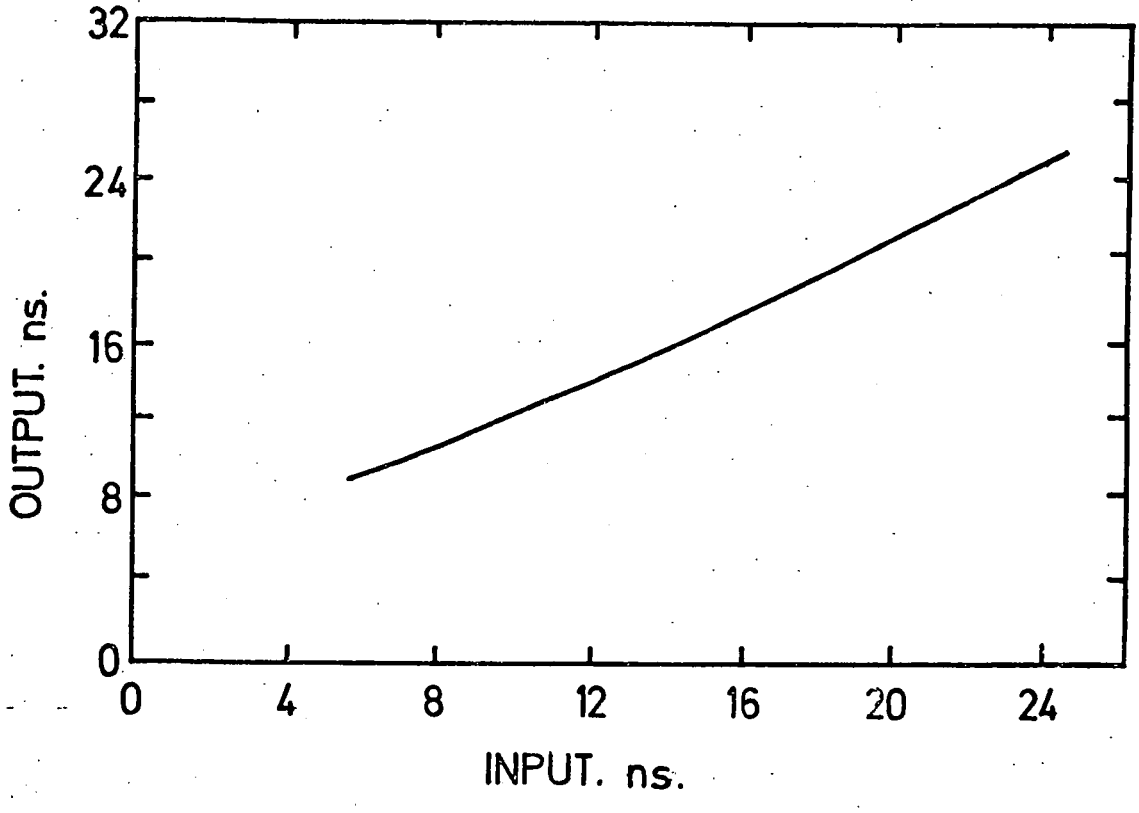

(a) PULSE RISE-TIME (10% - 90%).

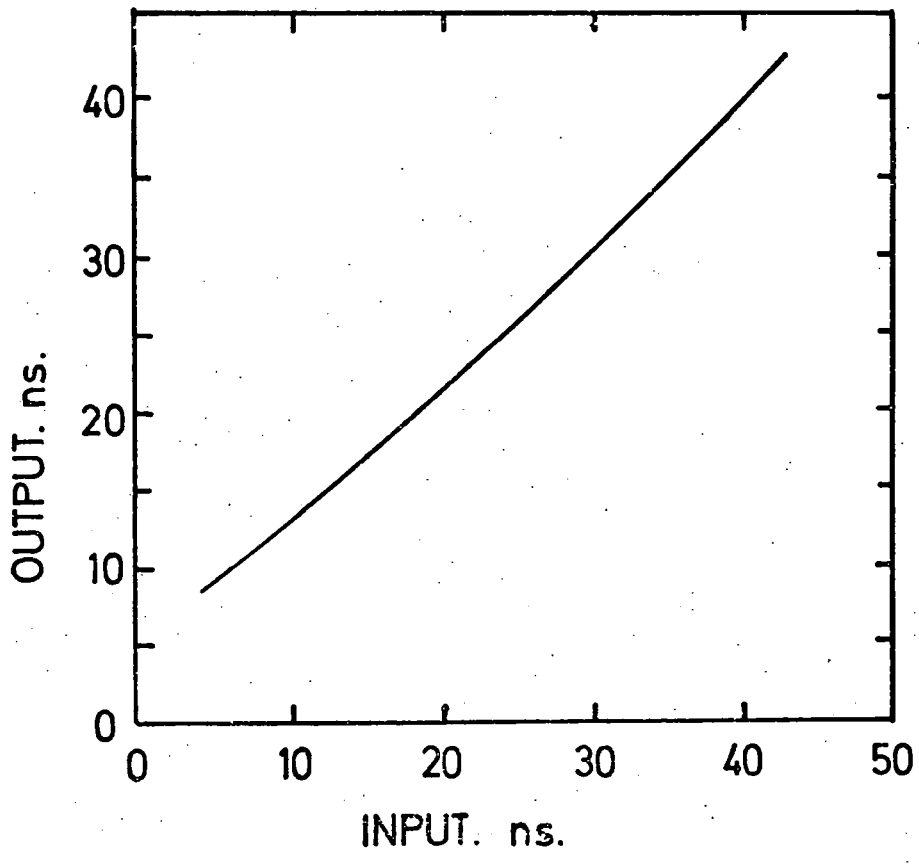

(b) PULSE FALL-TIME (90% - 10%).

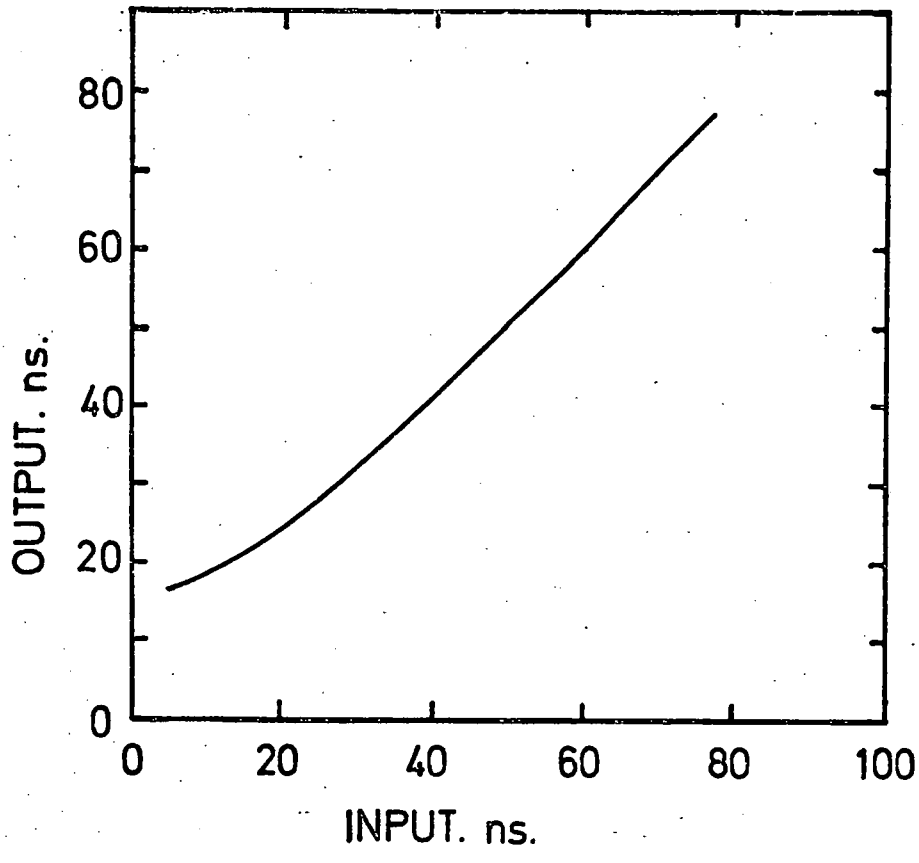

(c) PULSE FULL-WIDTH-HALF-MAXIMUM.

range purposes. A fast discriminator monitors the signal amplitude and on the arrival of a pulse too large for the oscilloscope Y-gain, switches on a 10 db attenuator connected in the signal line at the input of the recording oscilloscope. The signal passes through the attenuator delay cable, a nominal 100 ns of type U.R. 203 cable, to allow for the switching time of the attenuator, and arrives at the input of the recording oscilloscope. When the signal attenuator is activated by the pulse of a recorded event, i.e. in coincidence with the 150 m particle detector trigger that is fed to the signal interface, an L.E.D. in the camera field of view is illuminated to indicate that the recorded pulse has been attenuated.

* * *

Three recording oscilloscopes are used in all; two Tektronix type 7403, each with dual input amplifiers, and a Tektronix type 556 double beam, with two dual input amplifiers. Signals from two detectors are displayed on each oscilloscope trace and are distinguished by inverting one of each pair. The signals from the more centrally located detectors are recorded using timebase sweep speeds of 100 ns div^{-1}, and those from the remaining detectors are displayed on 200 ns div^{-1} timebases, the longer sweeps accommodating the larger arrival time jitters of the more distant detector signals. A type P.11 blue phosphor C.R.T. is used in each oscilloscope to make the photographic writing speed as fast as possbile and all the oscilloscopes have a bandwidth of 50 MHz.

Pulses of amplitude 0.3 div on the oscilloscope screens are about the smallest measurable and so the use of the one stage signal attenuator gives a dynamic range of about 50:1 for the recording system. The gain of all the oscilloscope amplifiers is 50 mV div^{-1}, and is such that the lower end of the dynamic range approximately

corresponds to the amplitude of the smallest signals readily distinguished from the background noise of a typical clear night sky, after they have passed through the complete detector channels.

* * *

The gain of each detector channel, and the oscilloscope timebase sweep speeds, are automatically calibrated at half-hourly intervals during operating periods. The master clock in the data recording system activates the calibration command generator, which then sends the positive going calibration command pulses, via the signal interfaces, back up the signal transit cables to each of the detectors. The calibration L.E.D.s of the detectors are illuminated, and the trigger distributor is informed at the appropriate instant, so that the calibration signals are recorded. The gains of the detectors can be calculated from the amplitudes of the "artificial" light pulses registered in such a "calibration event".

For the calibration of the recording oscilloscope timebase velocities, the z-blanking unit is also triggered by the calibration command generator. A series of avalanche transistors is used to produce a very short, high voltage spike, which is bounced down a fixed length of Aerialite type 4301 relay cable, the z-blanking delay (ii). The period between the initial voltage spike and its echo provides a constant time interval standard. The two voltage spikes are fed to the z-modulation inputs of the recording oscilloscopes and produce timing markers on the oscilloscope traces of the calibration events. The z-blanking delay (i), between the calibration command generator and the z-blanking unit, is included so that the first z-blank occurs just after the start of the timebase sweeps. The length of the time interval determining z-blanking delay (ii) is such that

Figure 3.7. Examples of the film records.

(a) The atmospheric Cerenkov light pulses registered in a shower selected by the Haverah Park particle detector array. The light detectors producing each of the signals are identified.

detector 12 detector 22

detector 24 detector 23

detector 5 detector 3

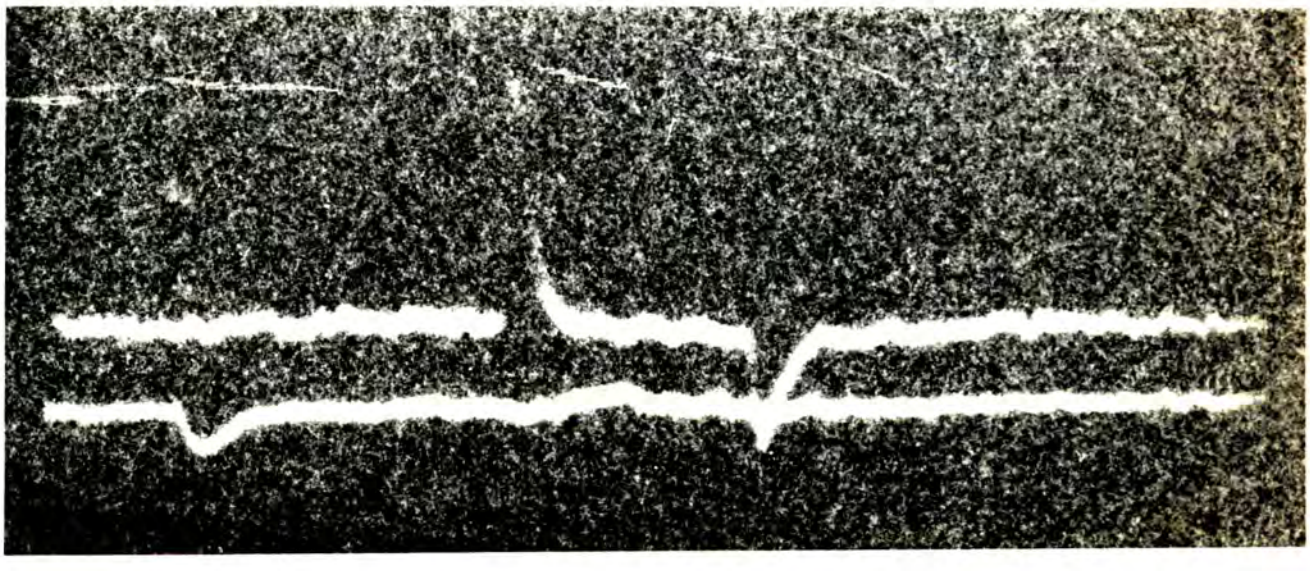

detector 2

(b) The "artificial" light pulses registered in a calibration event. The amplitudes of the pulses indicate the channel gains, and the z-blanks are timing markers for checking the oscilloscope timebase velocities.

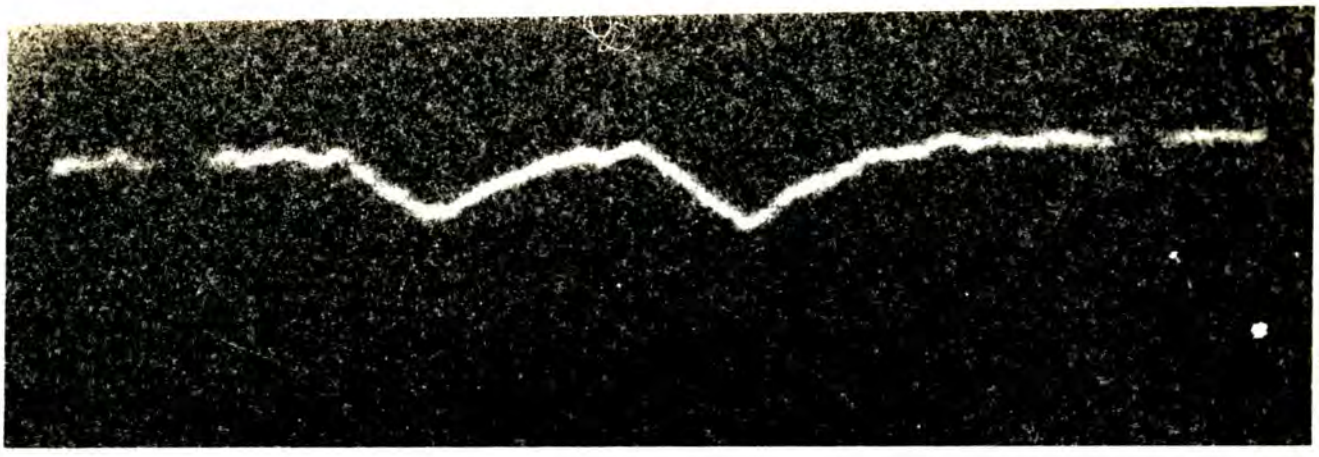

detector 12 detector 22

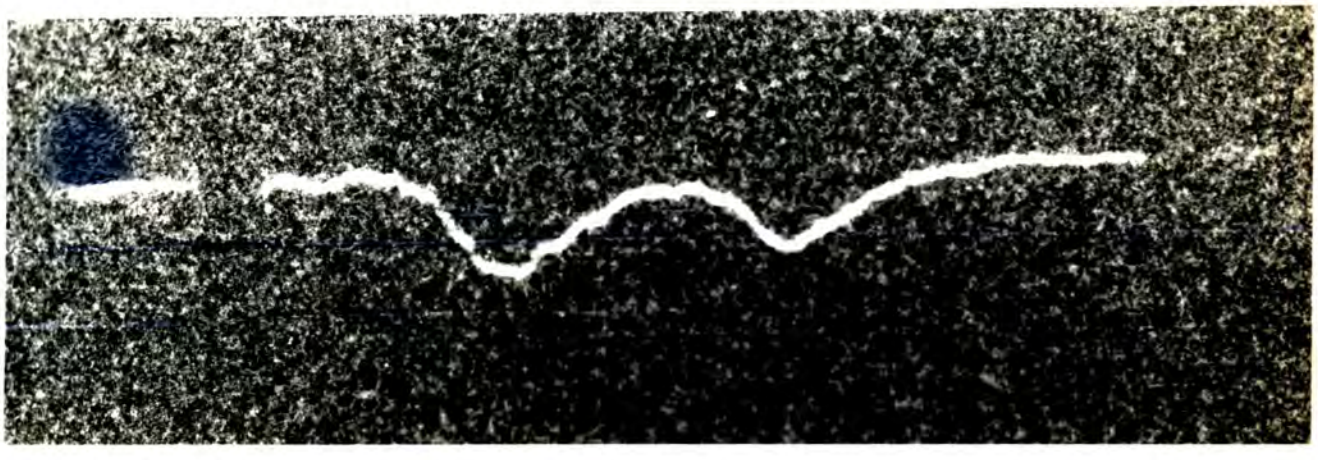

detector 24 detector 23

detector 3 detector 5

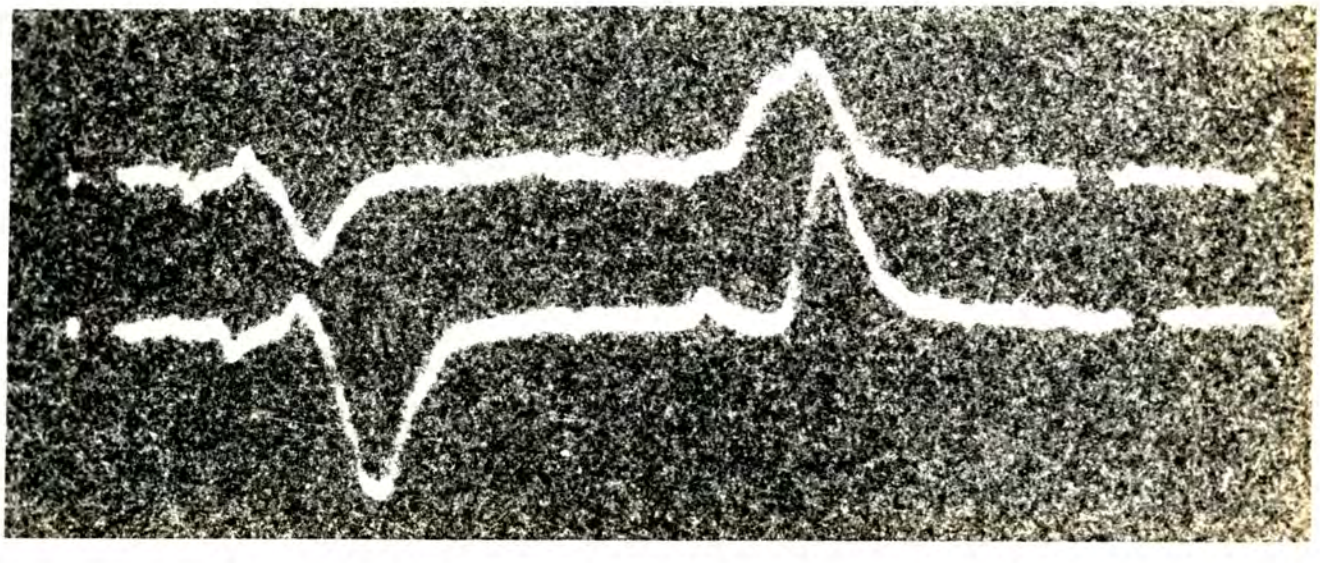

detector 2 detector 4

the second z-blank occurs just before the end of the sweeps.

* * *

The recording oscilloscopes are automatically photographed after each shower with Shackman type AC2/25 35 mm cameras fitted with f1.9 lenses. Kodak type 2485 high speed recording film is used, and with the type P.11 phosphor oscilloscope screens, a photographic writing speed of about 140 cm μs^{-1} is achieved. This is sufficient to show up the details of all but the very largest and fastest Cerenkov light pulses observed. A Haverah Park half-minute solar time register is illuminated in the field of view of each camera, immediately after each shower, before the film is advanced. A 7-segment L.E.D. display indicates which type of shower has occurred (either a 150 m event, a 500 m event or a calibration event). Examples of the film records of the light signals recorded in real showers, and in calibration events, are shown in fig.3.7.

* * *

Sky clarity is monitored by taking half-hour photographic exposures of the night sky with the sky camera, which views the zenith and has a field of view of about 40^{o}. It too is fitted with a Haverah Park solar time register, which is illuminated at the end of each exposure, allowing those showers recorded during clear periods (i.e. when star trails are visible) to be selected. Utmost care is taken in the selection of showers. The only ones considered for analysis are those recorded during clear periods of at least one hour duration when tracks of stars down to 7th order magnitude are visible. Showers recorded in misty conditions when a few stars may still be visible are not accepted. Fig.3.8 shows examples of the sky pictures obtained during acceptable and unacceptable weather conditions.

* * *

Figure 3.8. Examples of the time elapsed photographs of the night sky, illustrating:-

(a) Acceptably clear conditions.

(b) Unacceptably misty conditions, although a few star-trails are still visible.

The operation times of the light detectors and the data recording system are controlled by the master clock, which is programmed for periods of moonless astronomical darkness. During these periods the clock activates the command control and causes E.H.T. to be applied to the photomultipliers. The command control also gates the trigger distributor so that the recording system receives particle detector triggers only when the light detectors are operating. As a safety precaution, the sky sensor, which uses a photo-resistor located under the window of detector 12, overrides the master clock and turns off the detectors if the sky brightness exceeds a prescribed level.

3.3 The Performance of the Cerenkov Light Detection Equipment

The atmospheric Cerenkov light detection equipment described in the previous section has operated at the Haverah Park air shower array throughout the U.K. winter of 1975/76. Its performance during this period is now assessed. Described first is the use of the calibration facilities of the equipment, to interrelate the performances of the individual light detectors, and to account for slow variations of the characteristics of the system during the operating season. Then the duty cycle of the experiment is discussed and the way in which the gathered data were measured is described.

3.3.i Gain Calibration

In order to compare the amounts of Cerenkov light recorded by different detectors it is necessary to know the gains of the complete detector channels, at least relatively, and for some purposes absolutely, in terms of numbers of photons incident on the photocathodes.

The measurement of the relative gains of the complete detector channels was tackled in two stages. Firstly, the gain of each

individual complete channel was monitored throughout the operating season by the half-hourly L.E.D. calibrations. Changes in either photomultiplier gain, signal amplifier gain or oscilloscope Y-amplifier gain altered the amplitude of the calibration signals.

Then, on particular clear nights during the operating season, the half-hourly L.E.D. calibrations of the detectors were interrelated, to enable the gains of the various channels to be compared. A light source was taken to each detector in turn and positioned on the photomultiplier in a repeatable way such that the whole of the photocathode was illuminated. The amplitudes of the pulses produced by this light source, as well as those of the half-hourly L.E.D. calibration pulses, were measured on these nights. Interrelating the half-hourly L.E.D. calibrations of the individual detectors in this way, enabled the gain of any one detector channel, at any time during the operating season, to be compared with that of any other channel, at any other time, with an accuracy better than $\pm$5%.

The amplitudes of the signals from the type N.E. 130 radio-active light sources permanently mounted on the photomultiplier faces were also measured at various times during the operating season and used to confirm the L.E.D. gain calibration.

An attempt to measure absolutely the response of the detectors to a photon flux was made by relating the signals from each detector to the light output of one particular type N.E. 130 radio-active light source. The light pulse of this source was estimated by Hartman and Weekes (1976) to be 1725 $\pm$ 350 photons. The estimate of the absolute response of the detectors so obtained, was thus accurate to within $\pm$20%. In the following Chapters, the results of the present work are presented in terms of this absolute calibration. Of course, the precision with which photon density measurements made with different

detectors at different times are interrelated, does not depend on the absolute calibration. The relative calibration of the detectors is known to within ±5%.

* * *

The gain calibration showed that no gain changes occurred in any channel during the course of any one clear night. However, gains did vary from night to night and the photomultipliers showed an ageing effect during the course of the winter; their gains falling steadily by as much as a factor of two in some cases. This was thought to be due to bleaching of the photocathodes by sunlight during the day. Fig.3.9 shows the gain decrease of the most and least affected channels.

3.3.ii Timing Calibration

In order to measure the arrival time of the Cerenkov photons at one detector with respect to the arrival time of those at another, it is necessary to know the total delay in the signal path of the one channel - from the photons striking the photomultiplier to the appearance of the pulse on the recording oscilloscope timebase - relative to that of the other channel. To measure this, the delay through the signal transit cables and signal display delay cables must be taken into account, as well as the delay thrcugh the photomultipliers and signal amplifiers. The attenuator delay cable and other connecting leads in the data recording station will also contribute to the total signal delay. The velocity and linearity of the recording oscilloscope timebases, and the differences in the triggering time of each oscilloscope, must also be considered.

The delay of all cables in the signal path between the signal amplifier output and the oscilloscope input of one channel, was compared with that of another channel by simultaneously bouncing a pulse down the two cables and noting the time difference in the

Figure 3.9. Detector gain measurents made on clear nights, showing the gradual decrease in gains during the 1975/76 operation period. This was thought to be caused by sunlight bleaching the photocathodes during the day. The measurements shown are for the least and most affected detectors.

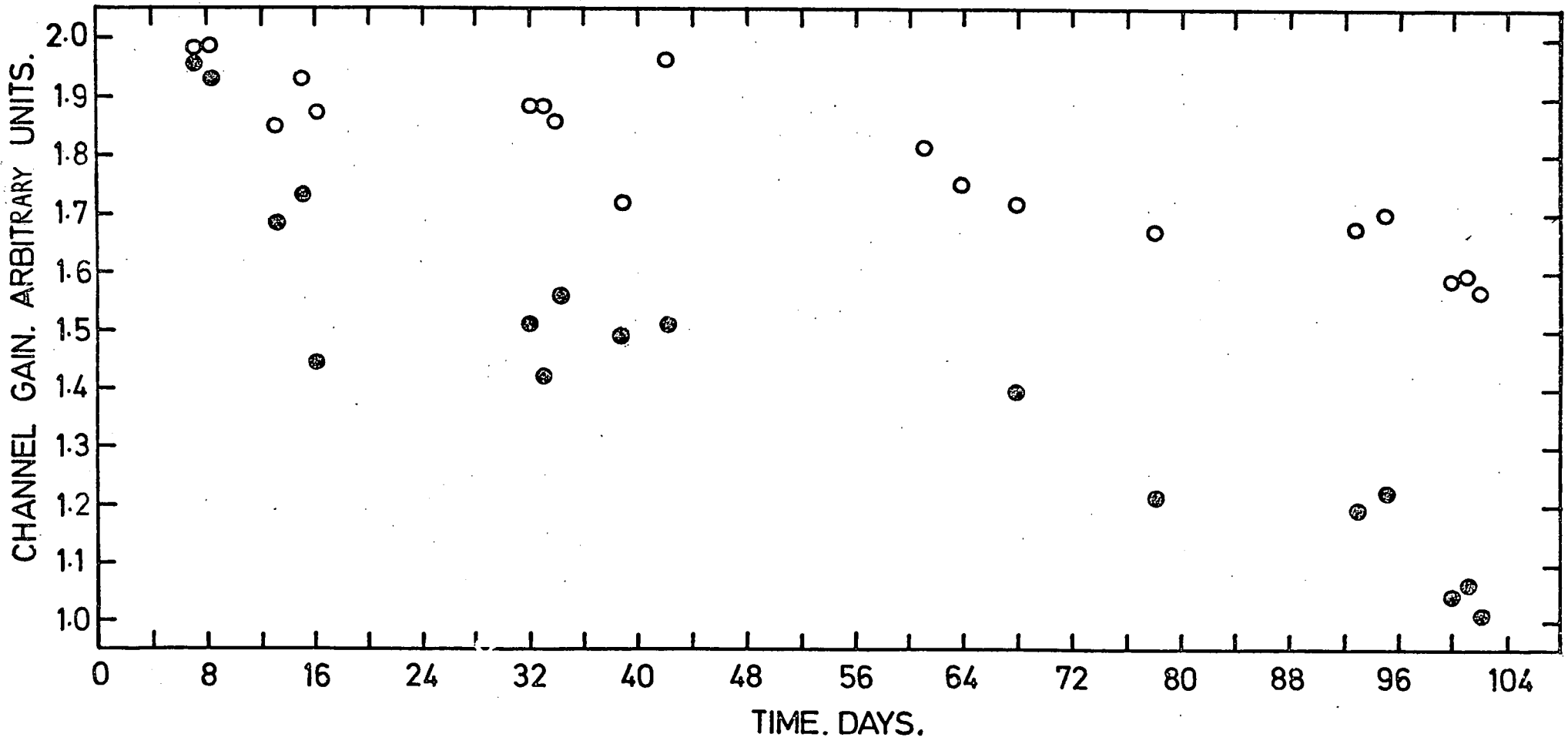
CHANNEL GAIN. ARBITRARY UNITS.
2·0
1·9
1·8
1·7
1·6
1·5
1·4
1·3
1·2
1·1
1·0
0
8
16
24
32
40
48
56
64
72
80
88
96
104
TIME. DAYS.

return of the echoes. Relative cable delays were found to better than $\pm$2 ns in this way.

The delay of each photomultiplier and signal amplifier was measured absolutely to better than $\pm$5 ns. This contributed typically 120 ns to the total signal delay, about 90 ns of which was the transit time through the photomultiplier.

Allowances for differences in the times taken for each recording oscilloscope to trigger were made by using the first z-blanks of calibration events as real-time coincidence markers. The time interval between the start of the timebase of a particular oscilloscope and the first blank, was subtracted from the time along the timebase of Cerenkov light pulses displayed on that oscilloscope. Delays of the light pulses from a well defined point in time were thus obtained.

Measurements of the recording oscilloscope timebase velocities made with the z-blanking unit every half-hour, showed that all sweep speeds remained constant to within the measuring accuracy of 1 ns div^{-1} during any one night. However, variations between nights were revealed and these were taken into account in the calculation of Cerenkov light pulse arrival times.

Non-linearity of the recording oscilloscope timebases was also considered in the calculation of light pulse arrival times. The timebase linearities were measured occasionally during the operating season using a crystal ocsillator. No evidence that they varied was seen.

By allowing for the above factors, the relative arrival time of the light pulses of a shower, could be found with a precision of $\pm$7 ns. It was convenient to relate all arrival times to that of the light pulse from detector 12, since there is always a signal recorded by this detector because it is located centrally in the array.

3.3.iii The Duty Cycle of the Experiment

The requirement of cloudless and moonless nights makes operating atmospheric Cerenkov light detection equipment in the U.K. worthwhile only during winter months, when the longest nights occur. The present system has run at Haverah Park for a period of 100 days between 25th November, 1975 and 6th March, 1976. During this operating season, 23 acceptably clear nights occurred and the equipment was operative on 20 of these, providing data from 70 hours running time. (Expressed as a fraction of a whole year, the running time efficiency was about 1% of a year.)

A total of 68 500 m events, together with a further 584 150 m events were recorded during the periods of acceptable sky conditions, and fig.3.10 shows a histogram of the number of atmospheric Cerenkov light signals registered in each of the showers. The light signals recorded in all of the 500 m events were measured, since shower analyses on the basis of particle detector measurements were available for these showers. However, of the 584 150 m events, only 255, in which four or more Cerenkov light signals had been recorded, were selected for study, since at least four detector signals are required for any sort of shower analysis on the basis of the Cerenkov light information alone.

3.3.iv The Measurement of the Recorded Cerenkov Light Signals

The photographic records of those events selected for analysis were printed to an enlargement of nominally twice life size and measured manually with a transparent graph paper overlay. The exact magnification of the print was determined from the sizes of the oscilloscope graticules, which were photographed at the beginning and end of each film. For each light pulse examined, the parameters measured were the pulse amplitude, and the positions along the time-

Figure 3.10. Histogram showing the number of measurable Cerenkov light signals registered in each shower recorded.

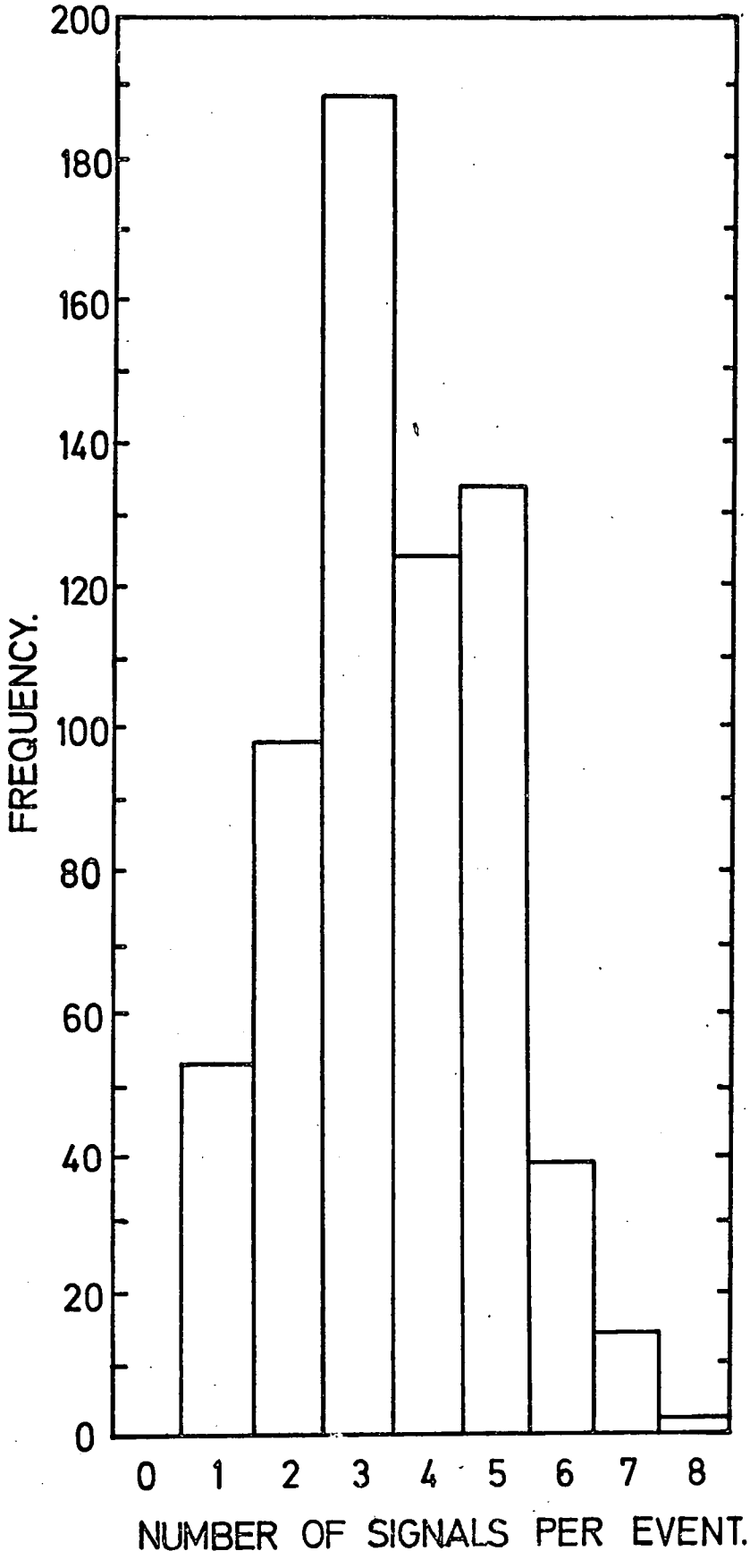
200
180
160
140
120
100
80
60
40
20
0
FREQUENCY.
0 1 2 3 4 5 6 7 8
NUMBER OF SIGNALS PER EVENT.

base at which the pulse reached 10%, 50% and 90% of its amplitude, on both the rising and falling edges of the pulse (refer to fig.3.11). From these measurements were determined:-

(i) The light pulse rise-time (10% up - 90% up)

(ii) The light pulse top-time (90% up - 90% down)

(iii) The light pulse full-width-half-maximum (50% up - 50% down)

(iv) The light pulse fall-time (90% down - 50% down)

(v) The light pulse area, by the use of a trapezoidal fit to the measured points.

(vi) The light pulse arrival time, determined from the time between the start of the timebase and the 10% point on the pulse leading edge.

(The light pulse fall-time, from 90% to 10% of the full amplitude on the falling edge, was not determined because it was found too difficult to reliably measure the 10% point in the presence of background noise.)

For the case of a calibration event, the parameters measured were the calibration pulse amplitudes, which allowed the complete channel gains to be checked, and the times between the z-blanks, which checked the oscilloscope timebase velocities. The times between the timebase starts and the first z-blanks, which were used to allow for the triggering times of the oscilloscopes in the calculation of the arrival times of the light pulses in real showers (as discussed in section 3.3.ii), were also measured.

Measurements could be made to within 0.5 mm on the prints, corresponding to timing accuracies of better than 2.5 ns for light pulses displayed on the type 7403 recording oscilloscopes, and better than 5.0 ns for those appearing on the type 556 oscilloscope.

Figure 3.11. Measuring the recorded light signals.

(a) The measured parameters of each Cerenkov light pulse.

(b) The measured calibration pulse parameters.

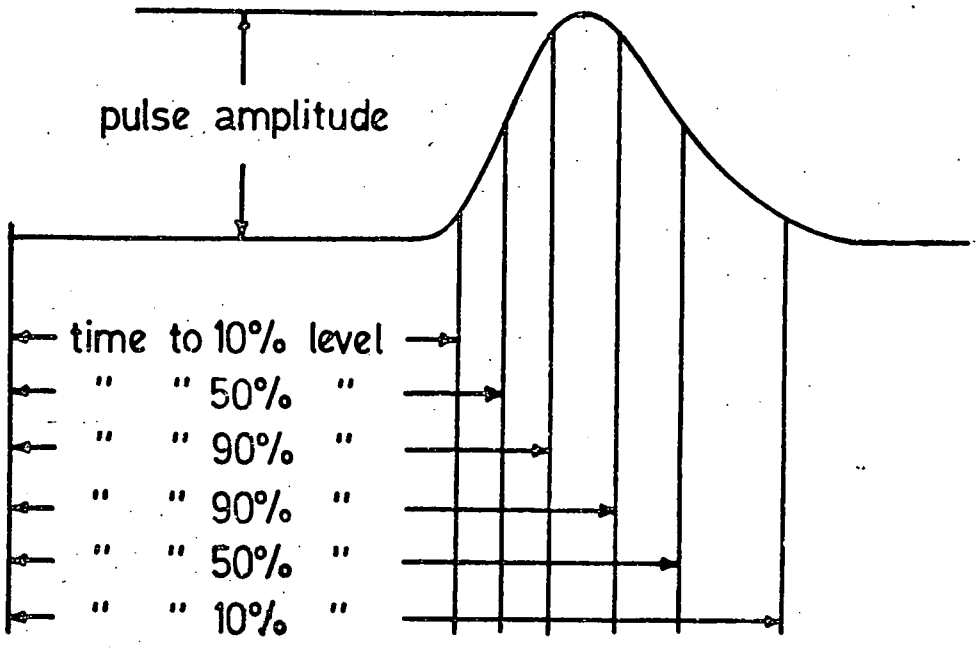
pulse amplitude
time to 10% level
" " 50% "
" " 90% "
" " 90% "
" " 50% "
" " 10% "

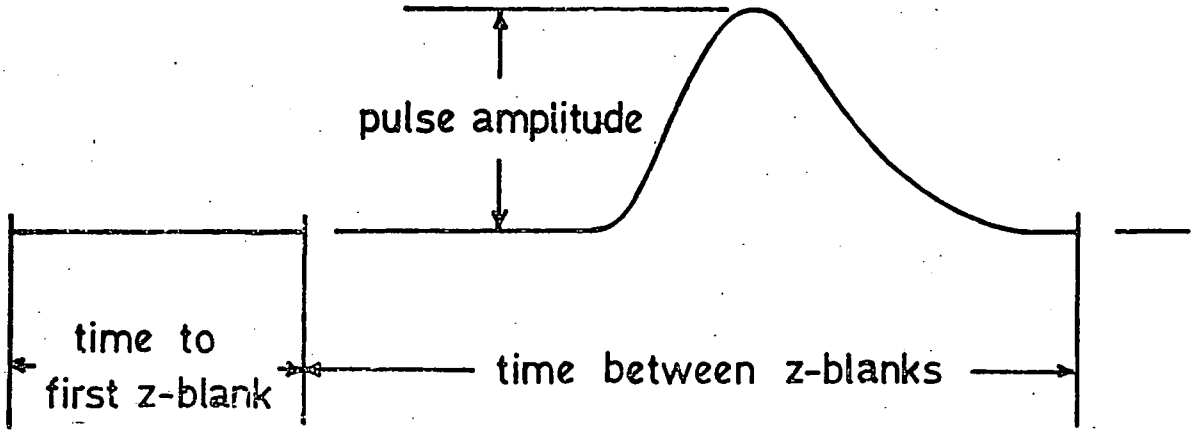
pulse amplitude
time to
first z-blank
time between z-blanks

Treatment of the data from the selected showers involved the measurement of more than 1500 light pulses. These measurements, and the further processing of the numbers obtained into computer compatible form, were handled on a "production line" basis to minimise the time spent on this part of the data analysis.

3.4 Conclusions

An array of widely spaced atmospheric Cerenkov light detectors and an analogue data recording system have been constructed and calibrated at the Haverah Park air shower array. Three independent sets of information about the Cerenkov light in each extensive air shower recorded, are obtained with the equipment:-

(i) The density of Cerenkov photons is sampled at different positions in the shower by measuring the areas of the light pulses registered by the detectors. The signal strength at each detector is interrelated with an accuracy of better than 5%, and the response of the detectors to a photon flux is known to within 20%.

(ii) Measurements are made of the temporal characteristics (the rise-time, top-time, fall-time, and full width-half-maximum) of the Cerenkov light pulses registered by the detectors. The equipment faithfully responds to light pulses with rise-times as short as 10 ns and full-width-half-maxima down to 18 ns. Each pulse shape parameter is measured with a precision of better than 5 ns.

(iii) Measurements of the positions of the light pulses along the recording oscilloscope timebases are made, and these lead to the calculation of the relative arrival times of the Cerenkov light front at the various detector positions. The timing measurements are made to within 7 ns.

The accuracy with which the various Cerenkov light parameters can be measured is not limited by any single part of the system; each section of the equipment being similarly matched in this respect.

The 1% duty cycle of the experiment in the unfavourable climate that occurs at Haverah Park is very low. Nevertheless, 100 winter nights operation have produced a worthwhile sample of data. Cerenkov light measurements have been made in 68 500 m events, for which shower analyses based on the Haverah Park particle detector measurements are available. Measurements have also been made in many more 150 m events, for about half of which, four or more light signals were recorded, making analyses on the basis of Cerenkov light data alone feasible.

CHAPTER FOUR

MEASUREMENTS OF THE AVERAGE CHARACTERISTICS OF ATMOSPHERIC CERENKOV LIGHT IN AIR SHOWERS

The average features of the Cerenkov light signals measured in the present work are reported in this Chapter. Data recorded in those extensive air showers registered by the Haverah Park 500 m array are considered here, since information on the arrival direction, core location and primary particle energy of each of these showers is available, from analyses of the deep water particle detector data by the University of Leeds group.

The features of the lateral Cerenkov light distribution and of the various light pulse shape parameters are each considered in turn. Dependences of each of these parameters on shower energy and inclination from the zenith are determined. Then, changes in shower energy and in shower zenith angle are related to changes in depth of shower cascade development maximum, in an attempt to quantify the sensitivity of the Cerenkov light parameters to depth of shower cascade maximum. A Cerenkov light measure of primary particle energy is identified, and finally, the curvature of the Cerenkov light front in extensive air showers is examined.

4.1 Data Handling

All of the measured Cerenkov light parameters vary with core distance as well as with primary particle energy and shower inclination to the vertical. This must be taken into account when determining the dependences of the parameters on shower energy and inclination. The showers studied were divided into intervals of zenith angle and vertical equivalent value of the Haverah Park particle detector array parameter, $\rho(500)$. $(\rho(500)_{VE}$ is an established measure of primary particle energy that is customarily employed by all supporting experiments at Haverah Park. See, for example, Allan et al. (1971), Blake et al. (1973), Dixon

et al. (1974).) The intervals used were:-

Energy Ranges	Zenith Angle Ranges
$\rho(500)_{VE} < 0.3\ m^{-2}$	$0^o < \theta < 25^o$
$0.3 < \rho(500)_{VE} < 0.6\ m^{-2}$	$25^o < \theta < 35^o$
$0.6 < \rho(500)_{VE} < 1.25\ m^{-2}$	$35^o < \theta < 45^o$
$\rho(500)_{VE} > 1.25\ m^{-2}$	$45^o < \theta < 65^o$

Within each interval, the measured values of each of the Cerenkov light parameters in turn, were expressed as functions of core distance using least squares fits of appropriate expressions. Average values of each parameter at selected core distances between 100 and 500 m, were then derived from the fitted expressions. In this way, the dependence of each parameter on core distance was removed, enabling the variation of the parameters with shower energy and inclination to the zenith, to be studied.

Before the curve fitting, the photon density measurements in each interval were normalized to the average interval energy, on the assumption that the Cerenkov photon density increases linearly with primary particle energy. Also, allowance was made for the fact that the area of a detector photocathode exposed to the Cerenkov light flux in an inclined shower, is effectively less than the area exposed in a vertically incident shower.

In the case of measurements of the pulse shape parameters, no attempt was made to account for the effect of the bandwidth of the experimental equipment.

All measurements made by detectors situated closer than 70 m, or further than 600 m, from the shower core were not used and showers with poor particle detector data analyses (i.e. with goodness of fit, χ^2, greater than 1.50) were rejected.

A total of 226 sets of Cerenkov light pulse measurements were contained in the final data sample. These were spread evenly amongst the shower energy and inclination intervals, although rather few measurements were made in small, vertical showers or in highly inclined ones. The sample of data was small, but sufficient to give useful results on the average characteristics of the Cerenkov light in extensive air showers.

4.2 The Lateral Cerenkov Light Distribution

4.2.i The Variation of the Cerenkov Photon Density with Core Distance

The variation of the Cerenkov photon density with core distance is illustrated in fig.4.1. The individual photon density measurements made in showers of energies in the interval $0.3 < \rho(500)_{VE} < 0.6\ m^{-2}$, and incident at zenith angles in the interval $25^{o} < \theta < 35^{o}$, are shown. The measurements are well represented over the restricted range of core distances by a simple power law structure function.

Power law structure functions were fitted to the photon density measurements made in the showers of each of the energy and zenith angle intervals. Over the range of core distances at which measurements were made, the light intensity, Φ, decreases with distance from the shower core, r, according to:-

$$\Phi(r) \propto r^{-\gamma} \qquad \ldots \text{ equ.4.1}$$

The structure function exponent, γ, is a constant particular to the showers in each interval. (The correlation coefficients of the fits of the power laws were all greater than 0.75, indicating critical significances less than 0.5%.)

Each measured lateral Cerenkov light distribution is completely defined by stating the value of the photon density at one core distance, as well as the value of the exponent of the power law structure function. The values of $\Phi(200)$, the photon density at 200 m core distance, and

Figure 4.1. Individual Cerenkov photon density measurements made in showers of energies in the interval $0.3 < \rho(500)_{VE} < 0.6\ m^{-2}$, and incident at zenith angles in the interval $25^{o} < \theta < 35^{o}$. The measurements are shown here as an illustration of the shape of the lateral Cerenkov light distribution.

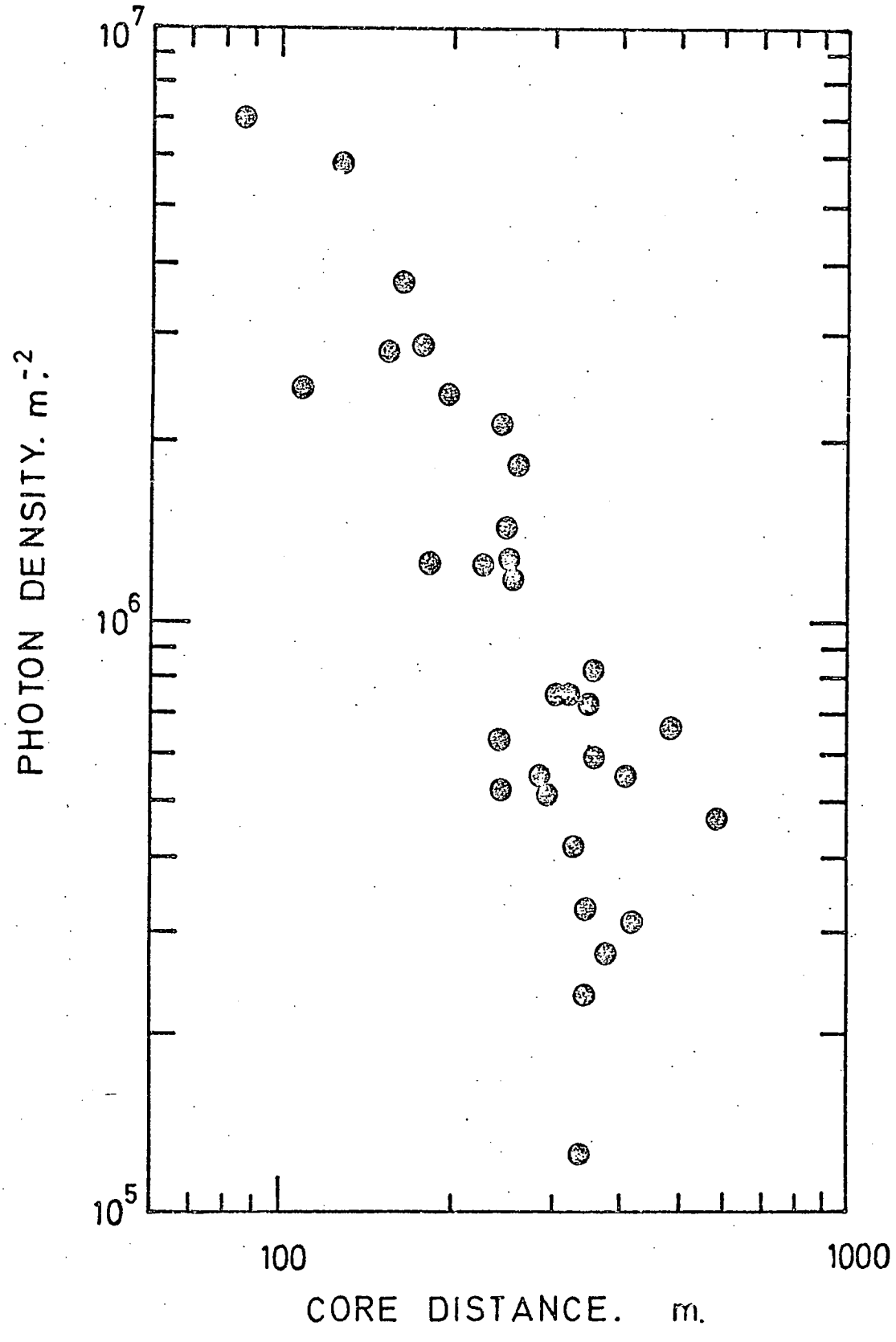
10^7
10^6
10^5
PHOTON DENSITY. m^{-2}
100
1000
CORE DISTANCE. m.

Table 4.1. Measurements of the lateral Cerenkov light distribution. The average features of the light distribution have been determined by fitting power law structute functions to the photon density measurements made in showers of various energies and incident at various zenith angles. Shown here are:

(a) The average values of $\phi(200)$, the Cerenkov photon density at 200 m core distance.

(b) The average values of γ, the structure function exponent.

Shower Zenith Angle	Primary Particle Energy			
	$\rho(500)_{VE} < 0.3$ m^{-2}	$0.3 < \rho(500)_{VE} < 0.6$ m^{-2}	$0.6 < \rho(500)_{VE} < 1.25$ m^{-2}	$\rho(500)_{VE} > 1.25$ m^{-2}
$0^{o} < \theta < 25^{o}$		$1.45 \pm 0.43 \times 10^{6}$ m^{-2}	$4.30 \pm 0.98 \times 10^{6}$ m^{-2}	$11.44 \pm 1.52 \times 10^{6}$ m^{-2}
$25^{o} < \theta < 35^{o}$	$0.87 \pm 0.11 \times 10^{6}$ m^{-2}	$1.74 \pm 0.30 \times 10^{6}$ m^{-2}	$1.93 \pm 0.71 \times 10^{6}$ m^{-2}	$7.44 \pm 3.60 \times 10^{6}$ m^{-2}
$35^{o} < \theta < 45^{o}$	$0.85 \pm 0.13 \times 10^{6}$ m^{-2}	$1.59 \pm 0.21 \times 10^{6}$ m^{-2}	$2.98 \pm 0.90 \times 10^{6}$ m^{-2}	
$45^{o} < \theta < 65^{o}$		$1.48 \pm 0.79 \times 10^{6}$ m^{-2}		

Table 4.1(a). Average values of $\Phi(200)$, the Cerenkov photon density at 200 m core distance. (The units are photons m^{-2}.)

Shower Zenith Angle	Primary Particle Energy			
	$\rho(500)_{VE} < 0.3\ m^{-2}$	$0.3 < \rho(500)_{VE} < 0.6\ m^{-2}$	$0.6 < \rho(500)_{VE} < 1.25\ m^{-2}$	$\rho(500)_{VE} > 1.25\ m^{-2}$
$0^o < \theta < 25^o$		1.91 ± 0.15	2.10 ± 0.13	2.28 ± 0.06
$25^o < \theta < 35^o$	1.67 ± 0.09	1.85 ± 0.07	1.89 ± 0.07	1.93 ± 0.14
$35^o < \theta < 45^o$	1.55 ± 0.10	1.21 ± 0.03	1.69 ± 0.10	
$45^o < \theta < 65^o$		1.00 ± 0.17		

Table 4.1(b). Average values of γ, the structure function exponent.

the values of γ, the structure function exponent, which together represent the data of each shower energy and zenith angle interval, are given in tables 4.1(a) and (b). The standard errors on these quantities are also given. (As explained in the previous Chapter, the photon calibration used in the present work is accurate only to within 20%, but the light fluxes measured in the showers of each interval are related to one another with an uncertainty of less than 5%.)

The trends of the values in table 4.1 indicate that the lateral Cerenkov light distribution is sensitive to both shower energy and shower inclination to the zenith. The values of the structure function exponent are seen to decrease with decreasing shower energy and with increasing shower zenith angle, showing that the light in smaller showers, and in more inclined showers, is more laterally spread out. In contrast, the value of the photon density at a core distance of 200 m, is seen to be substantially independent of shower inclination and to vary only with shower energy. These characteristics are now examined more closely.

4.2.ii The Sensitivity of the Lateral Cerenkov Light Distribution to Shower Energy and Zenith Angle

The dependance of the lateral Cerenkov light distribution on shower energy is illustrated in fig.4.2(a). The power law structure functions fitted to the photon density measurements made in showers arriving at zenith angles in the interval $25^{o} < \theta < 35^{o}$ are shown, for four different energy intervals that span about one decade. The value of the structure function exponent of each of the fitted expressions is shown and the spread of the individual photon density measurements is indicated by the error bars, which show the standard errors on the fitted photon density values. Besides the fact that

Figure 4.2. The dependence of the lateral Cerenkov light distribution on shower energy.

(a) The power law structure functions fitted to the photon density measurements made in showers incident at zenith angles in the interval $25^{o} < \theta < 35^{o}$, for four intervals of shower energy.

(b) The variation of the structure function exponent with shower energy.

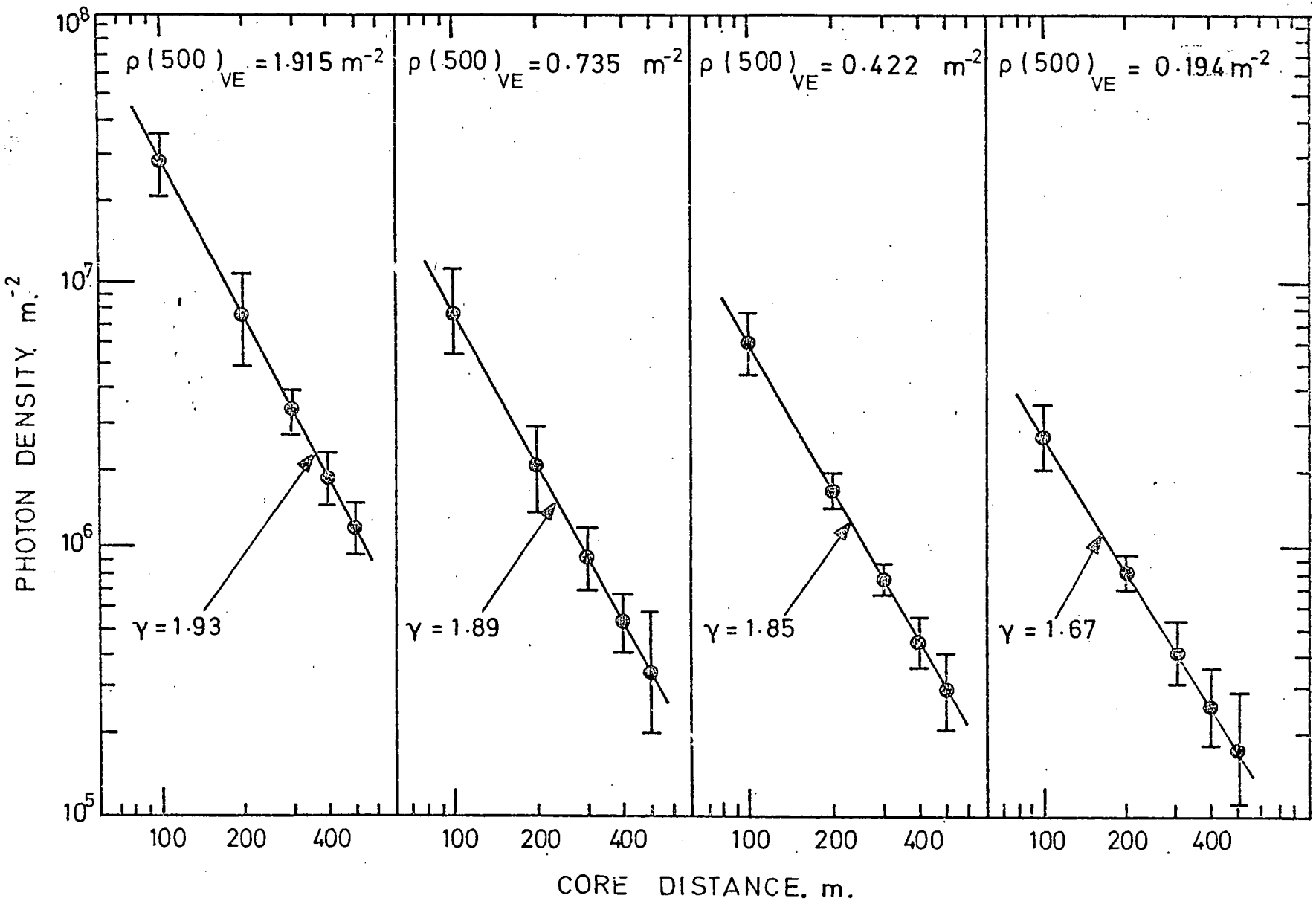
ρ (500)VE = 1·915 m-2
ρ (500)VE = 0·735 m-2
ρ (500)VE = 0·422 m-2
ρ (500)VE = 0·194 m-2
γ = 1·93
γ = 1·89
γ = 1·85
γ = 1·67
PHOTON DENSITY m.-2
CORE DISTANCE. m.
10^8
10^7
10^6
10^5
100
200
400

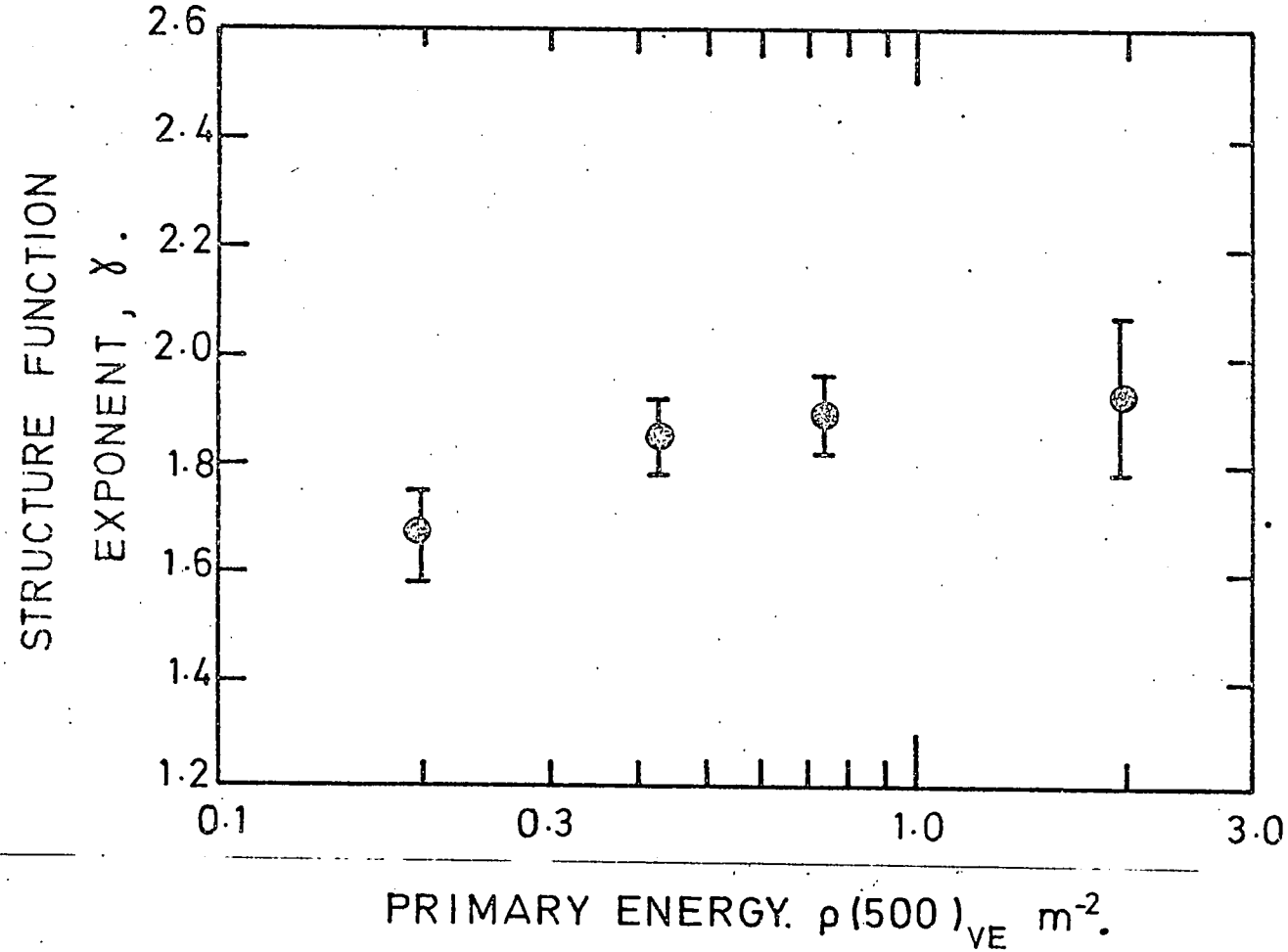
STRUCTURE FUNCTION
EXPONENT, γ.
2·6
2·4
2·2
2·0
1·8
1·6
1·4
1·2
0·1
0·3
1·0
3·0
PRIMARY ENERGY. ρ(500)VE m-2.

there is more light in higher energy showers, it is again seen that the value of γ, the structure function exponent, decreases with diminishing value of $\rho(500)_{VE}$. The lateral spread of the Cerenkov light is broader in showers of lower primary particle energy.

The variation of the structure function exponent with primary particle energy is shown more clearly in fig.4.2(b). Here, values of γ are plotted as a function of $\rho(500)_{VE}$. The small number of data points tentatively suggest that the value of the structure function exponent increases as the logarithm of primary particle energy, at least over the decade of energy in which the data were measured.

* * *

In a similar manner, the dependence of the lateral Cerenkov light distribution on shower zenith angle is illustrated in fig.4.3(a). The lateral spread of the light in showers of energies in the interval $0.3 < \rho(500)_{VE} < 0.6\ m^{-2}$ is shown, for four different zenith angle intervals. It is seen that the light spread is broader in the more inclined showers; the value of γ, the exponent of the fitted power law structure functions, decreasing with increasing shower zenith angle.

Values of the structure function exponent are plotted as a function of $\cos\theta$ in fig.4.3(b). The small number of data points suggest that the variation of the structure function exponent with shower zenith angle may be reasonably well represented by a dependence proportional to $\cos\theta$.

Returning to fig.4.3(a), the insensitivity of the photon density at 200 m core distance, to shower zenith angle, is also seen. Consequences of this are dealt with in section 4.6.

Figure 4.3. The dependence of the lateral Cerenkov light distribution on shower zenith angle.

(a) The power law structure functions fitted to the photon density measurements made in showers of energies in the interval $0.3 < \rho(500)_{VE} < 0.6\ m^{-2}$, for four zenith angle intervals.

(b) The variation of the structure function exponent with zenith angle.

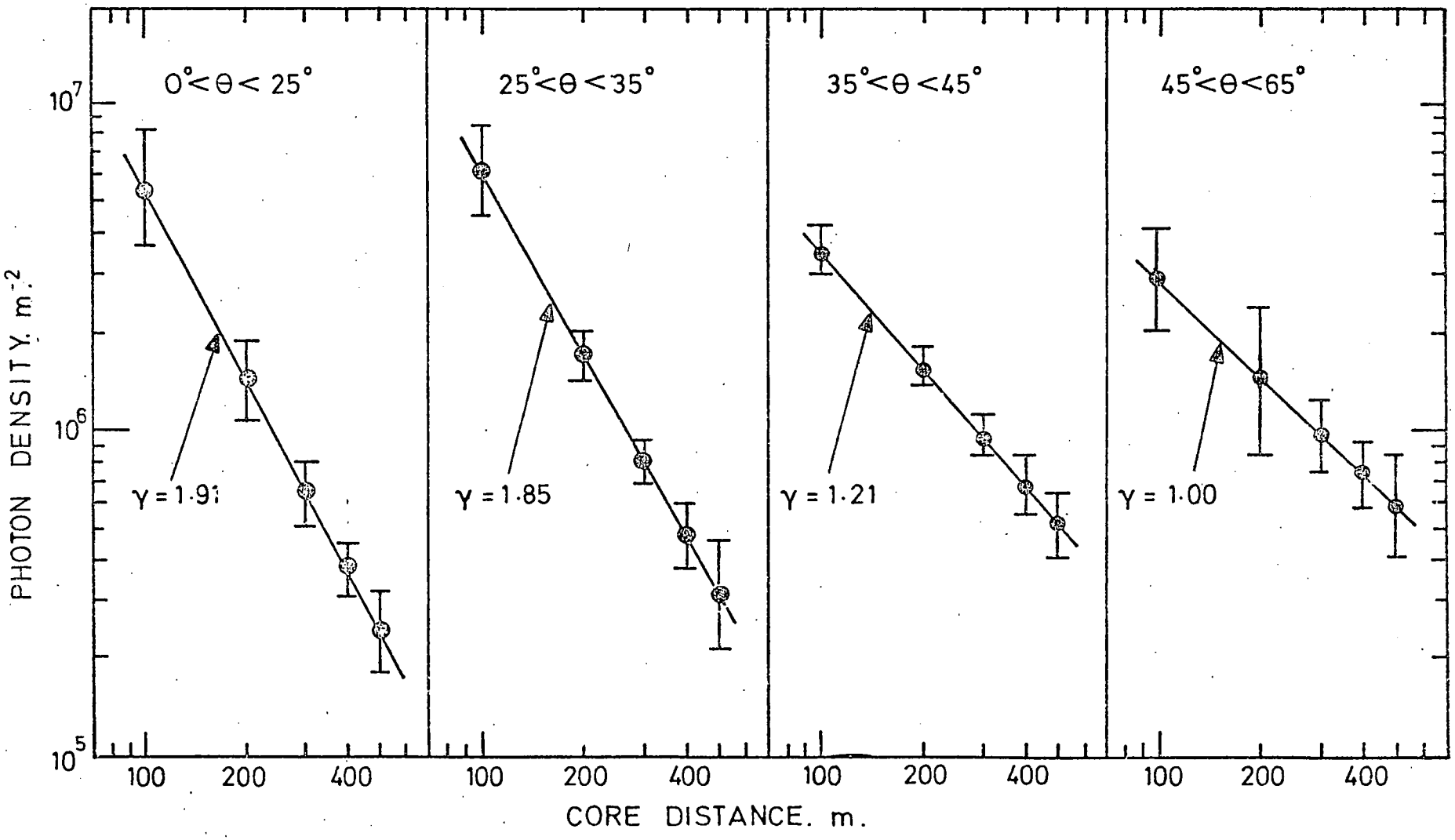
0°<θ< 25°
25°<θ<35°
35°<θ<45°
45°<θ<65°
γ = 1·91
γ = 1·85
γ = 1·21
γ = 1·00
PHOTON DENSITY. m.-2
10^7
10^6
10^5
100
200
400
CORE DISTANCE. m.

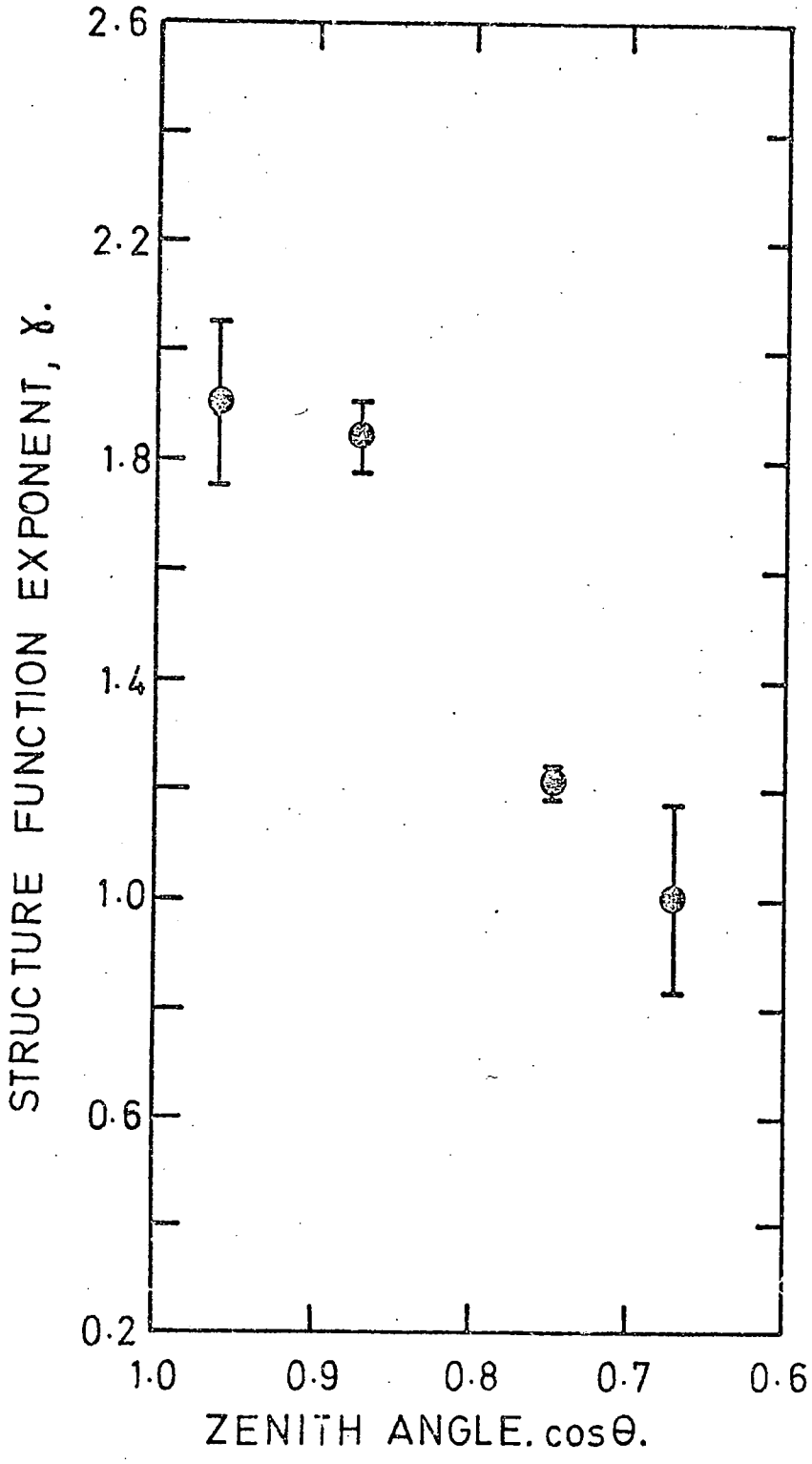
2·6
2·2
1·8
1·4
1·0
0·6
0·2
STRUCTURE FUNCTION EXPONENT, χ.
1·0
0·9
0·8
0·7
0·6
ZENITH ANGLE. cosθ.

4.3 The Cerenkov Light Pulse Shape

4.3.i The Variation of the Cerenkov Light Pulse Shape with Core Distance

All four of the parameters chosen to describe the shape of the Cerenkov light pulse; the rise-time, top-time, fall-time and full-width-half-maximum; were found to vary with core distance in a similar manner. The value of each of the pulse shape parameters increases exponentially with core distance, r, and an equation of the form:-

$$t = A + \exp(Br) \qquad \ldots \text{ equ.4.2}$$

was fitted to the measurements of each parameter, made in the showers of each of the shower energy and zenith angle intervals. (The correlation coefficients of the large majority of the fits were greater than 0.65, indicating critical significances less than 5%.)

At core distances greater than 200 m, the Cerenkov light pulses are slow enough to be essentially unaffected by the bandwidth of the experimental equipment. Thus it is at these large core distances, that dependences of the light pulse shape on shower energy and zenith angle are most marked. At core distances less than 200 m, any variations of the pulse shape with these shower parameters are likely to be masked by the bandwidth.

To study trends with shower energy and zenith angle, the exponential expressions fitted to the measurements of the light pulse shape parameters, were used to evaluate each parameter at a core distance of 400 m. Tables 4.2(a) - (d) show respectively the values of the light pulse rise-time, top-time, fall-time and full-width-half-maximum at this core distance. The standard errors on the values are also shown.

It is seen in table 4.2 that generally, the values of all the light pulse shape parameters decrease with increasing shower inclination from the zenith. The light pulses in inclined showers are faster in all

Table 4.2. Measurements of the shape of the Cerenkov light pulse. The average features of the shape of the Cerenkov light pulse have been determined by expressing measurements of the pulse shape parameters, made in showers of various energies and incident at various zenith angles, as exponential functions of core distance. Shown here, are the average values of the light pulse shape parameters at 400 m core distance.

Shower Zenith Angle	Primary Particle Energy			
	$\rho(500)_{VE} < 0.3\ m^{-2}$	$0.3 < \rho(500)_{VE} < 0.6\ m^{-2}$	$0.6 < \rho(500)_{VE} < 1.25\ m^{-2}$	$\rho(500)_{VE} > 1.25\ m^{-2}$
$0^{o} < \theta < 25^{o}$		24.6 ± 4.3 ns	24.9 ± 2.2 ns	25.9 ± 4.2 ns
$25^{o} < \theta < 35^{o}$	22.8 ± 6.2 ns	24.7 ± 3.4 ns	24.8 ± 3.1 ns	21.1 ± 3.8 ns
$35^{o} < \theta < 45^{o}$	16.1 ± 7.0 ns	17.3 ± 4.1 ns	16.1 ± 2.7 ns	15.5 ± 2.0 ns
$45^{o} < \theta < 65^{o}$		14.3 ± 2.2 ns		

Table 4.2(a). Average values of the Cerenkov light pulse rise-time (10% - 90%) at 400 m core distance.

Shower Zenith Angle	Primary Particle Energy			
	$\rho(500)_{VE} < 0.3$ m^{-2}	$0.3 < \rho(500)_{VE} < 0.6$ m^{-2}	$0.6 < \rho(500)_{VE} < 1.25$ m^{-2}	$\rho(500)_{VE} > 1.25$ m^{-2}
$0^{o} < \theta < 25^{o}$		22.1 $\pm$ 1.6 ns	17.8 $\pm$ 3.1 ns	24.1 $\pm$ 2.6 ns
$25^{o} < \theta < 35^{o}$	13.7 $\pm$ 3.4 ns	16.4 $\pm$ 1.8 ns	21.7 $\pm$ 1.9 ns	17.1 $\pm$ 2.3 ns
$35^{o} < \theta < 45^{o}$	18.1 $\pm$ 5.1 ns	12.1 $\pm$ 1.9 ns	14.8 $\pm$ 2.9 ns	11.6 $\pm$ 2.5 ns
$45^{o} < \theta < 65^{o}$		12.1 $\pm$ 1.8 ns		

Table 4.2(b). Average values of the Cerenkov light pulse top-time (90% - 90%) at 400 m core distance.

Shower Zenith Angle	Primary Particle Energy			
	$\rho(500)_{VE} < 0.3$ m^{-2}	$0.3 < \rho(500)_{VE} < 0.6$ m^{-2}	$0.6 < \rho(500)_{VE} < 1.25$ m^{-2}	$\rho(500)_{VE} > 1.25$ m^{-2}
$0^{o} < \theta < 25^{o}$		29.7 ± 3.9 ns	31.6 ± 3.1 ns	41.6 ± 4.4 ns
$25^{o} < \theta < 35^{o}$	21.6 ± 5.2 ns	24.3 ± 4.8 ns	31.4 ± 4.7 ns	27.8 ± 4.4 ns
$35^{o} < \theta < 45^{o}$	24.4 ± 10.2 ns	21.2 ± 3.6 ns	20.0 ± 5.9 ns	21.9 ± 3.0 ns
$45^{o} < \theta < 65^{o}$		19.2 ± 3.7 ns		

Table 4.2(c). Average values of the Cerenkov light pulse fall-time (90% - 50%) at 400 m core distance.

Shower Zenith Angle	Primary Particle Energy			
	$\rho(500)_{VE} < 0.3\ m^{-2}$	$0.3 < \rho(500)_{VE} < 0.6\ m^{-2}$	$0.6 < \rho(500)_{VE} < 1.25\ m^{-2}$	$\rho(500)_{VE} > 1.25\ m^{-2}$
$0^{o} < \theta < 25^{o}$		65.5 ± 6.1 ns	62.3 ± 5.1 ns	82.4 ± 7.9 ns
$25^{o} < \theta < 35^{o}$	43.2 ± 8.3 ns	54.4 ± 4.8 ns	66.1 ± 4.7 ns	55.5 ± 6.2 ns
$35^{o} < \theta < 45^{o}$	50.8 ± 11.1 ns	41.8 ± 6.1 ns	43.8 ± 8.6 ns	40.1 ± 4.7 ns
$45^{o} < \theta < 65^{o}$		37.6 ± 5.7 ns		

Table 4.2(d). Average values of the Cerenkov light pulse full-width-half-maximum (50% - 50%) at 400 m core distance.

respects than those in vertical showers. However, there is little evidence for any trend with shower primary particle energy. In the next section, the dependence of the light pulse shape on shower inclination is examined more closely. All the pulse shape parameters are considered together, since they exhibit very similar characteristics.

4.3.ii The Sensitivity of the Cerenkov Light Pulse Shape to Shower Zenith Angle

The shower zenith angle dependences of the four Cerenkov light pulse shape parameters are illustrated in figs.4.4(a) to 4.7(a). The exponential expressions fitted to the measurements made in showers of energies in the interval $0.3 < \rho(500)_{VE} < 0.6$ m^{-2} are shown, for four different zenith angle intervals. The spread of the individual measurements is indicated by the error bars, which show the standard errors on the fitted pulse shape values. It is seen that the rise-time, top-time, fall-time and full-width-half-maximum of the Cerenkov light pulse, all decrease in value with increasing shower inclination to the zenith. This trend is most marked at core distances greater than about 200 m, since the bandwidth of the recording equipment has no effect on the light signals recorded at these core distances.

The variation of the light pulse shape parameters with shower inclination is illustrated in an alternative way in figs.4.4(b) to 4.7(b). Here, the values of each parameter at 400 m core distance, are plotted as functions of the cosine of shower zenith angle. Although the number of measurements in each case is small, the data suggest that the variation of all the light pulse shape parameters with zenith angle, can be adequately represented by a dependence proportional to $\cos\theta$ (at least over the range of shower zenith angles for which data are available). It is noted, however, that results of simulations by the Soviet group indicate that the light pulse full-width-half-maximum varies as $\cos^2\theta$

Figure 4.4. The dependence of the Cerenkov light pulse rise-time on shower zenith angle.

(a) The exponential expressions fitted to the rise-time measurements made in showers of energies in the interval $0.3 < \rho(500)_{VE} < 0.6$ m^{-2}, for four zenith angle intervals.

(b) The variation of the pulse rise-time at 400 m core distance with zenith angle.

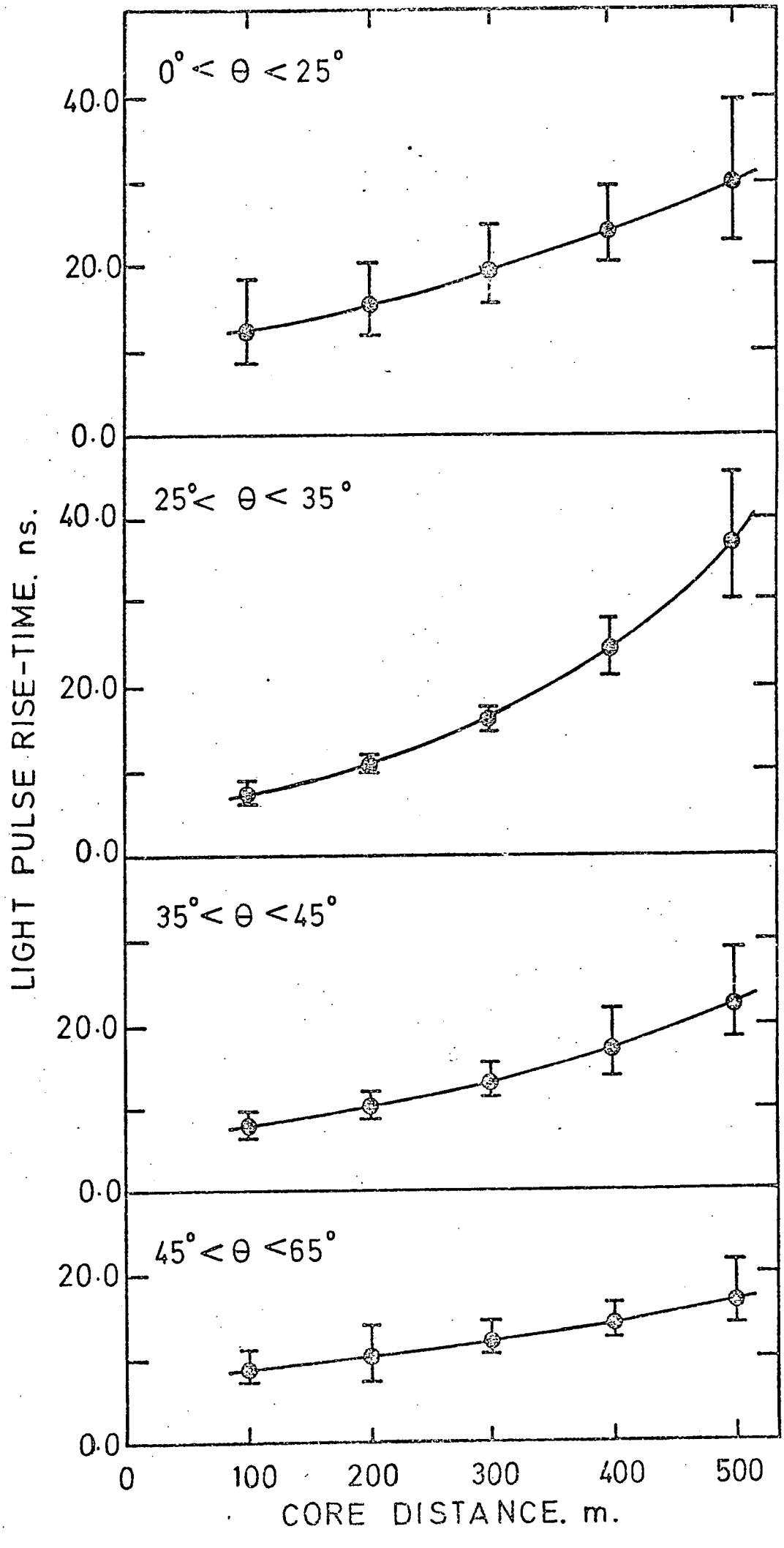
0° < θ < 25°
25° < θ < 35°
35° < θ < 45°
45° < θ < 65°
40·0
20·0
0·0
LIGHT PULSE RISE-TIME. ns.
0
100
200
300
400
500
CORE DISTANCE. m.

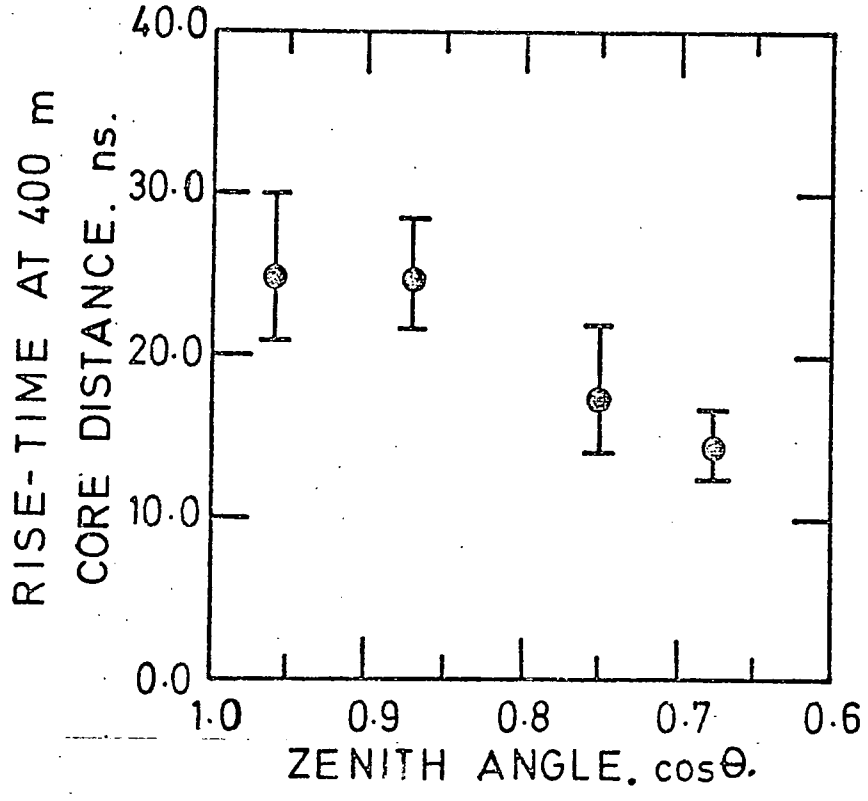
RISE-TIME AT 400 m CORE DISTANCE. ns.
40·0
30·0
20·0
10·0
0·0
1·0
0·9
0·8
0·7
0·6
ZENITH ANGLE. cosΘ.

Figure 4.5. The dependence of the Cerenkov light pulse top-time on shower zenith angle.

(a) The exponential expressions fitted to the top-time measurements made in showers of energies in the interval $0.3 < \rho(500)_{VE} < 0.6$ m^{-2}, for four zenith angle intervals.

(b) The variation of the pulse top-time at 400 m core distance with zenith angle.

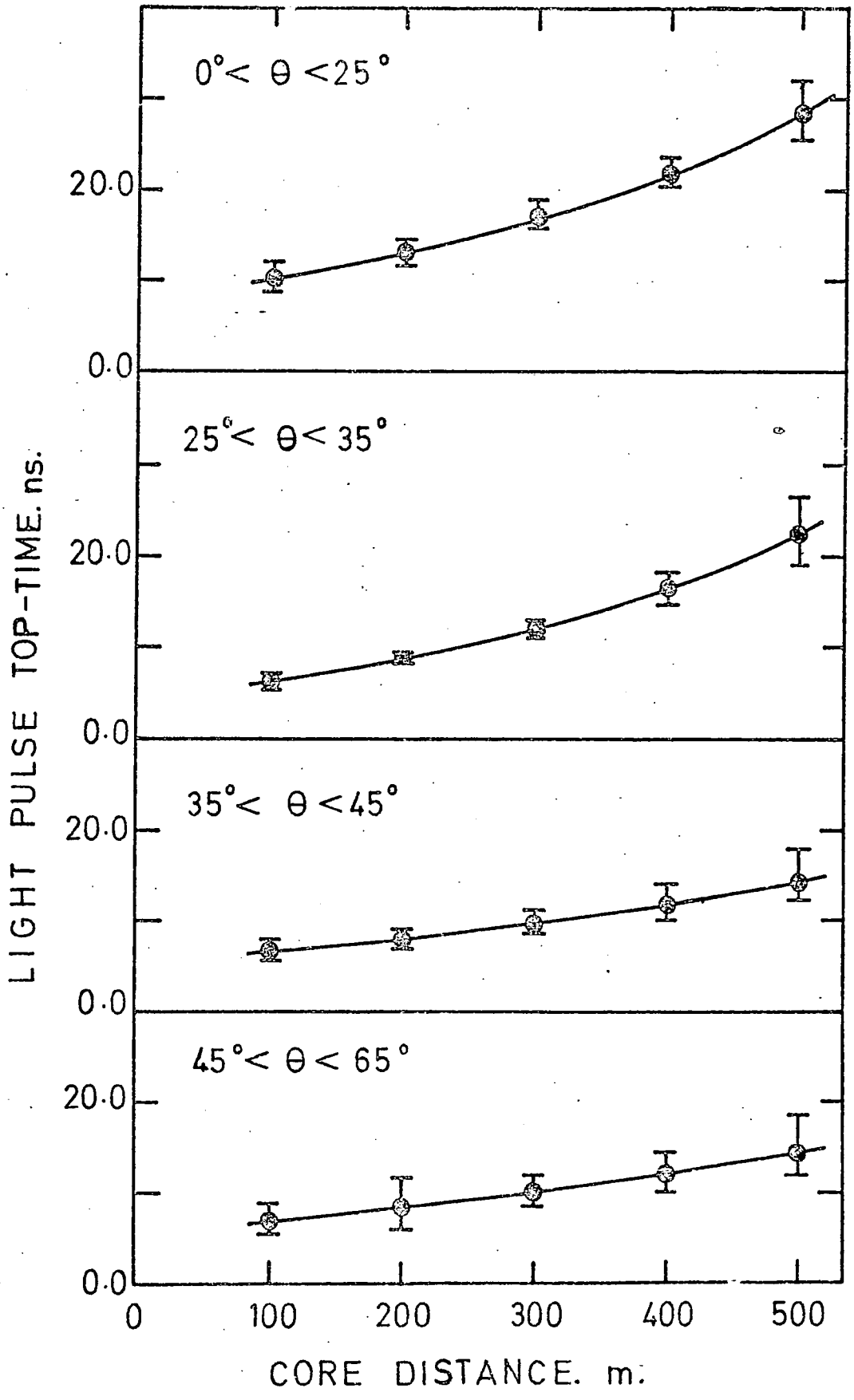
0°< θ <25°
25°< θ< 35°
35°< θ <45°
45°< θ < 65°
20·0
0·0
LIGHT PULSE TOP-TIME. ns.
0
100
200
300
400
500
CORE DISTANCE. m.

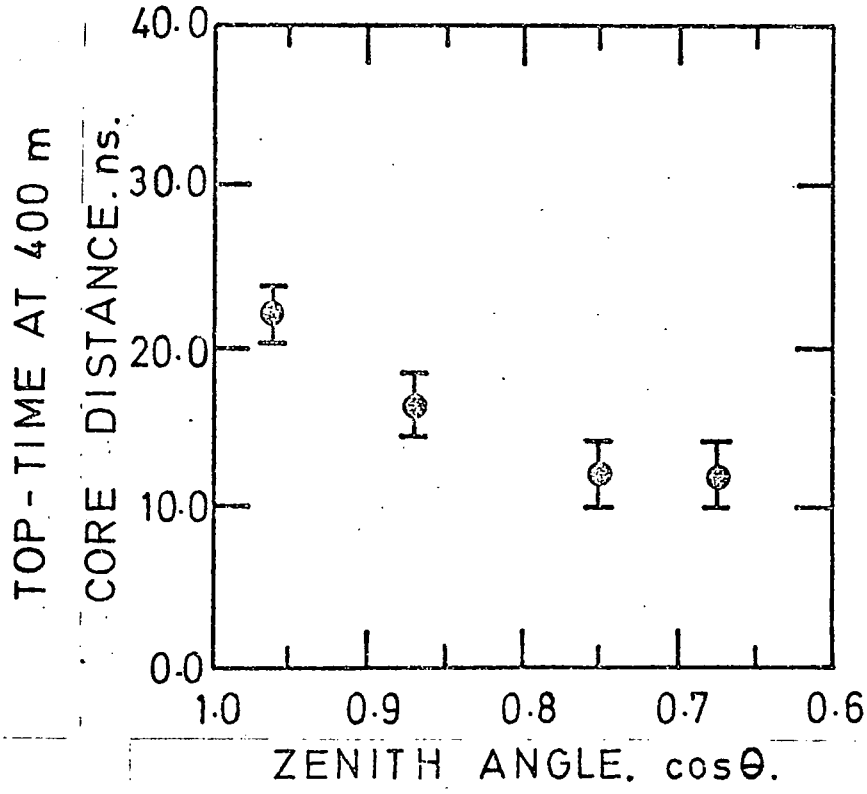
TOP-TIME AT 400 m
CORE DISTANCE. ns.
40·0
30·0
20·0
10·0
0·0
1·0
0·9
0·8
0·7
0·6
ZENITH ANGLE. cosθ.

Figure 4.6. The dependence of the Cerenkov light pulse fall-time on shower zenith angle.

(a) The exponential expressions fitted to the fall-time measurements made in showers of energies in the interval $0.3 < \rho(500)_{VE} < 0.6$ m^{-2}, for four zenith angle intervals.

(b) The variation of the pulse fall-time at 400 m core distance with zenith angle.

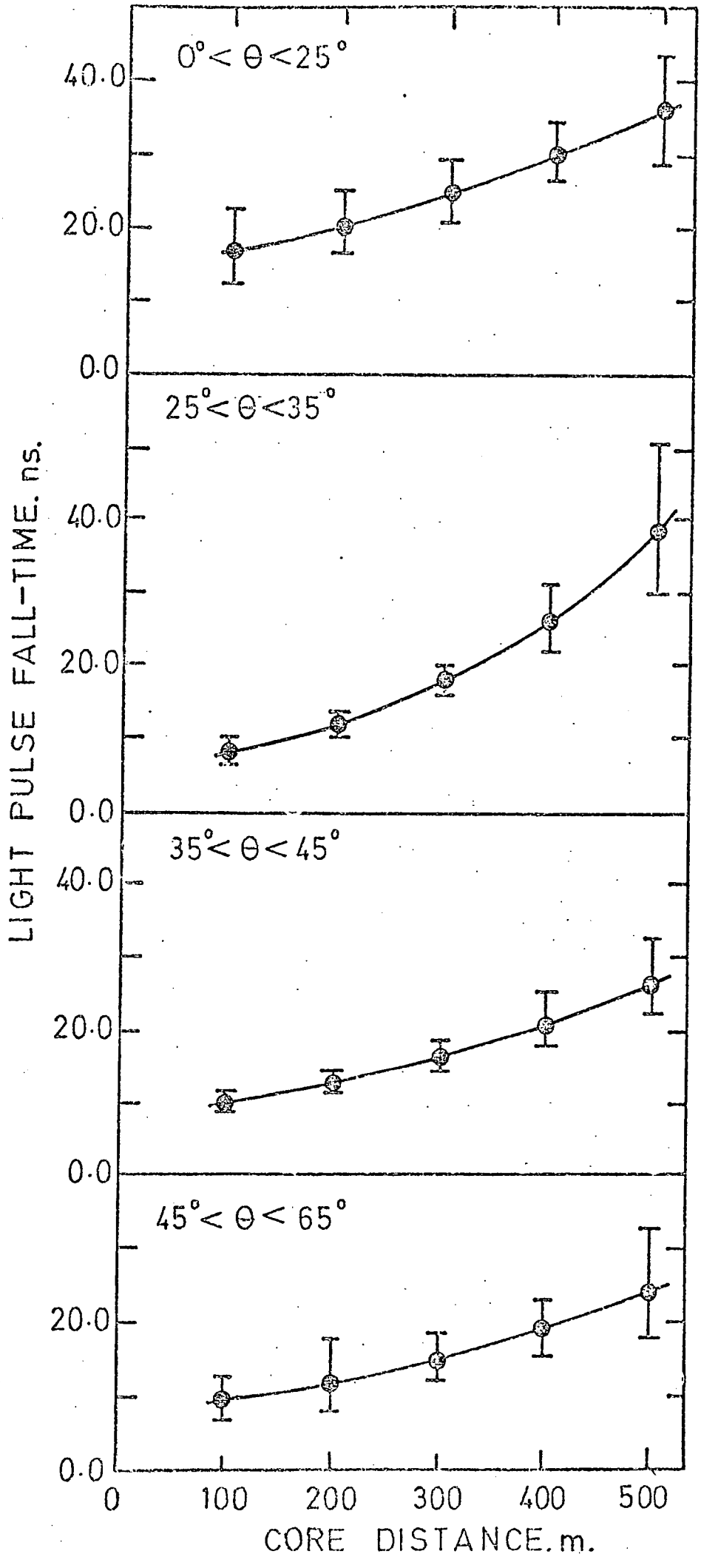
0°< θ <25°
25°< θ <35°
35°< θ <45°
45°< θ < 65°
40.0
20.0
0.0
LIGHT PULSE FALL-TIME. ns.
0
100
200
300
400
500
CORE DISTANCE. m.

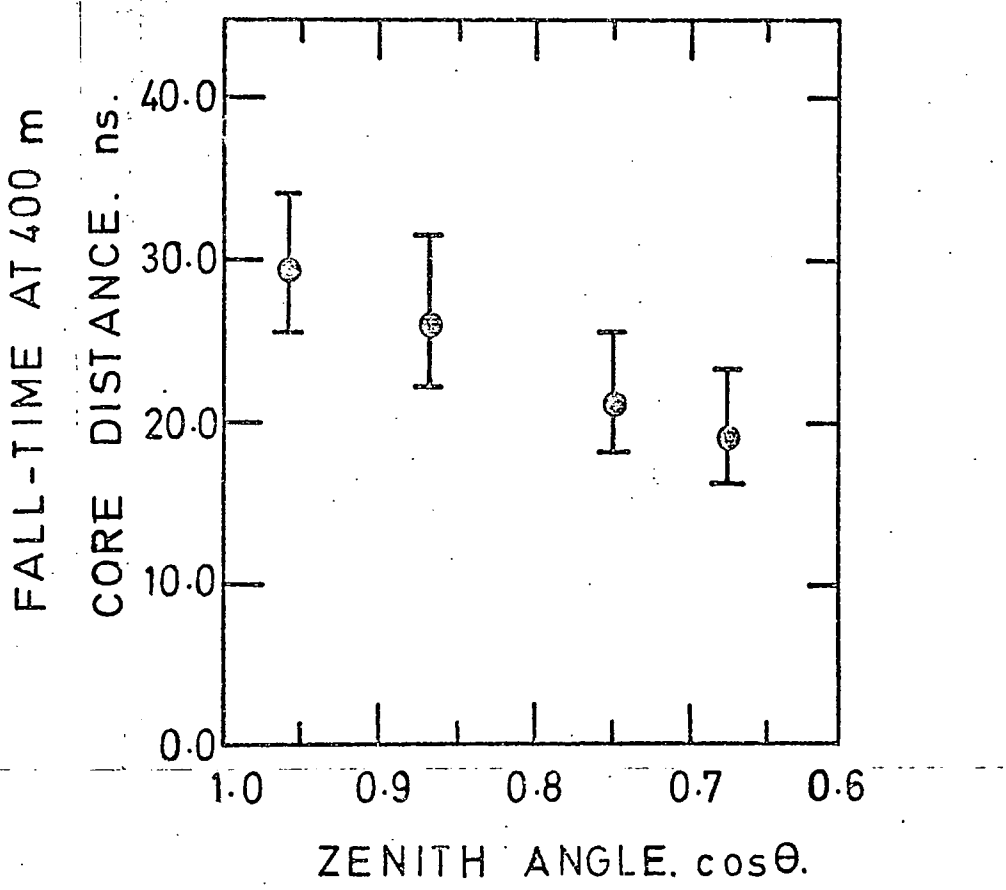
FALL-TIME AT 400 m
CORE DISTANCE. ns.
40·0
30·0
20·0
10·0
0·0
1·0
0·9
0·8
0·7
0·6
ZENITH ANGLE. cosθ.

Figure 4.7. The dependence of the full-width-half-maximum of the Cerenkov light pulse on shower zenith angle.

(a) The exponential expressions fitted to the measurements of the full-width-half-maximum made in showers of energies in the interval $0.3 < \rho(500)_{VE} < 0.6$ m^{-2}, for four zenith angle intervals.

(b) The variation of the full-width-half-maximum at 400 m core distance with zenith angle.

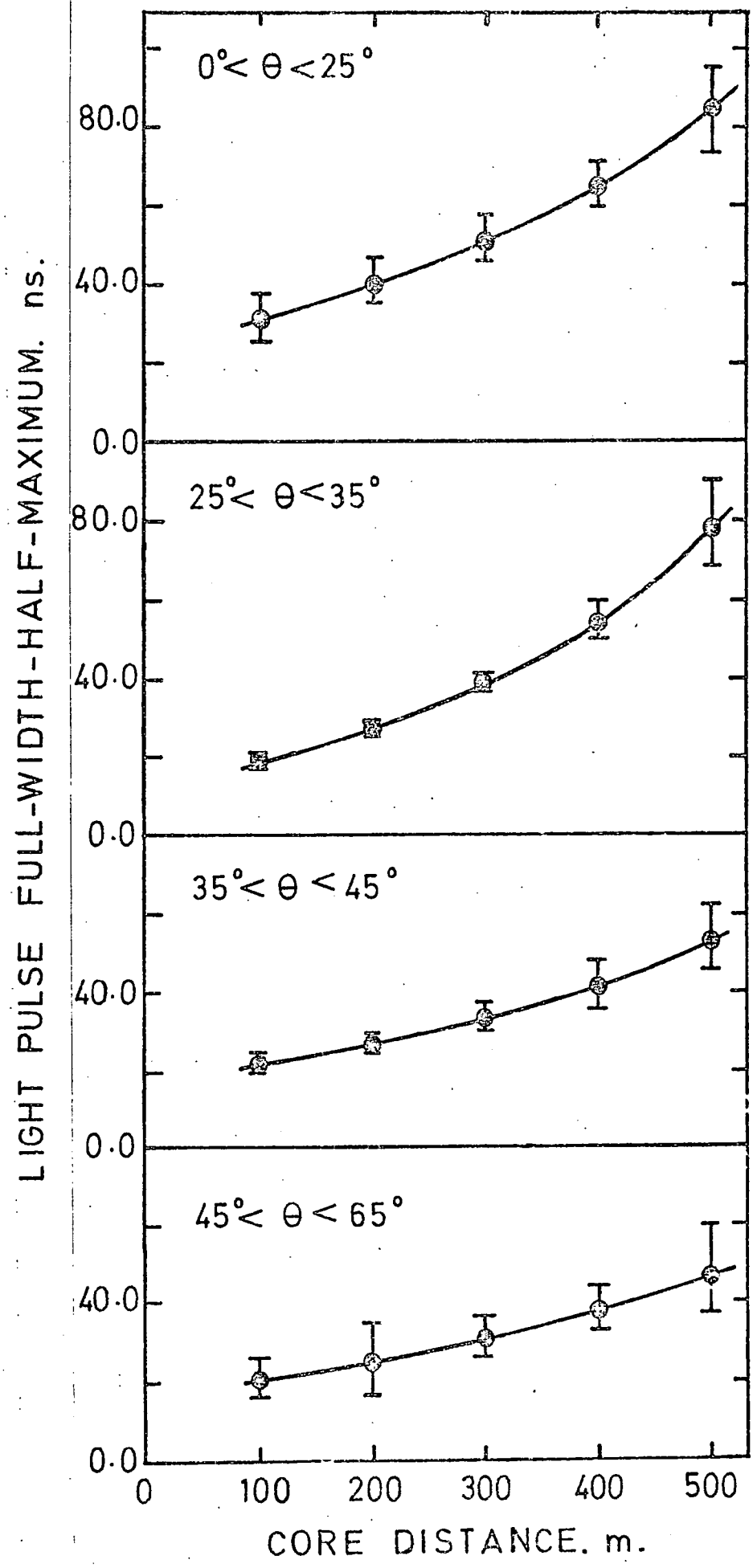
0°< θ <25°
25°< θ <35°
35°< θ < 45°
45°< θ < 65°
80.0
40.0
0.0
0
100
200
300
400
500
LIGHT PULSE FULL-WIDTH-HALF-MAXIMUM. ns.
CORE DISTANCE. m.

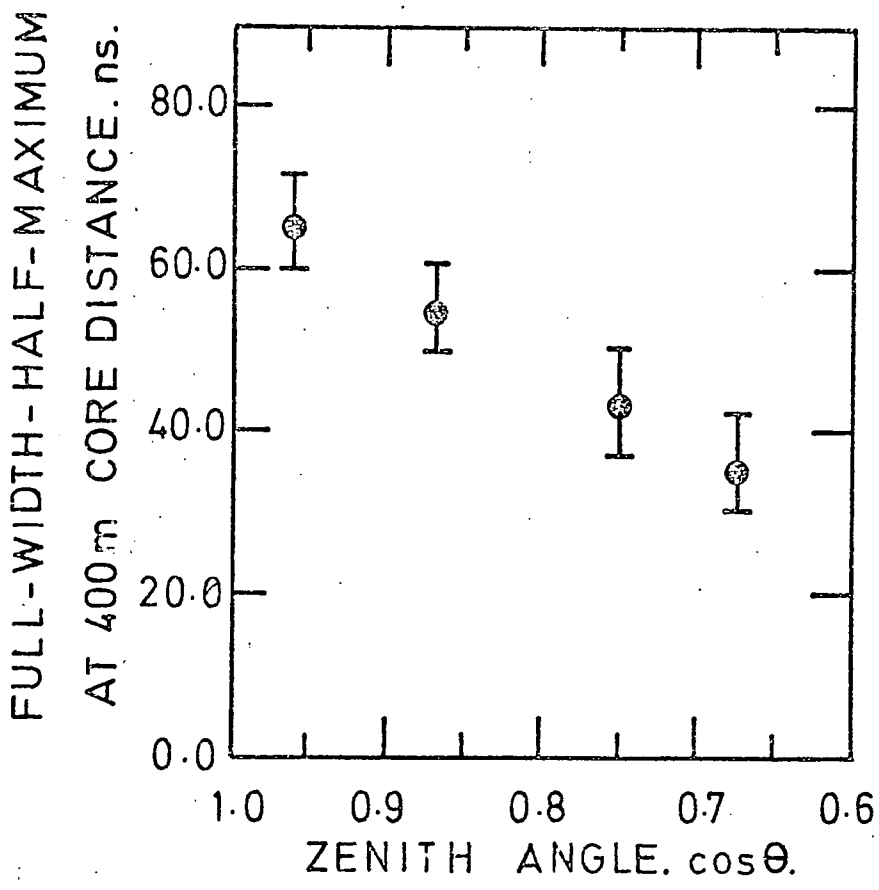
FULL-WIDTH-HALF-MAXIMUM
AT 400m CORE DISTANCE. ns.
80.0
60.0
40.0
20.0
0.0
1.0
0.9
0.8
0.7
0.6
ZENITH ANGLE. cosθ.

(Efimov et al. (1973)). More numerous and accurate experimental measurements would enable the form of the variation of the Cerenkov light pulse shape with shower zenith angle, to be defined with greater certainty.

4.4 Quantifying the Sensitivity of the Cerenkov Light Measures to Shower Energy and Zenith Angle

It has been illustrated in the last two sections, that most of the measured Cerenkov light parameters vary with shower energy and inclination. It is necessary to quantify these variations in order that values of the parameters appropriate to showers of specific energies and zenith angles, can be calculated (for comparison of the data measured here with simulation results, for example). This has been achieved by using a multi-parametric analysis procedure. The average values of the measurements of each of the parameters, made in the showers of each of the energy and zenith angle intervals, were expressed as linear combinations of the average values of $\log_{10}\left(\rho(500)_{VE}\right)$ and $\cos\theta$ of each interval. These functions were chosen following the empirical suggestions from the data presented in figs.4.2(b) to 4.7(b) (see sections 4.2.ii and 4.3.ii, above).

The structure function exponent of the lateral light distribution, and the pulse shape parameters evaluated at 400 m core distance, were observed to depend on shower energy and inclination according to:-

Structure Function Exponent

$$\gamma = 1.199 - 3.547 \times \cos\theta - 0.277 \times \log_{10}\left(\rho(500)_{VE}\right) \quad \ldots \text{ equ.4.3}$$

(The multiple correlation coefficient of the fit was 0.95, indicating a critical significance less than 0.1%. The standard error on the

predicted exponent values was 0.133.)

Rise-Time at 400 m Core Distance

$$t_r(400) = -16.55 + 43.75 \times \cos\theta + 0.119 \times \log_{10}\left(\rho(500)_{VE}\right) \text{ ns.} \quad \ldots \text{ equ.4.4}$$

(The multiple correlation coefficient of the fit was 0.94, indicating a critical significance less than 0.1%. The standard error on the predicted rise-time values was 1.7 ns.)

Top-Time at 400 m Core Distance

$$t_t(400) = -13.29 + 36.27 \times \cos\theta + 1.201 \times \log_{10}\left(\rho(500)_{VE}\right) \text{ ns.} \quad \ldots \text{ equ.4.5}$$

(The multiple correlation coefficient of the fit was 0.79, indicating a critical significance of 0.2%. The standard error on the predicted top-time values was 2.9 ns.)

Fall-Time at 400 m Core Distance

$$t_f(400) = -16.84 + 52.96 \times \cos\theta + 6.91 \times \log_{10}\left(\rho(500)_{VE}\right) \text{ ns.} \quad \ldots \text{ equ.4.6}$$

(The multiple correlation coefficient of the fit was 0.86, indicating a critical significance of 0.1%. The standard error on the predicted fall-time values was 3.6 ns.)

Full-Width-Half-Maximum at 400 m Core Distance

$$t_{\frac{1}{2}}(400) = -45.14 + 120.3 \times \cos\theta + 9.92 \times \log_{10}\left(\rho(500)_{VE}\right) \text{ ns.} \quad \ldots \text{ equ.4.7}$$

(The multiple correlation coefficient of the fit was 0.87, indicating a critical significance of 0.1%. The standard error on the predicted full-width-half-maximum values was 7.4 ns.)

Equs.4.3 to 4.7 are a statement of the average characteristics of Cerenkov light in extensive air showers, as measured in the present work. From them, values of each of the Cerenkov light

parameters in showers of any energy and zenith angle can be evaluated.

4.5 The Sensitivity of Cerenkov Light Measures to Depth of Shower Cascade Development Maximum

The variations of the various Cerenkov light parameters with shower zenith angle, can be used to investigate the sensitivity of the parameters to changes in depth of shower cascade development maximum. An inclined shower traverses a greater thickness of atmosphere before reaching ground level than does a vertical shower. Consequently, on average, inclined showers reach cascade development maxima at greater altitudes than vertically incident showers. Assuming that no significant changes arise from the differing air densities at different atmospheric levels, increasing the inclination of a vertical shower to 24.4°, is equivalent to changing the depth of the cascade development maximum of the shower by 100 g cm^{-2}.

A second estimate of the sensitivity of the Cerenkov light parameters to changes in depth of shower cascade development maximum, is made possible by using the information from model simulations, that showers initiated by higher energy primary particles reach cascade maxima lower in the atmosphere than those initiated by lower energy primary particles. (Here there is no possible complication arising from the showers developing in parts of the atmosphere of differing density.) Many plausible simulations, including those of Protheroe and Turver (1977), suggest a difference of about 100 g cm^{-2} between the depths of the cascade maxima of showers initiated by primary particles of energies differing by one decade.

The variations of each of the Cerenkov light parameters with both shower energy and shower inclination, have been used to estimate the sensitivities of the parameters to depth of shower cascade development maximum. The changes in the value of each parameter, that

Parameter	Change due to increase of 100 g cm^{-2} in depth of shower cascade maximum, estimated from:-	
	Zenith Angle	Energy
Structure function exponent	+ 0.32	+ 0.28
Rise-time at 400 m core distance	+ 3.9 ns	+ 0.1 ns
Top-time at 400 m core distance	+ 3.3 ns	+ 1.2 ns
Fall-time at 400 m core distance	+ 4.7 ns	+ 6.9 ns
Full-width-half-maximum at 400 m core distance	+ 10.8 ns	+ 9.9 ns

Table 4.3. The sensitivities of the various Cerenkov light parameters to depth of shower cascade development maximum. Shown here, are the changes in the values of each parameter that result from alterations of shower energy and inclination, that are each equivalent to an increase in depth of maximum of 100 g cm^{-2}.

result from alterations of shower energy and inclination that are each equivalent to an increase in depth of maximum of 100 g cm^{-2}, were calculated from equs.4.3 to 4.7. These changes are shown in table 4.3. It is seen that alterations in shower energy and in shower zenith angle, that correspond to similar variations in position of shower cascade maximum above the detector array, each lead to similar changes in the values of the Cerenkov light parameters (although the rise-time values are a possible exception). This consistency supports the validity of interpreting alterations in shower energy and in shower zenith angle, as being equivalent to variations in depth of shower cascade development maximum.

Both the lateral light distribution and the light pulse shape are sensitive to depth of shower cascade development maximum. On average, the lateral light spread is narrower in showers reaching cascade development maxima lower in the atmosphere, and the light pulses in these showers are slower. The Cerenkov light parameters most sensitive to changes in depth of shower cascade maximum, appear to be the structure function exponent, and the light pulse fall-time and full-width-half-maximum. The changes in these parameters resulting from a change of 100 g cm^{-2} in depth of shower maximum, are greater than the errors on individual measurements of these quantities. This then, gives some indication of the resolution in depth of shower cascade development maximum, that is potentially available with the existing experimental equipment and measuring techniques.

4.6 A Cerenkov Light Measure of Primary Particle Energy

It has been observed that the Cerenkov photon density at core distances in the region of 200 m, is substantially independent of shower zenith angle. It varies only with shower energy. (See table 4.1 and fig.4.3(a) .) This supports the suggestion from the computer

simulations by Smith and Turver (1973), and also from those by Protheroe and Turver (1977), that the Cerenkov photon density at this core distance is insensitive to shower longitudinal development. The Cerenkov photon density at 200 m core distance relates well to primary particle energy, according to the simulations.

As a test of this idea, fig.4.8 shows the average values of $\phi(200)$, the Cerenkov photon density at 200 m core distance, as a function of the established Haverah Park primary particle energy measure, $\rho(500)_{VE}$. The values of $\phi(200)$ are derived from photon density measurements made in showers of all zenith angles, by averaging the values in each of the energy intervals of table 4.1. The standard error on the average values is shown by the error bars. It is seen that the Cerenkov photon density at 200 m core distance relates very well to the Haverah Park particle detector array parameter - at least for the range of shower energies spanned by the present measurements. The relation is described by:-

$$\phi(200) = 3.93 \times 10^{6} \times \left(\rho(500)_{VE}\right)^{1.101} \text{ photon m}^{-2} \quad \ldots \text{ equ.4.8}$$

(The correlation coefficient of the fit was 0.995, indicating a critical significance of 2%.)

* * *

Cerenkov light measurements have been made in many showers for which no analyses of data from the Haverah Park deep water particle detectors are available. An estimate of the primary particle energies of these showers is necessary if the measurements are to be fully exploited in the future. The method of determining primary particle energy from the Cerenkov photon density at 200 m core distance, that has been demonstrated here, may fulfil this requirement.

Figure 4.8. A Cerenkov light measure of primary particle energy. Shown here is the variation of average values of $\Phi(200)$, the Cerenkov photon density at 200 m core distance, with the established Haverah Park primary particle energy measure, $\rho(500)_{VE}$. (The values of $\Phi(200)$ have been determined from measurements made in showers incident at all zenith angles.)

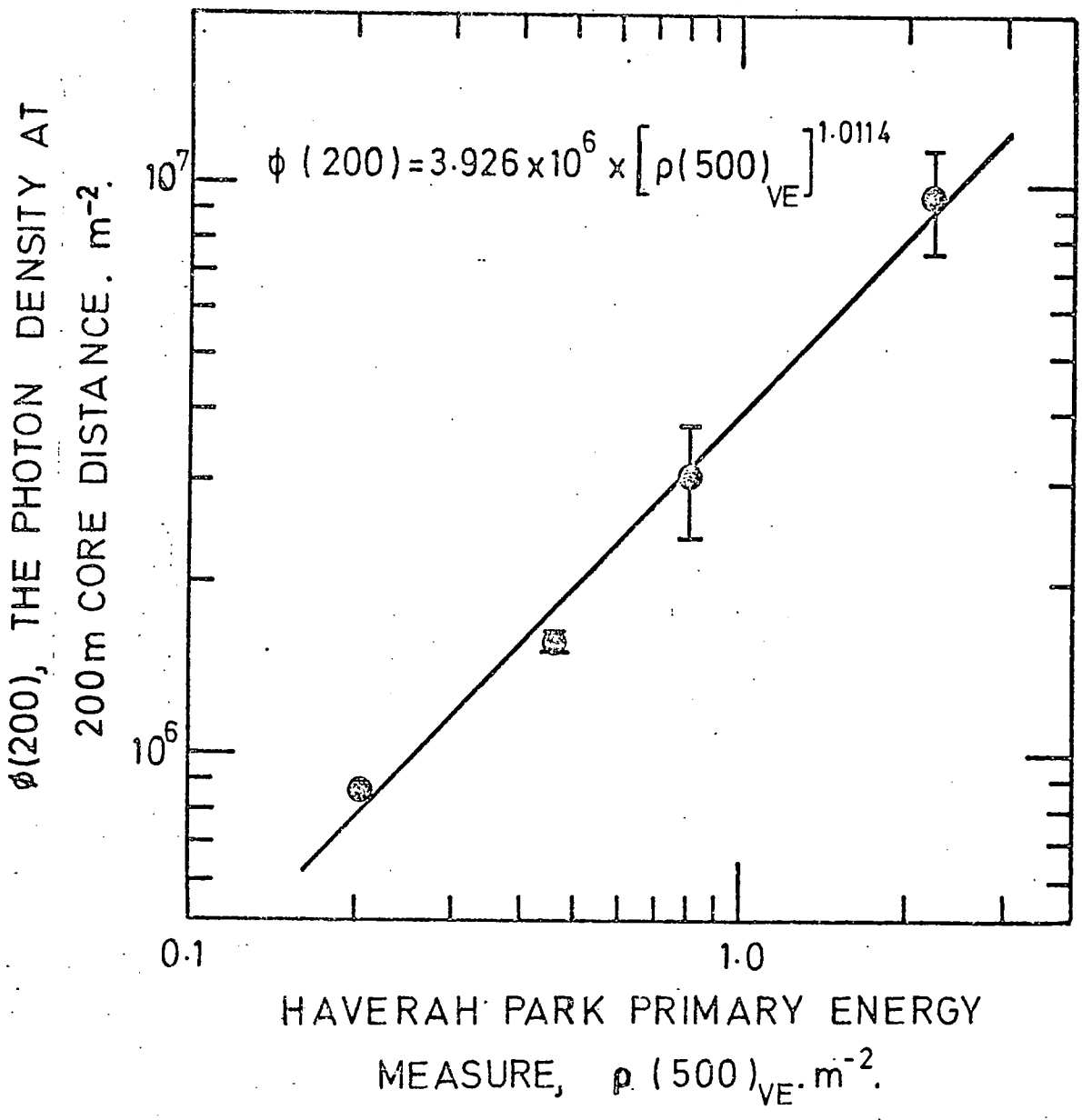
$\phi(200) = 3.926 \times 10^6 \times [\rho(500)_{VE}]^{1.0114}$
10^7
10^6
0·1
1·0
$\phi(200)$, THE PHOTON DENSITY AT 200 m CORE DISTANCE. m^{-2}.
HAVERAH PARK PRIMARY ENERGY MEASURE, $\rho(500)_{VE}$. m^{-2}.

Figure 4.9. A further illustration of the possible use of Cerenkov photon density measurements for estimating primary particle energy. Here, values of $\Phi(200)$ determined from photon density measurements made in individual showers, are plotted as a function of $\rho(500)_{VE}$. (At least five photon density measurements were made in each of the showers considered. The showers were incident at zenith angles up to 40^{o}.)

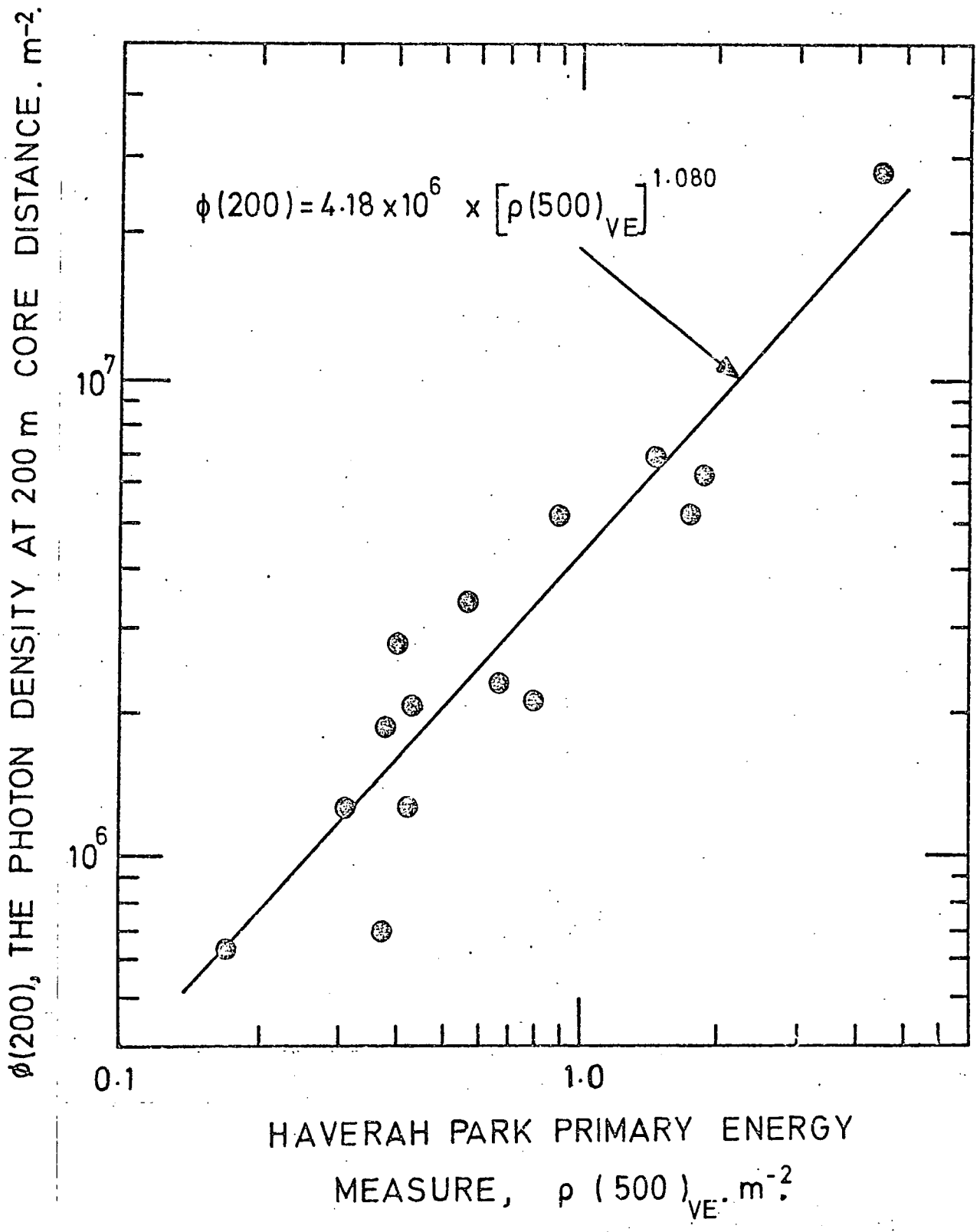
$\phi(200) = 4.18 \times 10^6 \times [\rho(500)_{VE}]^{1.080}$
10^7
10^6
0·1
1·0
$\phi(200)$, THE PHOTON DENSITY AT 200 m CORE DISTANCE. m^{-2}.
HAVERAH PARK PRIMARY ENERGY MEASURE, $\rho(500)_{VE}$. m^{-2}.

Fig.4.9 illustrates the possible use of photon density measurements for estimating the energies of individual showers. Values of $\Phi(200)$ have been determined for each of those showers registered by the Haverah Park particle detector array, in which at least five photon density measurements were made. The values of $\Phi(200)$ are plotted against the $\rho(500)_{VE}$ values of the showers. Of course, the values of $\Phi(200)$ are based on shower core locations indicated by the particle detector data, and similar core location information must be provided from Cerenkov light measurements if this energy estimate is to be used in the absence of particle detector data.

4.7 The Curvature of the Cerenkov Light Front

The measurements of the relative times at which the Cerenkov light in individual showers, arrives at the various detector positions, are now reported. From these measurements, the curvature of the Cerenkov light front in the showers can be calculated. As stated in Chapter 2, the simulations by Protheroe and Turver (1977) suggest that the light observed earliest at each detector position, originates highest in the atmosphere. The timing measurements made to the points at which the observed light pulses reach 10% of full amplitude, will therefore, lead to the determination of the curvature of the light front arising from the Cerenkov photons produced high up in showers. This quantity should be closely related to the early cascade development of the showers.

To fit a spherically shaped light front, a minimum of four light arrival times need to be measured in a shower. However, because of the experimental errors of the timing measurements, some redundancy of information is desirable. In the present work, the light front curvatures of those 25 showers in which five or more

light arrival times were measured, have been calculated. The showers spanned a range of primary energy from $\rho(500)_{VE} = 0.11\ m^{-2}$ to $\rho(500)_{VE} = 4.33\ m^{-2}$, and arrived at zenith angles up to 45^{o}.

The spherical light fronts were computed by Dr K.J. Orford and Mr K. Appleby, using the computer program "Minuit" - a multi-parameter minimization procedure. The differences between the observed photon arrival times and those predicted from spherical light front fits were minimized. The observed Cerenkov light arrival times were found to be very well represented by spheres - r.m.s. deviations of 4 ns from light fronts of radius 10 km were typical.

The average radius of curvature of the Cerenkov light fronts in the small sample of showers studied here, was 13.19 km. (The distribution of the light front radius values had a standard deviation of 6.75 km,) It is interesting to note that the fitting procedure did not require a knowledge of the positions of the cores of the showers studied, nor the gains of the light detectors. Only the relative times at which the Cerenkov light in a shower reached the various detector positions were needed.

* * *

The Cerenkov light front radius itself is not directly related to shower cascade development, since it also depends on shower zenith angle. Showers incident at large inclinations traverse a greater thickness of atmosphere than vertically incident showers, and so on average, develop at a greater distance (in km) from the detector array. However, a knowledge of both the Cerenkov light front radius and the zenith angle of a shower, enables the thickness of atmosphere that the shower penetrates while producing those Cerenkov photons that reach ground level before the observed light pulses reach 10%

of full amplitude, to be calculated. This quantity is independent of shower zenith angle, and should be a direct measure of the early cascade development of showers. The "depth of the light front origin" of each of the showers studied here, was calculated in this way. The mean of the values obtained was 314 g cm^{-2}, and the distribution of the values had a standard deviation of 168 g cm^{-2}.

Calculation of the correlation between the values of the depth of the light front origin and the energy of the showers studied, showed that these two parameters are not related (the correlation coefficient was less than 0.1). This is expected, provided that the mean free path for interaction between nucleons and air nuclei varies only very slowly with the nucleon energy.

* * *

Before closing this section, some mention must be made of the effects of experimental measurement errors on the values obtained for both the light front radius and the depth of the light front origin. As stated above, the average deviation from sphericity, of the Cerenkov light arrival times observed in a shower, was about 4 ns. Simple considerations suggest that this corresponds to uncertainties of about 2 km in the light front radius values, and about 150 g cm^{-2} in the values of the depth of the light front origin. However, the exact interpretation of the timing measurement errors is a complex problem and is the subject of further studies currently being undertaken. Clearly, improving the accuracy of the timing measurements would be well worthwhile for future measurements of the curvature of the Cerenkov light front in extensive air showers.

4.8 Conclusions

The average characteristics of the Cerenkov light signals recorded in showers of energies in the range $0.11 < \rho(500)_{VE} < 4.33$ m^{-2}, and incident at zenith angles up to 65^{o}, have been measured. Variations of both the lateral light distribution and the light pulse shape, with shower energy and with shower inclination from the zenith, have been determined.

The steepness of the lateral Cerenkov light distribution is observed to vary with both shower energy and zenith angle. The spread of the light is broader in lower energy showers and also in more inclined showers.

The shape of the Cerenkov light pulses in vertically incident showers is slower than that of the light pulses in more inclined showers. However, variations of the light pulse shape with varying shower energy are not so clearly seen. This may be because the range of energies of the showers in which measurements have been made, is too small for any dependences to be readily apparent.

An attempt has been made to relate changes in shower energy and in shower inclination, to changes in depth of shower cascade development maximum. The sensitivities of the various Cerenkov light parameters to depth of shower cascade maximum that are derived from changes in shower energy, are similar to those determined from changes in shower zenith angle. An increase of 100 g cm^{-2} in the depth of shower cascade maximum, alters the values of several of the parameters by amounts which are greater than the uncertainties of individual measurements of the parameters. Estimates of depth of shower cascade maximum to within 100 g cm^{-2} should, therefore, be possible with the presently available measuring equipment.

The photon density at 200 m core distance is seen to be substantially independent of shower zenith angle and to vary only with shower energy. This supports the suggestions from recent computer simulations, that this quantity relates well to primary particle energy. Measurements of the photon density at 200 m core distance may, therefore, be a useful measure of the energy of those showers in which Cerenkov light measurements have been made, but for which no analyses of the Haverah Park deep water particle detector data are available.

The Cerenkov light arrival times measured in a small sample of showers have been found to be very well represented by spherically shaped light fronts. The thickness of atmosphere that each of the showers penetrated while "igniting", has been determined from the radii of these light fronts. These atmospheric thicknesses should be closely related to the early cascade developments of the showers, and light arrival time measurements made in a large sample of showers may be important for future studies of the mass of the primary cosmic radiation. Improving the accuracy of the timing measurements would be well worthwhile for such future studies.

CHAPTER FIVE

COMPARISON WITH COMPUTER SIMULATIONS AND OTHER WORK

In this Chapter, the average characteristics of the Cerenkov light in extensive air showers, that were reported in Chapter 4, are compared with results from the most recent computer simulations and with experimental measurements of other workers. The simulation results considered are those by Protheroe and Turver (1977), and the experimental measurements examined were made at the Yakutsk air shower array in U.S.S.R.

5.1 Comparison with the Computer Simulations by Protheroe and Turver (1977)

As mentioned in Chapter 2, Protheroe and Turver (1977) have simulated the average characteristics of the Cerenkov light produced in showers initiated by vertically incident protons, alpha particles, and iron nuclei, of energies 10^{16}, 10^{17} and 10^{18} eV. The results of these simulations suggest that while many of the observed characteristics of the light vary with both primary particle energy and mass, they do not uniquely reflect either of these quantities. The average features of the light are, however, well correlated with the depth of shower cascade development maximum. In the following comparison of theoretical and experimental results, the depths of the cascade maxima of the simulated showers are indicated, rather than the energies and masses of the primary particles. This makes it possible to comment on the depths of the cascade maxima of the real showers, in which the experimental measurements were made.

The experimental measurements of the present work need to be corrected to the case of vertically incident showers for comparison with the results of the simulations, which are for vertical showers only. It is also convenient to reduce the experimental data to

correspond to measurements made in showers of energies similar to those of the simulated showers. Equs.4.3 to 4.7 of the previous Chapter, and others like them, have been used to do this. The values of the lateral light structure function exponent, together with the values of the photon density and the various light pulse shape parameters at given core distances between 100 and 500 m, have been evaluated for vertical showers of energies $\rho(500)_{VE} = 0.2\ m^{-2}$ and $\rho(500)_{VE} = 2.0\ m^{-2}$. Direct comparison of the experimental and simulation results can then be made.

5.1.i The Lateral Cerenkov Light Distribution

It will be recalled from Chapter 2, that the simulation results suggest that depth of shower cascade development maximum is indicated by the extent of the lateral Cerenkov light distribution. The light is less widely spread in showers developing lower in the atmosphere, than it is in showers developing higher in the atmosphere. The exponent of a power law description of the lateral light distribution, increases monotonically with increasing depth of shower cascade development maximum.

The experimental values of the structure function exponents of the lateral Cerenkov light distributions, after correction to vertically incident showers of energies $\rho(500)_{VE} = 0.2\ m^{-2}$ and $\rho(500)_{VE} = 2.0\ m^{-2}$, are $\gamma = 2.16 \pm 0.13$ and $\gamma = 2.43 \pm 0.13$, respectively. According to the simulations, these values indicate depths of shower cascade maxima at $610 \pm 98\ g\ cm^{-2}$ and $810 \pm 98\ g\ cm^{-2}$ into the atmosphere. Fig.5.1 shows the simulation results for the lateral Cerenkov light distributions in showers of energies 10^{17} and 10^{18}eV, with cascade maxima at such atmospheric depths. The present experimental results, corrected to vertical shower incidence, are also given. The values of the photon density observed at various core distances between

Figure 5.1. Comparison of measurements of the lateral Cerenkov light distribution made in the present work, with results from the computer simulations by Protheroe and Turver (1977). The experimental measurements have been corrected to vertical showers of energies $\rho(500)_{VE} = 0.2\ m^{-2}$ and $\rho(500)_{VE} = 2.0\ m^{-2}$. The depths of the cascade development maxima of the simulated showers which resemble the experimental data closest, are indicated. (Note: the photon density scale refers to the simulation results only.)

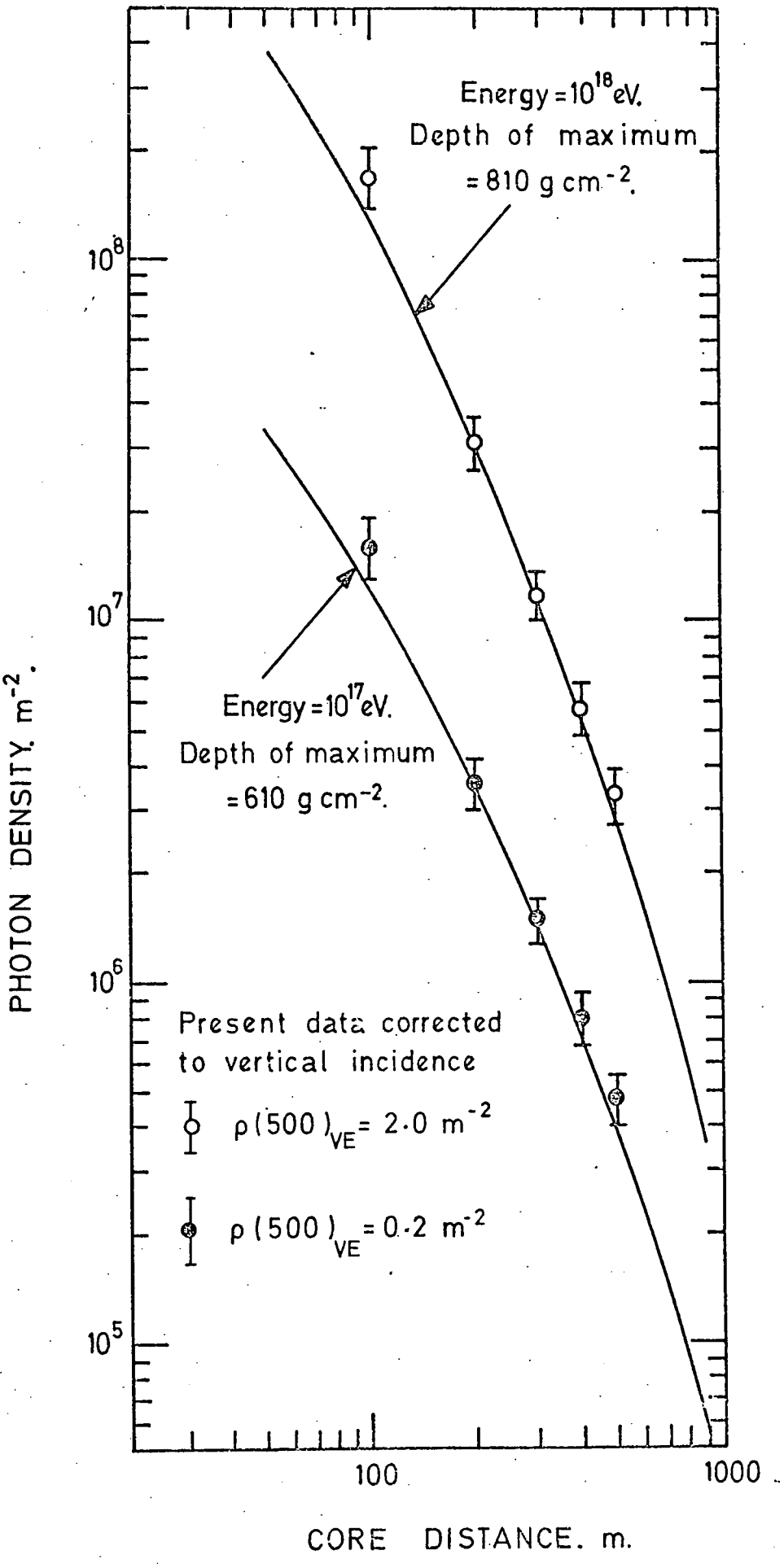
Energy = 10^{18} eV.
Depth of maximum
= 810 g cm^{-2}.
Energy = 10^{17} eV.
Depth of maximum
= 610 g cm^{-2}.
Present data corrected
to vertical incidence
$\rho(500)_{VE}$ = 2·0 m^{-2}
$\rho(500)_{VE}$ = 0·2 m^{-2}
10^8
10^7
10^6
10^5
100
1000
PHOTON DENSITY. m^{-2}.
CORE DISTANCE. m.

100 and 500 m are shown and the standard errors on these values are indicated by the error bars.

It is seen in fig.5.1 that the shapes of the lateral Cerenkov light distributions predicted by the simulations, are in excellent agreement with those observed in the present work. For the comparison of the shapes, the experimental results have been normalized at one point, by adjusting the ordinates of the measurements to make the photon density observed at 200 m core distance in the lower energy showers agree with the simulation data.

The photon density scale of fig.5.1 refers to the simulation results. Comparison with the measured photon density values, gives the result that the density of Cerenkov photons observed in showers with values of the Haverah Park array parameter of $\rho(500)_{VE} = 7.60\ m^{-2}$, is the same as the density predicted by the simulations (which incorporate the Feynman scaling hypothesis) for showers of energies around 10^{18}eV. However, this result should be regarded cautiously because the wavelength distribution of the photon source used for the absolute calibration of the experimental results is unknown, and may well be significantly different from the production spectrum of the Cerenkov photons, that is used in the simulations.

The dependence of the Cerenkov photon density on primary particle energy, predicted by the simulations, is confirmed by the experimental results without reference to an absolute calibration. Both the measured and simulated light distributions shown in fig.5.1 are for showers differing by one decade of primary particle energy. The predicted relative excess of the Cerenkov light in the higher energy showers, over that in the lower energy showers, is the same as that observed. This agreement does not depend on the normalization mentioned above.

5.1.ii The Cerenkov Light Pulse Shape

As was outlined in Chapter 2, depth of shower cascade development maximum is also indicated by the rise-time and the full-width-half-maximum of the Cerenkov light pulse, according to the simulation results. At all core distances, both these parameters increase monotonically with increasing depth of cascade maximum, although the variation of the pulse rise-time is much less than that of the full-width-half-maximum. The other light pulse shape parameters - the top-time and fall-time - also vary with depth of shower cascade development maximum, but not in such a simple way.

The experimental measurements of the four Cerenkov light pulse shape parameters, after correction to vertically incident showers of energies $\rho(500)_{VE} = 0.2\ m^{-2}$ and $\rho(500)_{VE} = 2.0\ m^{-2}$, are shown in figs.5.2(a) - (d). The values of each parameter observed at various core distances between 100 and 500 m are given, and the standard errors on these values are shown by the error bars. The results of the simulations are also shown in fig.5.2(a) - (d). For each pulse shape parameter, the predicted values which best describe the measured results are given, and the depths of shower cascade development maxima which lead to these values are indicated.

It is seen in fig.5.2(a) that the measured values of the Cerenkov light pulse rise-time are well represented by the simulation results for showers reaching maximum cascade development between 810 and 865 g cm^{-2} into the atmosphere.

Fig.5.2(b) shows that the measured Cerenkov light pulse top-time values indicate depths of shower cascade maxima at atmospheric levels between 650 and 695 g cm^{-2}, according to the simulations.

In fig.5.2(c) the measured values of the fall-time of the Cerenkov light pulse are seen to be reasonably well described by the

Figure 5.2. Comparison of measurements of the shape of the Cerenkov light pulse made in the present work, with results from the computer simulations by Protheroe and Turver (1977). The experimental measurements have been corrected to vertical showers of energies $\rho(500)_{VE} = 0.2\ m^{-2}$ and $\rho(500)_{VE} = 2.0\ m^{-2}$. For each pulse shape parameter, the depths of the cascade development maxima of the simulated showers which resemble the experimental data closest, are indicated.

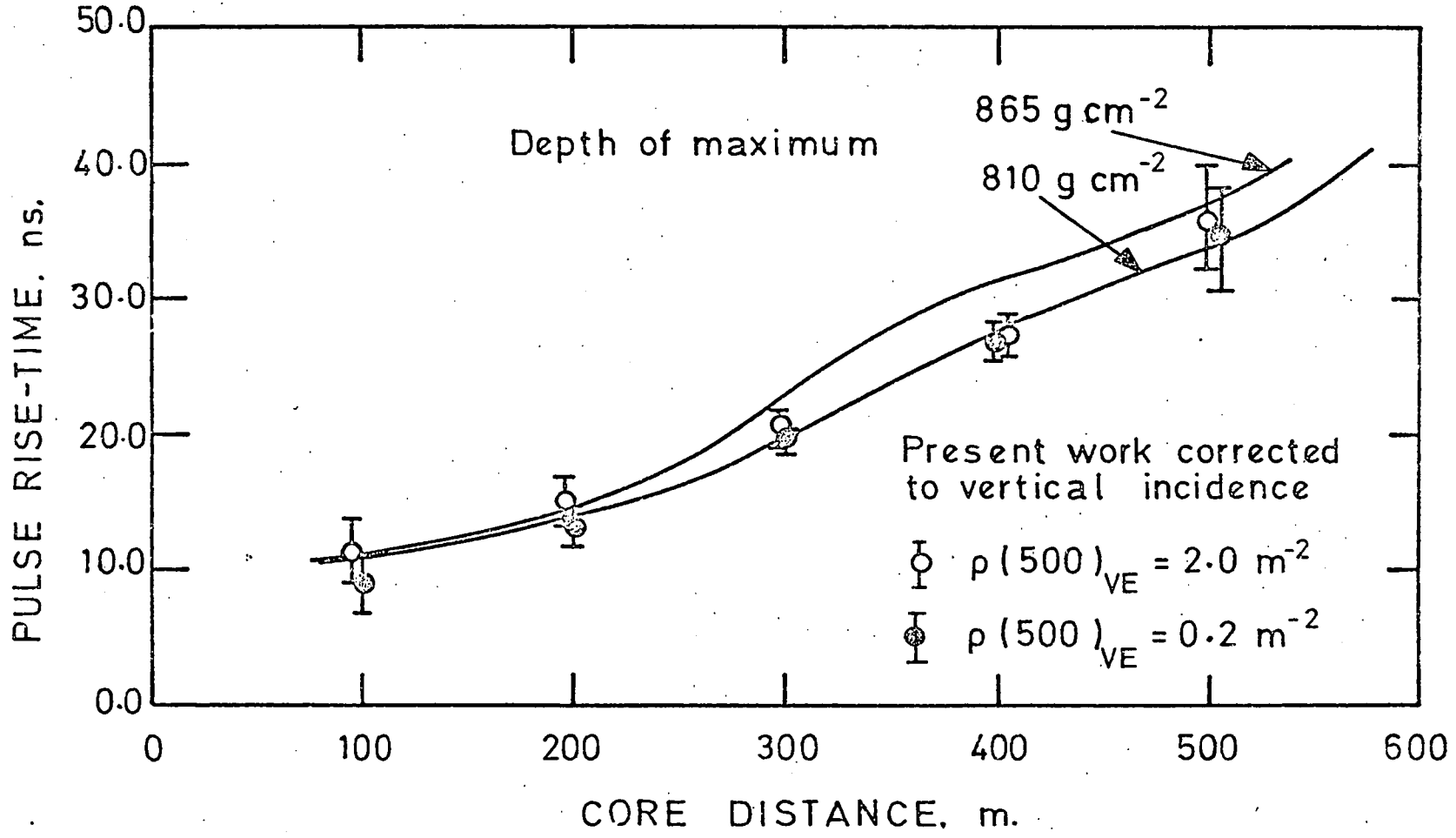
50·0
40·0
30·0
20·0
10·0
0·0
PULSE RISE-TIME, ns.
0
100
200
300
400
500
600
CORE DISTANCE, m.
Depth of maximum
865 g cm⁻²
810 g cm⁻²
Present work corrected
to vertical incidence
ρ(500)VE = 2·0 m⁻²
ρ(500)VE = 0·2 m⁻²

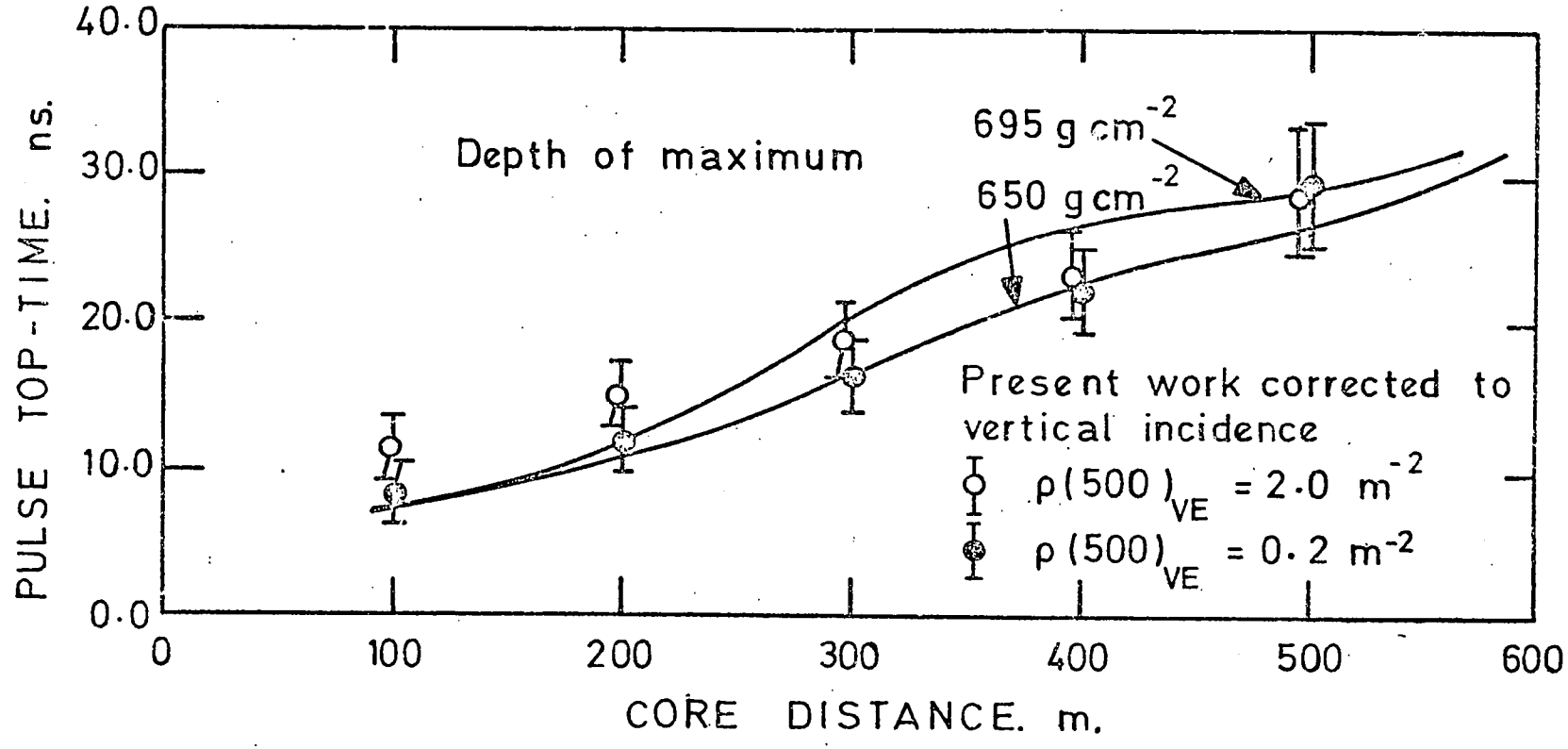
40·0
30·0
20·0
10·0
0·0
PULSE TOP-TIME. ns.
Depth of maximum
695 g cm^{-2}
650 g cm^{-2}
Present work corrected to vertical incidence
$\rho(500)_{VE}$ = 2·0 m^{-2}
$\rho(500)_{VE}$ = 0·2 m^{-2}
0
100
200
300
400
500
600
CORE DISTANCE. m.

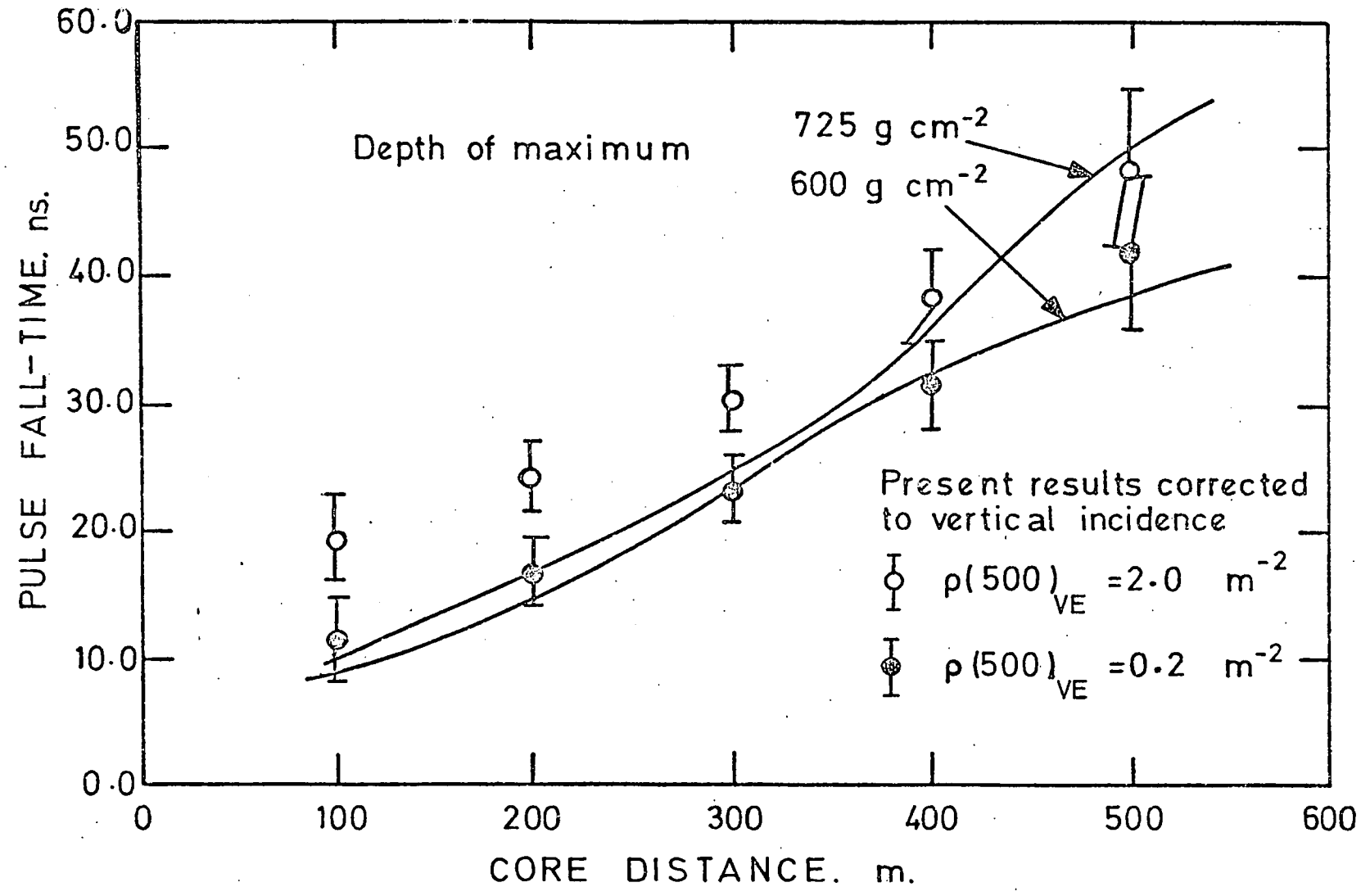
60·0
50·0
40·0
30·0
20·0
10·0
0·0
PULSE FALL-TIME. ns.
Depth of maximum
725 g cm-2
600 g cm-2
Present results corrected
to vertical incidence
ρ(500)VE =2·0 m-2
ρ(500)VE =0·2 m-2
0
100
200
300
400
500
600
CORE DISTANCE. m.

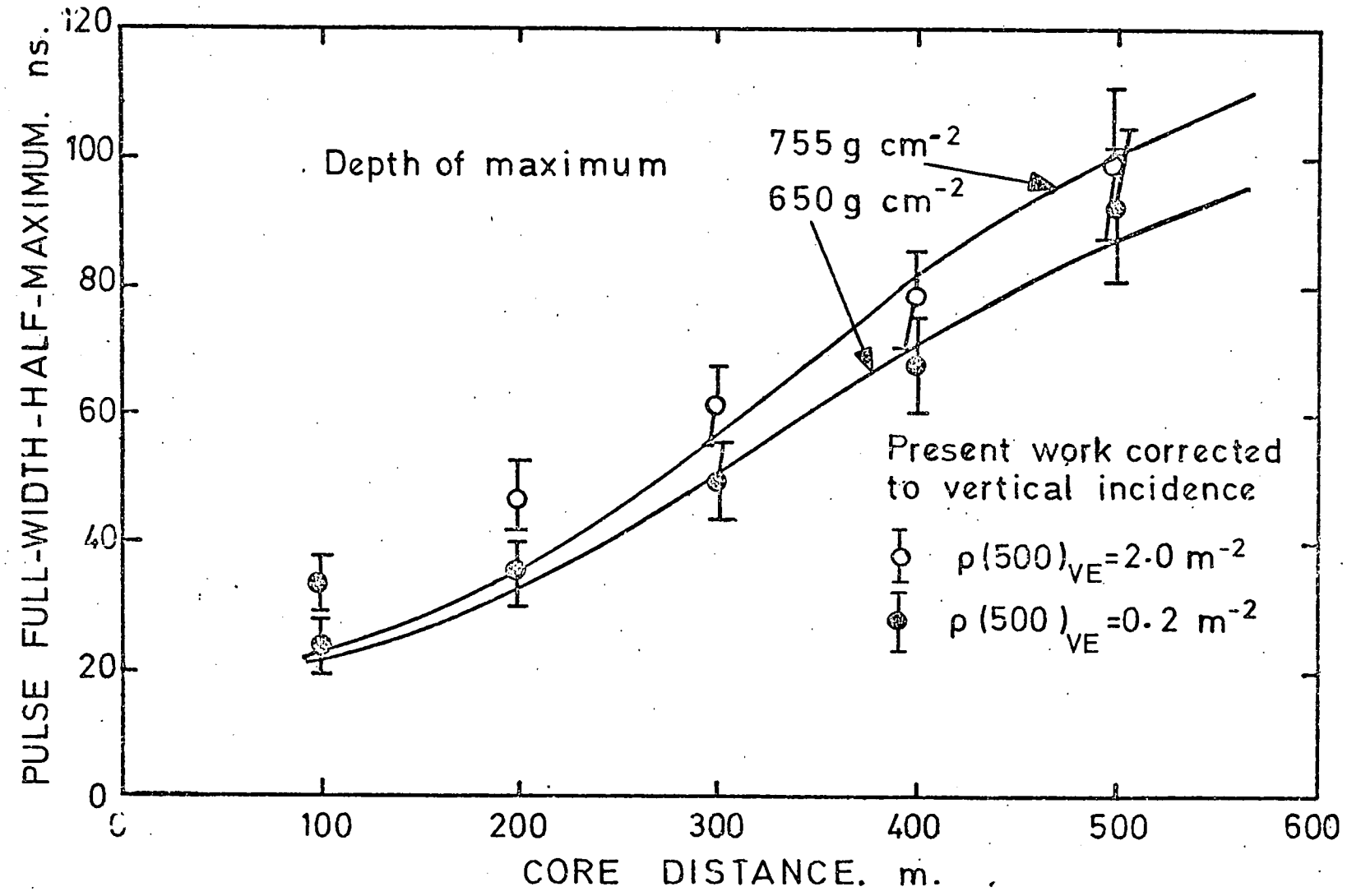
PULSE FULL-WIDTH-HALF-MAXIMUM. ns.
120
100
80
60
40
20
0
100
200
300
400
500
600
CORE DISTANCE. m.
Depth of maximum
755 g cm-2
650 g cm-2
Present work corrected to vertical incidence
ρ(500)VE=2·0 m-2
ρ(500)VE=0·2 m-2

simulation results for showers with depths of cascade development maxima between 600 and 725 g cm^{-2} into the atmosphere.

Lastly, the measured values of the Cerenkov light pulse full-width-half-maximum shown in fig.5.2(d), are in reasonable agreement with the simulation results for showers reaching maximum cascade development at atmospheric levels between 650 and 755 g cm^{-2}.

* * *

It is apparent in figs.5.2(a) - (d), that the experimental values of the pulse shape parameters at core distances less than 300 m in the higher energy showers, are consistently greater than the corresponding predicted values. (The light pulse fall-time and full-width-half-maximum show this most.) This may have been caused by an instrumental effect, and should not be regarded as evidence that the simulation results are incorrect. The light pulses observed close to the core in showers of these energies were the largest signals recorded, and it possible that they were slightly distorted by the signal amplifier. Amplifier distortion would broaden the signals, accounting for the apparent discrepancy. (Of course, at core distances greater than 300 m, the light signals are smaller, and would not have been at all distorted by the signal amplifier.)

5.1.iii Depth of Shower Cascade Development Maximum and Primary Particle Mass

In the previous two sections, estimates of the depths of the cascade development maxima of the showers studied in the present work, have been obtained by comparing experimental measurements with the results of the simulations by Protheroe and Turver (1977). A more detailed comparison is now made, in table 5.1. Shown here are the observed values of the various Cerenkov light parameters at 350 and 500 m core distance, after correction to vertical showers of

Table 5.1. The depths of shower cascade development maxima inferred by comparing the measured values of the various Cerenkov light parameters, with results from the simulations by Protheroe and Turver (1977). The experimental measurements have been corrected to vertical showers of energies $\rho(500)_{VE} = 0.2\ m^{-2}$ and $\rho(500)_{VE} = 2.0\ m^{-2}$.

Parameter	$\rho(500)_{VE} = 0.2$ m^{-2}		$\rho(500)_{VE} = 2.0$ m^{-2}	
	Observed value	Inferred depth of maximum	Observed value	Inferred depth of maximum
Structure funtion exponent	2.16 ± 0.13	610 g cm^{-2}	2.43 ± 0.13	810 g cm^{-2}
Rise-time at 350 m core distance	23 ± 2 ns	805 g cm^{-2}	24 ± 2 ns	810 g cm^{-2}
Rise-time at 500 m core distance	36 ± 4 ns	865 g cm^{-2}	35 ± 4 ns	860 g cm^{-2}
Top-time at 350 m core distance	19 ± 3 ns	640 g cm^{-2}	21 ± 3 ns	660 g cm^{-2}
Top-time at 500 m core distance	29 ± 4 ns	690 g cm^{-2}	29 ± 4 ns	690 g cm^{-2}
Fall-time at 350 m core distance	27 ± 3 ns	585 g cm^{-2}	34 ± 3 ns	650 g cm^{-2}
Fall-time at 500 m core distance	42 ± 6 ns	630 g cm^{-2}	48 ± 6 ns	690 g cm^{-2}
Full-width-half-maximum at 350 m core distance	59 ± 7 ns	655 g cm^{-2}	70 ± 7 ns	785 g cm^{-2}
Full-width-half-maximum at 500 m core distance	93 ± 12 ns	695 g cm^{-2}	99 ± 12 ns	750 g cm^{-2}
Average values		686 ± 31 g cm^{-2}		745 ± 25 g cm^{-2}

energies $\rho(500)_{VE} = 0.2\ m^{-2}$ and $\rho(500)_{VE} = 2.0\ m^{-2}$. The depths of shower cascade maxima inferred by comparing each of these experimental values with the simulation results, are also shown. It is seen that, with the possible exception of the light pulse rise-time, the observed values of all the Cerenkov light parameters measured in the showers of each energy, indicate fairly similar depths of shower cascade maxima. (The rise-time is the most difficult parameter to measure, and probably does not give such reliable estimates of depth of shower maximum as the other measurements.)

Taking the average of the values in table 5.1, gives the result that vertical showers of energy $\rho(500)_{VE} = 0.2\ m^{-2}$, reach cascade development maxima at an atmospheric depth of $686 \pm 31\ g\ cm^{-2}$, on average. Those of energy $\rho(500)_{VE} = 2.0\ m^{-2}$, reach cascade maxima at $745 \pm 25\ g\ cm^{-2}$. According to the simulations by Protheroe and Turver (1977), showers of these energies, reaching cascade development maxima at these atmospheric depths, are initiated by primary particles heavier than protons. However, this conclusion is entirely a consequence of the Feynman scaling model of the high energy nuclear physics, that is used in these simulations. Other plausible simulations which employ the model of the hadron cascade proposed by Cocconi et al. (1961) (e.g. the simulations by Smith and Turver (1973)) suggest that showers initiated by protons of such energies, can reach cascade development maxima at such atmospheric depths.

Thus, although comparison of the experimental results with model simulations gives an estimate of the average depth at which the showers studied in the present work reached cascade development maxima, no statement about the mass of the primary particles can be made. The most significant feature of the comparison, is the fact that simulated showers reaching cascade development maxima at one

particular atmospheric depth, give values of the various Cerenkov light parameters which are all in consistent agreement with the experimental results.

5.2 Comparison with other Measurements at Sea-Level

The results of the present work are now compared with measurements made at the Yakutsk air shower array, which like Haverah Park, is at sea-level.

5.2.i The Lateral Cerenkov Light Distribution

Measurements of the lateral Cerenkov light distribution made in the present work, are compared in fig.5.3 with results from the earlier work carried out at the Yakutsk array by Dim nstein et al. (1972). The measurements of the Russian workers shown, were made in showers of mean sea-level sizes $\bar{N} = 1.4 \times 10^7$ particles, and $\bar{N} = 1.7 \times 10^8$ particles, incident at zenith angles less than 30^o. From the present work, measurements made in showers of energies in the intervals $\rho(500)_{VE} < 0.3$ m^{-2} and $\rho(500)_{VE} > 1.25$ m^{-2}, and incident at zenith angles in the interval $25^o < \theta < 35^o$, are shown. (The data in these two intervals have average values of the Haverah Park array parameter of $\bar{\rho}(500)_{VE} = 0.194$ m^{-2} and $\bar{\rho}(500)_{VE} = 1.915$ m^{-2}, respectively.) The photon density values observed at various core distances between 100 and 500 m are given and the standard errors on these values are indicated by the error bars.

It is seen in fig.5.3 that the shapes of the lateral Cerenkov light distributions measured in the present work, agree very well with the shapes of those reported by Dim nstein et al. (1972). For the comparison of the shapes, the present experimental data have been normalized at one point, by adjusting the ordinates of the measurements so that the photon fluxes observed in the lower energy showers of each work agree at 200 m core distance.

Figure 5.3. Comparison of measurements of the lateral Cerenkov light distribution made at the Yakutsk air shower array by Diminstein et al. (1972), with measurements from the present work. (Note: the photon density scale refers only to the Russian work.)

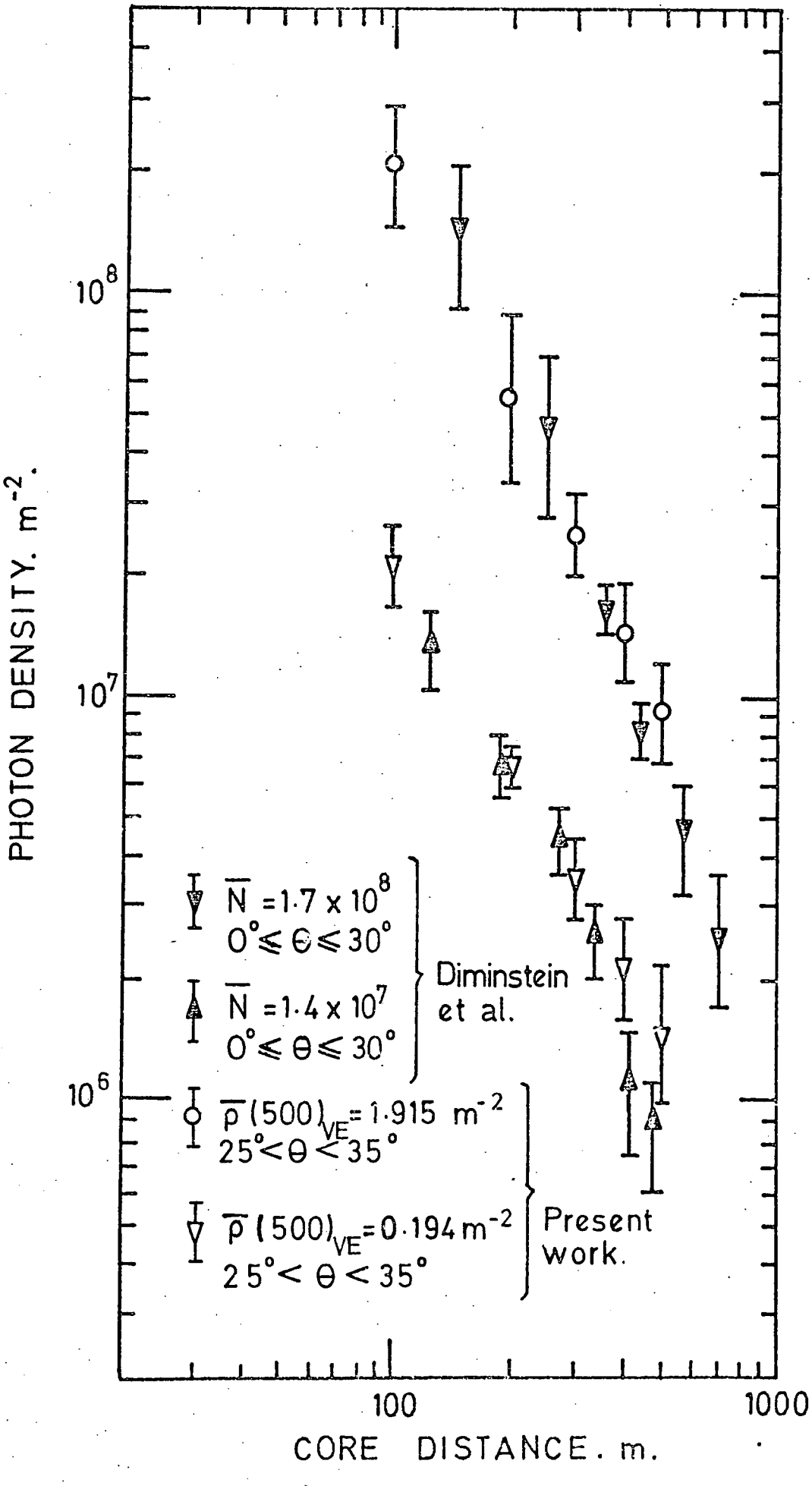
PHOTON DENSITY. m^{-2}.
10^8
10^7
10^6
$\bar{N} = 1.7 \times 10^8$
$0° \leq \theta \leq 30°$
$\bar{N} = 1.4 \times 10^7$
$0° \leq \theta \leq 30°$
Diminstein et al.
$\bar{\rho}(500)_{VE} = 1.915$ m^{-2}
$25° < \theta < 35°$
$\bar{\rho}(500)_{VE} = 0.194$ m^{-2}
$25° < \theta < 35°$
Present work.
100
1000
CORE DISTANCE. m.

The photon density scale of fig.5.3 refers to the results of the Russian workers. Comparison with the absolute light intensities observed in the present experiment, gives the result that the density of Cerenkov photons in showers with a value of the Haverah Park array parameter of $\rho(500)_{VE} = 1.00\ m^{-2}$, is the same as that in showers specified by a sea-level particle number of $N = 9.4 \times 10^6$, as measured by the Yakutsk array. However, comparing photon density measurements made by experiments employing photomultipliers that have different cathode quantum efficiencies and spectral responses, and that have been calibrated with different photon sources, is difficult. This result should, therefore, be regarded cautiously.

The variation of the Cerenkov photon density with changing Haverah Park array parameter value, and with changing sea-level particle size, can be compared without reference to the absolute calibration of each experiment. The results shown in fig.5.3 suggest that an increase of one decade in the value of $\rho(500)_{VE}$, increases the observed light intensity by the same proportion as increasing the sea-level particle size by 1.09 decades.

5.2.ii The Cerenkov Light Pulse Shape

The full-width-half-maximum is the only measure of the shape of the Cerenkov light pulse that has been investigated in other experiments. The first measurements of this parameter in showers of energies similar to those of the showers studied in the present work, were made at the Yakutsk array by Efimov et al. (1973). These measurements are compared with the present results in fig.5.4. The Russian data were measured in showers of sea-level sizes in the range $3 \times 10^6 < N < 3 \times 10^8$ particles, and have been corrected by the authors to correspond to measurements made in vertical showers with

Figure 5.4. Comparison of measurements of the Cerenkov light pulse full-width-half-maximum made at the Yakutsk air shower array by Efimov et al. (1973), with measurements from the present work. Both sets of data have been corrected to vertical shower incidence. The Russian results have been further corrected to correspond to measurements made with equipment of zero response time.

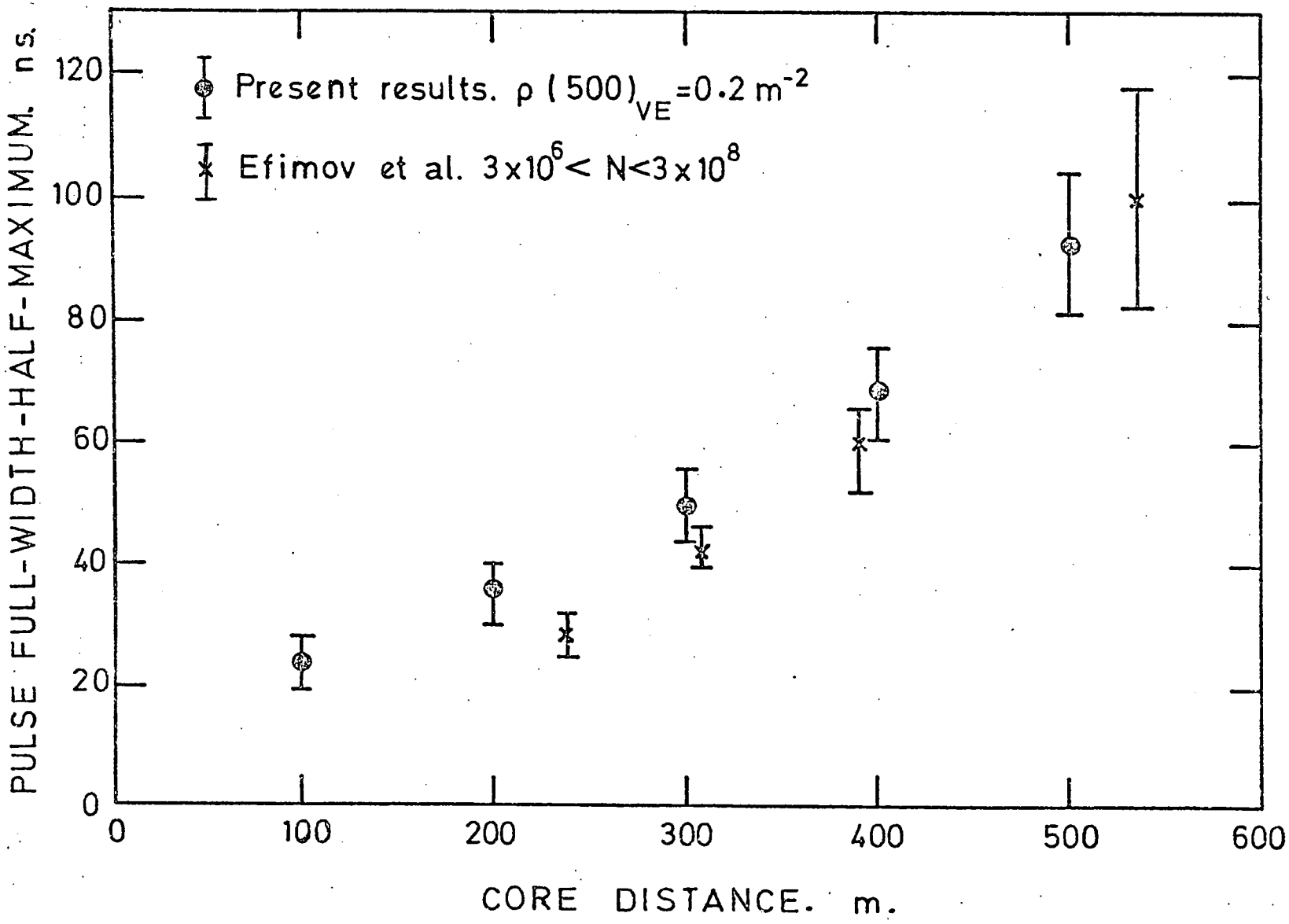
Present results. ρ (500)VE=0.2 m-2
Efimov et al. 3x10^6< N<3x10^8
PULSE FULL-WIDTH-HALF-MAXIMUM. ns.
CORE DISTANCE. m.
0
20
40
60
80
100
120
0
100
200
300
400
500
600

a system of zero response time. The measurements from the present work have been corrected to vertical showers of energy $\rho(500)_{VE}$ = 0.2 m^{-2}, but no attempt to remove the effect of the bandwidth of the recording equipment has been made. The values of the light pulse full-width-half-maximum observed at various core distances between 100 and 500 m are given and the standard errors on these values are shown by the error bars.

It is seen in fig.5.4 that the two sets of data are in good agreement, especially at core distances greater than about 300 m. Closer to the shower core than this, the light pulses observed in the present work are slightly wider, as expected, because of the effect of the bandwidth of the recording equipment.

5.3 Conclusions

The average characteristics of the Cerenkov light that have been measured in the present work, have been compared with model simulations and with other experimental results. The present experimental measurements are in good agreement with results from the simulations by Protheroe and Turver (1977). All the observed features of the Cerenkov light - the lateral light distribution and the details of the light pulse shape - are adequately described by the predicted light signals from showers reaching electron cascade development maxima, at atmospheric depths between about 686 and 745 g cm^{-2}. This estimate of depth of shower cascade development maximum, cannot however, be related to primary particle mass, without first making assumptions about the high energy nuclear physics occuring in shower hadron cascades.

The experimental results of the present work are in good agreement with available comparable measurements made at the Yakutsk air shower array in U.S.S.R.

CHAPTER SIX

MEASUREMENTS OF CERENKOV LIGHT IN INDIVIDUAL AIR SHOWERS

6.1 Introduction

In the previous Chapter, experimental measurements of the average characteristics of the Cerenkov light in extensive air showers, were compared with results from the computer simulations by Protheroe and Turver (1977). This comparison led to an estimate of the average depth in the atmosphere, at which the showers studied in the present work, reached cascade development maximum. However, any interpretation of this estimate, in terms of the masses of the primary particles which initiated the showers, depended entirely on assumptions about the nature of the high energy nuclear physics which took place in the showers.

Information about shower longitudinal development which is more directly related to primary particle mass composition, may be contained in the amounts by which individual Cerenkov light measurements fluctuate from the average characteristics of the light. Variations in the ways that the nucleons in shower cascades interact, cause showers to reach cascade development maxima at different atmospheric depths. The fluctuations in the values of shower parameters measured at ground level, arise from such variations in shower cascade development.

It is plausible that the primary particle mass itself, may be reflected by the fluctuations in the values of measured shower parameters. As outlined in Chapter 1, the mean free path of protons in air, is much larger than that of heavier particles, such as iron nuclei. The range of depths in the atmosphere at which primary protons initially interact, will therefore, be correspondingly larger than the range of atmospheric depths at which primary iron nuclei interact.

Variations in the depth at which the first interaction of the primary particle takes place, will cause showers to reach cascade development maxima at different atmospheric levels. This will be reflected by fluctuations in the values of the shower parameters measured at ground level.

According to many computer simulations, the fluctuations in showers initiated by protons, are about five times larger than those in showers initiated by iron nuclei. Furthermore, since it is only protons that can be expected to occasionally penetrate very deeply into the atmosphere before interacting, the presence of protons in the primary cosmic ray flux, would be indicated by extreme fluctuations in the values of shower parameters.

* * *

This Chapter is an attempt to demonstrate a means which might be used to evaluate the fluctuation values of Cerenkov light measurements. Fluctuation values are calculated here, by removing the recognisable effects of shower energy and zenith angle, from measurements made in individual showers. The average variation of the Cerenkov light parameters with core distance, shower energy and shower zenith angle, that were determined empirically in Chapter 4, are used to do this. It is assumed that the fluctuation values obtained, depend only on variations in shower cascade development caused by differences in the interactions of the nucleons in the shower cascades, and on the effects of measurement errors.

To investigate whether the calculated fluctuation values relate to shower cascade development, the correlations between the fluctuation values of several independent parameters, are studied. Then an attempt to quantify the differences between the cascade developments of showers, is made. Studies of the masses of the primary cosmic ray

particles, however, must await measurements of Cerenkov light in a much larger sample of showers. The procedures described in this Chapter, illustrate techniques for interpreting Cerenkov light data, that are presently being developed.

6.2 Fluctuations in the Cerenkov Light Measures

6.2.i Data Handling

The fluctuation values of the Cerenkov light signals measured in a sample of 25 showers have been studied. In each of these showers, light signals were recorded by at least five detectors, at core distances evenly distributed between 70 and 600 m. The showers in this small sample spanned a range of primary energy from $\rho(500)_{VE}$ = 0.11 m^{-2} to $\rho(500)_{VE}$ = 4.33 m^{-2}, and arrived at zenith angles less than 45^{o}.

The data of each shower was treated in a manner similar to that used in Chapter 4, for the determination of the average characteristics of the Cerenkov light in extensive air showers. A power law structure function was fitted to the photon density measurements, and the various light pulse shape measurements were expressed as exponential functions of core distance. (The correlation coefficients of these fits were all greater than 0.75, indicating critical significances less than 10%.) A spherical light front was fitted to the times at which the light pulses reached 10% of full amplitude. Fig.6.1 illustrates the complete set of information contained in the Cerenkov light measurements made in a typical individual shower.

Five independent Cerenkov light parameters were evaluated for each shower studied:-

(i) The exponent, γ, of the power law structure function fitted to the photon density measurements made at core distances between 70 and 600 m.

Figure 6.1. The complete set of information contained in the Cerenkov light measurements made in a typical individual shower. Five independent parameters can be evaluated from this information.

EVENT NO: 516 826.

θ 24°

ϕ 327°

$\rho(500)_{VE}$ 0·90 m^{-2}

RADIUS OF LIGHT FRONT CURVATURE 13216 m

DEPTH OF ORIGIN OF LIGHT FRONT 212 g cm^{-2}

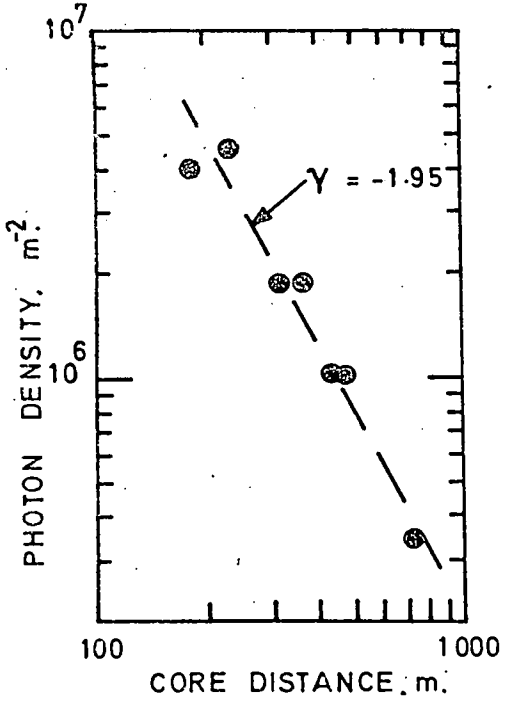

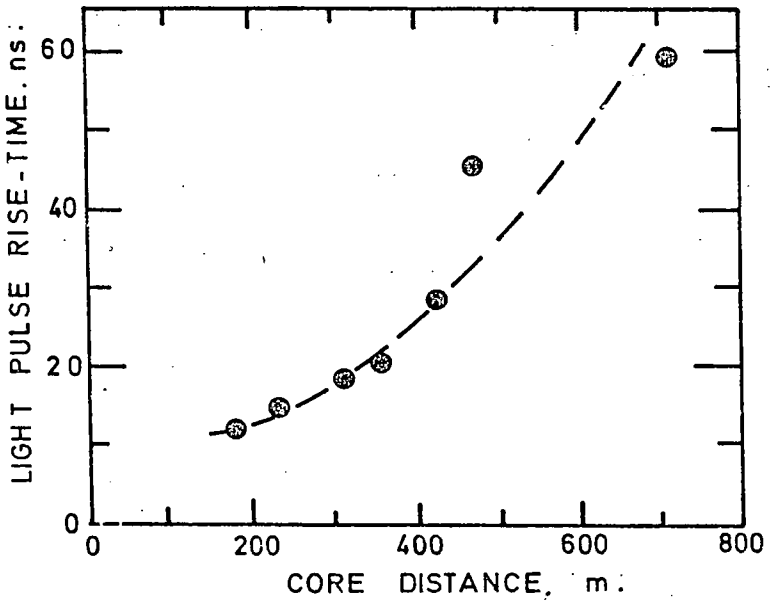

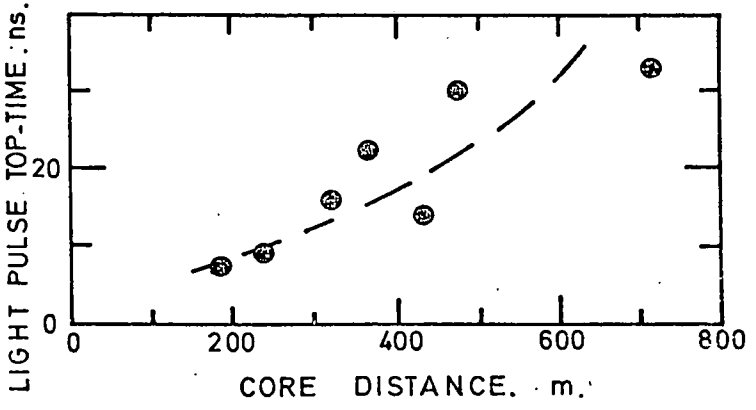

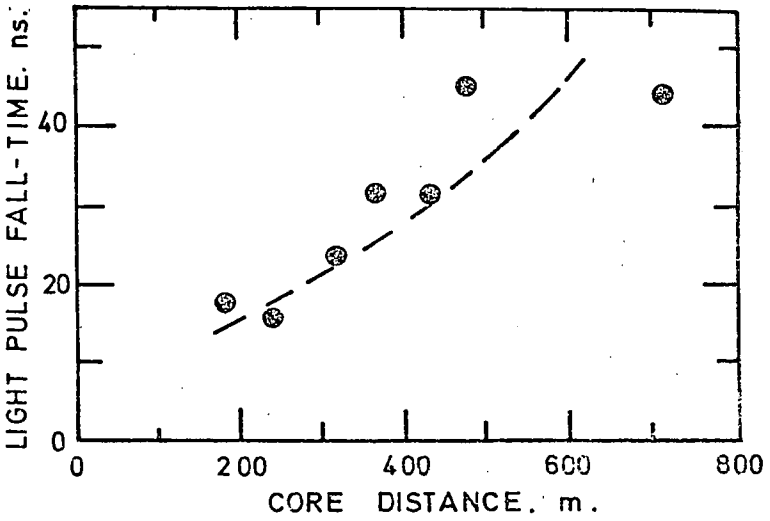

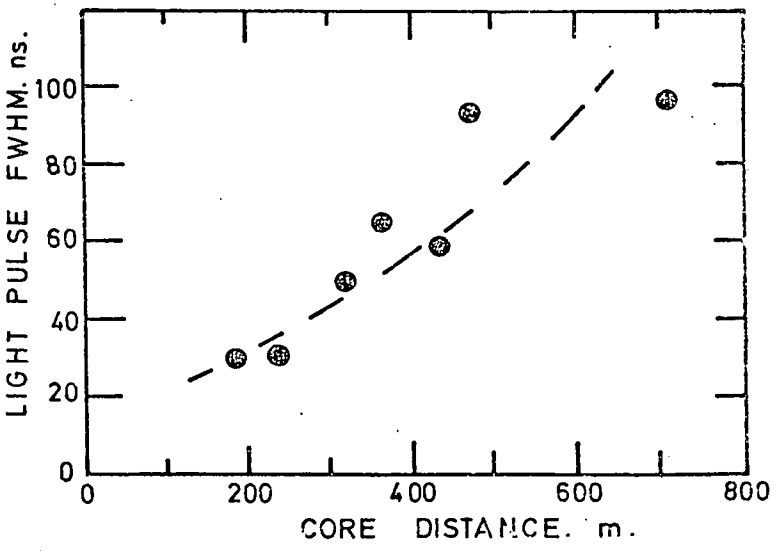

(ii) The light pulse rise-time at a core distance of 400 m (evaluated from the exponential expression fitted to the rise-time measurements).

(iii) The light pulse top-time at 400 m core distance.

(iv) The light pulse fall-time at 400 m core distance.

(v) The thickness of atmosphere (in g cm^{-2}) through which the shower penetrated while producing those Cerenkov photons which reached ground level before the observed light pulses reached 10% of full amplitude. (This is calculated from a knowledge of the radius of the Cerenkov light front and the shower zenith angle, as explained in Chapter 4.)

These quantities are an exhaustive list of the independent parameters that can be evaluated from the Cerenkov light data alone, since together they fully specify the area, shape and relative time of arrival of the light pulses observed in each shower.

6.2.ii Calculating the Fluctuation Values

The fluctuation values of the independent Cerenkov light parameters, were computed by calculating the deviations of individual measurements of the parameters, from appropriate average values of the parameters. The average values needed for the calculation, were derived from the average characteristics of the Cerenkov light in extensive air showers, that were established in Chapter 4. Equs.4.3 to 4.6 were used to determine the average values of the lateral light structure function exponent, and those of the light pulse rise-time, top-time and fall-time at 400 m core distance, that were appropriate to the energies and zenith angles of each of the showers studied. Differencing these average values and the individual measurements removed the effects of shower energy and zenith angle, leaving the

fluctuation values.

For the case of the depth of the light front origin, no allowance for the effects of shower energy and zenith angle was necessary. As discussed in Chapter 4, this quantity does not depend on shower zenith angle, and is observed to be substantially independent of shower energy. The fluctuation values of the depth of the light front origin were given directly, by differencing individual measurements of the parameter and the average value of the parameter, arrived at in Chapter 4.

The fluctuation values obtained in the ways described above, were independent of shower energy and zenith angle. They were assumed to depend only on variations in the cascade developments of individual showers, caused by differences in the details of the interactions of the nucleons in the nuclear cascades of the showers, and on the effects of measurement errors. The fluctuation values of the independent Cerenkov light parameters, provide five independent measures of shower cascade development.

To quantify the typical amounts by which variations in shower cascade development cause the measured Cerenkov light parameters to fluctuate, the distributions of the fluctuation values of each of the parameters were examined. The standard deviations of these distributions are shown in table 6.1.

It is seen in table 6.1, that the typical fluctuation values are not large compared with the precision with which the Cerenkov light parameters are measured. Further evidence to substantiate the assumption that the fluctuation values reflect variations in shower cascade development, is therefore needed. This evidence is sought in the next section, by studying the correlations between the independent fluctuation values measured in each shower. Then, in the last section,

	Standard deviation of the distribution of fluctuation values
Structure function exponent,	0.38
Rise-time at 400 m core distance	5.6 ns
Top-time at 400 m core distance	4.5 ns
Fall-time at 400 m core distance	8.2 ns
Depth of origin of light front	141 g cm^{-2}

Table 6.1. Typical fluctuations in the values of the independent Cerenkov light parameters, caused by variations in shower cascade development.

(Fluctuation values were calculated by removing the effects of shower energy and zenith angle from individual measurements of the parameters. For each parameter, the standard deviation of the distribution of these fluctuation values, is shown here.

the magnitudes of the fluctuation values, are related to variations in depth of shower cascade development maximum.

6.2.iii Correlations Between Independent Fluctuation Values.

More evidence that the various fluctuation values reflect variations in shower cascade development, would be provided if the independent fluctuation values measured in each individual shower, were found to be correlated. Such correlations would show that it is possible to resolve the effects of variations in shower cascade development, from the effects of measurement error.

In Chapter 4, the average characteristics of the Cerenkov light in extensive air showers were established. There, relating changes in shower energy and zenith angle, to changes in depth of shower cascade development maximum, indicated that in showers developing deeper in the atmosphere than usual:-

(i) The lateral light distributions are steeper (i.e. the values of the structure function exponent, γ, are larger);

(ii) The light pulse rise-times are slower;

(iii) The light pulse top-times are slower;

(iv) The light pulse fall-times are slower.

(v) In addition, the depths of the light front origins in showers developing deeper into the atmosphere will be greater.

If the fluctuation values of the independent Cerenkov light parameters measured in individual showers, reflect shower cascade development, they should be related in the same way as the average characteristics of the light.

To investigate the relations between the fluctuation values of the independent Cerenkov light parameters, it was necessary to express

each of the fluctuation values in equivalent units. This was achieved by making use of the sensitivities of the average values of the Cerenkov light parameters, to depth of shower cascade development maximum. These sensitivities were established in Chapter 4 and are shown in table 4.3. The mean of the two values given for each parameter in the table, was used to relate the fluctuation values of the parameter, to equivalent changes in depth of shower cascade development maximum (in g cm^{-2}). (The fluctuation values of the depth of the light front origin, were already expressed as thicknesses of atmosphere and so were not treated in this way.)

Two tests were then used to study the relations between the fluctuation values of the independent Cerenkov light parameters. Firstly, an "f-ratio" analysis of variance, showed that the variance of the samples consisting of the five independent fluctuation values obtained for each shower, was 2.3 times smaller than the variance between different shower samples. This corresponded to a probability of less than 0.5%, that within shower effects (which were due to experimental measurement errors) completely accounted for between shower effects (which therefore, must have been due in part to variations in shower cascade development).

Secondly, the correlation coefficients between the fluctuation values of pairs of the independent parameters were calculated. These are shown in table 6.2. For the size of sample considered, correlation coefficients greater than 0.34 are significant at the 10% level, and it is seen that there are 4 such correlations.

The two tests indicate that, despite the effects of experimental measurement errors, there are weak correlations between the fluctuation values of the independent Cerenkov light parameters measured in individual showers. The set of five fluctuation values obtained for a

	Structure function exponent	Rise-time at 400 m core distance	Top-time at 400 m core distance	Fall-time at 400 m core distance	Depth of origin of the light front
Structure function exponent	1.00	0.04	0.03	-0.45	0.22
Rise-time at 400 m core distance		1.00	0.09	0.13	0.51
Top-time at 400 m core distance			1.00	0.45	0.23
Fall-time at 400 m core distance				1.00	0.34
Depth of origin of the light front					1.00

Table 6.2. The correlation coefficients between the fluctuation values of the independent Cerenkov light parameters. Each parameter is an independent measure of shower cascade development. (For the sample size considered, coefficients greater than 0.34 are significant at the 10% level.)

shower, when considered together, enable the effects of variations in shower cascade development, to be resolved from the effects of experimental measurement errors. A larger sample of data would establish the correlations between the independent fluctuation values with more certainty.

6.2.iv Relating the Fluctuation Values to Variations in Shower Development

Having established in the previous section, that the fluctuation values of the various Cerenkov light parameters arise, at least in part, from variations in the cascade developments of individual showers, consideration was given to the magnitudes of the fluctuation values. The sizes of the fluctuation values were used to estimate the range of atmospheric depths over which showers reach cascade development maxima, as a result of variations in the nucleon interactions in their cascades.

For each shower studied, the deviation of the depth of the cascade development maximum, from an appropriate (but unspecified) average depth, was estimated. The fluctuation values of the five independent parameters measured in each shower, were treated in the manner described in the previous section. Each of the fluctuation values was related to an equivalent change in depth of shower cascade maximum, by using the sensitivities of the average values of the Cerenkov light parameters, to depth of shower maximum. The mean of the five values so obtained for each shower, was the best estimate of the deviation from average, of the position of the shower cascade development maximum.

The distribution of the deviations of the depths of the shower cascade maxima, had a standard deviation of 111 g cm^{-2}. This then, is an indication of the amount by which the depths of shower cascade development maxima vary, owing to variations in the

nucleon interactions in the shower cascades. The value is an upper limit, since it includes an, as yet, undetermined error of measurement. It was derived without recourse to any specific simulation results and, with the exception of information from analyses of the Haverah Park particle detector data, was based only on Cerenkov light measurements.

6.3 Conclusions

The fluctuation values of various Cerenkov light parameters measured in a small sample of showers have been examined. It has been demonstrated that these fluctuation values contain information about shower cascade development which is additional to the information derived from the average characteristics of the Cerenkov light in extensive air showers.

The fluctuation values have been calculated by removing the recognisable effects of shower energy and zenith angle from measurements made in individual showers. Correlations between the fluctuation values of independent parameters, have shown that it is possible to resolve the effects of variations in the details of shower cascades, from the effects of measurement errors. The estimates of the average sensitivities of the Cerenkov light parameters, to depth of shower cascade development maximum, have been used to relate the fluctuation values to changes in depth of cascade maximum. In this way, an upper limit of 111 g cm^{-2}, was obtained for the range of depths over which showers reach cascade development maxima, as a result of variations in the nucleon interactions in their cascades.

Perhaps the most significant feature of the fluctuation measurements is that information on the cascade developments of individual showers is obtained, without recourse to any detailed simulation results. Measurements of the fluctuation values of

Cerenkov light parameters made in a large sample of showers may well, therefore, play a useful rôle in further studies of the masses of the primary cosmic ray particles. The sample of data considered here, however, is much too small to begin such studies.

CHAPTER SEVEN

CONCLUSIONS AND FURTHER CERENKOV LIGHT DETECTION EXPERIMENTS

It has been clearly demonstrated that the Cerenkov light that is produced in large extensive air showers, can be readily observed with an array of simple light detectors and an analogue signal recording system. Measurements of the lateral distribution of the light, the shape of the light pulses, and the arrival time of the light have been made with such equipment, operated at the Haverah Park air shower array. The indications are that these measurements contain very detailed information about air showers.

Further work by the Durham University group to fully exploit the potential of Cerenkov light measurements is already underway. During the preparation of this thesis, portable light detectors have been operated at an established air shower array in U.S.A. A completely new method of analysing Cerenkov light data, in a manner which gives direct information on shower cascade development, has been developed. More sophisticated Cerenkov light detection equipment, which is to be operated independently at a site with good seeing conditions, has been constructed and is being installed.

7.1 Conclusions from the Present Work

The characteristics of the Cerenkov light averaged over many showers of energies around 5×10^{17} eV have been established. Measurements of both the photon density and the details of the light pulse shape have been made at core distances up to about 600 m. The curvature of the Cerenkov light front has also been determined, from measurements of the arrival times of the light made in a small sample of showers. The dependences of the average characteristics of the light on shower energy and zenith angle have been quantified. This has led to estimates of the sensitivities of the various Cerenkov light

parameters, to variations in depth of shower cascade development maximum. The data measured in the present work compare well with earlier measurements, where such comparisons may be made.

The measured average features of the Cerenkov light are in good agreement with the predictions from the simulations of shower development by Protheroe and Turver (1977). The comparison of the experimental and theoretical results has shown that, on average, the showers studied in the present work penetrated between 686 and 745 g cm^{-2} of atmosphere, before reaching cascade development maxima. While this estimate is not strongly affected by the details of the simulations, its interpretation in terms of primary particle mass, however, depends entirely on the model of the high energy nuclear physics that is used in the simulations.

It has been shown that further information on the cascade developments of air showers, is contained in the fluctuation values of Cerenkov light parameters. The fluctuation values of various parameters have been calculated, by removing the recognisable effects of shower energy and zenith angle from measurements of the parameters made in a small sample of individual showers. The fluctuation values of independent parameters have been found to be weakly correlated, and this has been taken as evidence that the fluctuations arise from variations in the details of the cascade developments of the individual showers. The estimates of the average sensitivities of the Cerenkov light parameters, to depth of shower cascade development maximum, have been used to relate the fluctuation values to changes in depth of cascade maximum. In this way, an upper limit of 111 g cm^{-2} for the range of depths over which showers reach cascade development maxima, as a result of variations in the nucleon interactions in their cascades, was obtained, without recourse to detailed simulation results.

The measurements made in the present work suggest that the shower information that is presently obtained from analyses of the Haverah Park particle detector data, should also be available from Cerenkov light measurements alone. Already, a Cerenkov light measure of shower energy - the photon density at 200 m core distance - has been identified. Cerenkov light measurements made with an array of several detectors, should also give information on shower core locations, since several parameters have been found to vary monotonically with core distance. Accurate shower arrival directions can be obtained from the measurements of the times at which the Cerenkov light arrives at the various detector positions. In fact, the feasibility of using the measurements made in the present work, for this sort of shower analysis, is currently being investigated and will be reported by Hammond et al. (1977).

The observation of Cerenkov light in extensive air showers, is now well established at Haverah Park. During the preparation of this thesis, the light detector array has continued to operate, essentially in an unaltered form. However, one important change to the equipment has been made and is worth mentioning here. The times of arrival of the Cerenkov light at the detectors, are now measured with greater precision. Improved real-time coincidence marker pulses at the starts of the timebase sweeps of the recording oscilloscopes, enable timing measurements to within 2 ns to be achieved. The measurements of the curvature of the Cerenkov light front are now much more precise than those described in this thesis.

The continued operation of the Cerenkov light detector array at Haverah Park, would be in conjunction with other new experiments there, which will also give information about shower cascade development. These experiments are the Durham University muon arrival

direction experiment (see Gibson (1976)): the "array infilling" experiment, conducted jointly by Durham and Leeds Universities (see Edge et al. (1977)): and the deep water particle detector pulse profile experiment (see Wild (1975)). Information from a number of experiments should give a much greater insight into the problems of determining the details of shower cascade development and primary particle mass, than the information from any one experiment. Ideally, in a finite sample of showers, Cerenkov light measurements would be available, as well as data from these other experiments. However, the low duty cycle for Cerenkov light observation in the British climate, makes this possibility rather remote.

7.2 A New Method of Analysing Cerenkov Light Measurements

As already stated, the results presented in this thesis indicate that it should be quite feasible to employ the methods currently used for the analysis of the Haverah Park particle detector data, to find arrival directions, core locations, and energies of showers, purely from Cerenkov light measurements. However, a new method of analysing Cerenkov light measurements, in a way that gives more direct information on shower cascade development, has recently been proposed. Details of the shapes of the light pulses registered by several well spaced detectors are used to accurately reconstruct images of shower cascades.

The computer simulations by Protheroe and Turver (1977), indicate that at core distances greater than about 100 m, the temporal structures of the Cerenkov light pulses observed in a shower, mirror the development of the shower. The first light to reach ground level is produced highest in the atmosphere. The light at any given point on each light pulse profile, is produced at a particular stage of the shower development and originates from a compact region of the atmosphere.

In the present work, spherical light fronts have been fitted to measurements of the relative times at which the Cerenkov light in a shower arrived at the various detector positions. The timing measurements were made to the points on the light pulse profiles at which 10% of full amplitude was reached. The new analysis method extends this procedure by also fitting spherical light fronts to other points on the light pulse profiles - the 50% and 90% of full amplitude levels, on both the leading and trailing edges. The radii of these light fronts determine the positions in the atmosphere of various stages of shower cascade development, and allow an image of the shower cascade to be constructed. Furthermore, the shower core is represented by the path through the light front centres of curvature. From this, the arrival direction of the shower, and the impact point of the core on the ground plane, can be determined without any reference to the photon densities at the detector positions.

This method of analysing Cerenkov light measurements seems particularly appropriate for further studies aimed at determining primary particle mass, since it gives such direct information on shower cascade development. A more detailed discussion of the analysis procedure, together with preliminary results obtained by analysing a small sample of suitable showers selected from the data recorded in the present work, have been presented by Orford and Turver (1976). As far as the design of an experiment to observe Cerenkov light is concerned, the salient point is that, should this method of analysis be used for dealing with showers recorded in the future, good timing measurement accuracy will become much more important than precise detector gain measurement.

7.3 Further Cerenkov Light Detection Experiments

The Durham University group is now involved with two further

experiments to detect the Cerenkov light in large cosmic ray showers. One of these has already been carried out, and the other is presently under construction. Both the experiments involve taking portable light detectors to overseas sites.

The first of the experiments was to make Cerenkov light measurements at a different altitude from that of Haverah Park. Equipment was operated for a period of about three weeks at the Volcano Ranch air shower array, in New Mexico, U.S.A., which is at an atmospheric depth of 834 g cm^{-2}. Four light detectors and an analogue signal recording system, that were very similar to the equipment described in this thesis, were used to make measurements of the Cerenkov photon density at 200 m core distance, in showers recorded by the Volcano Ranch array. The results of the experiment are soon to be described by Waddoup (1977). A possible extension of this work would be to make similar Cerenkov light measurements at the world's other established air shower arrays.

The second experiment, at present under construction, is to make measurements of Cerenkov light in a large sample of showers, and to use them for further studies of shower cascade development and primary particle mass. Eight light detectors have been dispatched to a site with good seeing conditions, in Utah, U.S.A. These will be operated independently of any established air shower array, and coincidences between the light signals registered by the various detectors, will be used to trigger the system. The light signals detected will be recorded completely digitally, facilitating the handling of a large sample of data. The bandwidth of the system will be higher than that of the equipment described in this thesis, enabling the shapes of light pulses registered at shorter core distances to be faithfully recorded. The showers detected will be analysed

solely on the basis of the Cerenkov light measurements, in all probability by using the new analysis method described in section 7.2, above.

* * *

In closing, it is fair to say that the work described in this thesis has established the techniques necessary to make detailed measurements of the Cerenkov light in large extensive air showers. The work has given rise to a number of new experiments, and the data obtained have been used for preliminary testing of a new method of shower analysis. While the present work goes no further than to present initial results on shower cascade development, the indications are, that the future measurements of Cerenkov light in a large sample of showers, should make a significant contribution to the identification of the masses of high energy primary cosmic ray particles.

REFERENCES

Allan, H.R., Jones, J.K., Mandolezi, N., Prah, J.H. and Shutie, P., (1971), Proc. 12th Int. Conf. on Cosmic Rays, 3, 1102.

Allen, C.W., (1955), Astrophysical Quantities (2nd Edition), The Athlone Press, University of London, 134.

Anderson, C.D., (1932), Science, 76, 238.

Auger, P., Maze, R. and Grivet-Mayer, T., (1938), G.R. Acad. Sci. Paris, 206, 1721.

Blackett, P.M.S., (1948), Emission Spectra of the Night Sky and Aurora, Physical Society of London Gassiot Committee Report, 34.

Blackwell, D.E., Ingham, M.F. and Rundle, H.N., (1960), Astrophys. J., 131, 15.

Blake, P.J., Armitage, M.L. and Nash, W.F., (1973), Proc. 13th Int. Conf. on Cosmic Rays, 4, 2539.

Boley, F.I., (1964), Rev. Mod. Phys., 36, 792.

Cerenkov, P.A., (1934), Dokl. Akad. Nauk, 2, 451.

Cerenkov, P.A., (1937), Phys. Rev., 52, 378.

Chudakov, A.E., Nesterov, N.M., Zatsepin, V.I. and Tukish, E.I., (1960), Proc. Moscow Conf. on Cosmic Rays, 2, 50.

Cocconi, G., Koester, L.G. and Perkins, D.H., (1961), Lawrence Radiation Lab. Seminars, 28, pt.2, UCID-144, 1.

Diminstein, O.C., Kolosov, V.A., Krasilnikov, D.D., Kusmin, A.I., Kulakovskaya, V.P., Orlov, V.A., Sleptsov, I.Ye., Yefimov, N.N., and Yegerov, T.A., (1972), paper presented to the European Symposium on Air Showers, Paris.

Dixon, H.E., (1974), Ph.D. Thesis. University of Durham.

Dixon, H.E., Machin, A.C., Pickersgill, D.R. and Turver, K.E., (1974), J. Phys. A., 7, 1016.

Dyakanov, M.N., Knurenko, S.P., Kolosov, V.A., Krasilnikov, D.D., Kulakovskaya, V.P., Kuzmin, A.I., Orlov, V.A., Sleptsov, I.Ye., Yefimov, N.N. and Yegorov, T.A., (1973), Proc. 13th Int. Conf. on Cosmic Rays, 4, 2389.

Edge, D., (1974), Ph.D. Thesis. University of Leeds.

Edge, D.M., Lapikens, J., McComb, T.J.L., Reid, R.J.O., Ridgway, S., Turver, K.E., Watson, A.A. and Wray, A.M., (1977), Proc. 15th Int. Conf. on Cosmic Rays.

Efimov, N.N., Krasilnikov, D.D., Khristiansen, G.B., Shikalov, F.V. and Kuzmin, A.I., (1973), Proc. 13th Int. Conf. on Cosmic Rays, 4, 2378.

Elterman, L., (1968), Air Force Cambridge Research Labs. Ref. AFC RL-68-0153.

Feynman, R.P., (1969), Phys. Rev., Letters, 23, 1415.

Fowler, P.H., Adams, R.A., Cowen, V.G. and Kidd, J.M., (1967), Proc. Roy. Soc. A, 301, 39.

Frank, I.M. and Tamm, Ig., (1937), Dokl. Akad. Nauk, 14, 109.

Galbraith, W. and Jelley, J.V., (1953), Nature, 171, 349.

Gibson, A.I., (1976), M.Sc. Thesis. University of Durham.

Grigorov, N.L., Gubin, Yu.V., Rapoport, I.D., Savenko, I.A., Yakovlev, S.M., Akimov, V.V. and Nesterov, V.E., (1971), Proc. 12th Int. Conf. on Cosmic Rays, 5, 1746.

Grigorov, N.L., Nesterov, V.E., Rapoport, I.D., Savenko I.A. and Skuridin, G.A., (1967), Proc. 10th Int. Conf. on Cosmic Rays, A, 512.

Hammond, R.T., Orford, K.J., Shearer, J.A.L., Turver, K.E., Waddoup, W.D. and Wellby, D.W., (1977), to be published.

Hartman, D. and Weekes, T.C., (1976), Private Communication.

Hess, V.F., (1912), Phys. Z., 13, 1084.

Jelley, J.V., (1958), Cerenkov Radiation and its Applications, Pergamon Press, London.

Jelley, J.V., (1967), Proc. Cosmic Ray Phys., 10, 41.

Kolhorster, W., (1914), Ber deutsch. Phys. Ges., 16, 719.

Kolhorster, W., Matthes, I. and Webster, E., (1938), Naturwissenschaften, 26, 576.

Kriegar, A.S. and Bradt, H.V., (1969), Phys. Rev., 185, 1629.

La Pointe, M., Kamata, K., Gaebler, J., Escobar, I., Domingo, V., Suga, K., Murakami, K., Toyoda, Y. and Shibata, S., (1968), Can. J. Phys., 46, 569.

Messel, H. and Crawford, D.F., (1969), Electron-Photon Shower Distribution Function - Tables for Lead, Copper and Tin Absorbers, Pergamon Press, London.

Orford, K.J. and Turver, K.E., (1976), Nature, 264, 727.

Orford, K.J., Stubbs, R.J., Turver, K.E., Waddoup, D.W. and Wellby, D.W., (1975), Proc. 14th Int. Conf. on Cosmic Rays, 8, 3014.

Orford, K.J., Turver, K.E. and Wellby, D.W., (1975), Proc. 14th Int. Conf. on Cosmic Rays, 8, 3019.

Protheroe, R.J. and Turver, K.E., (1977), to be published.

R.C.A. Photomultiplier Manual, Technical Series PT-61.

Rossi, B. and Greisen, K., (1941), Rev. Mod. Phys., 13, 240.

Smith, G.J. and Turver, K.E., (1973), J. Phys. A., 6, L121.

Sreekantan, B.V., (1972), Space Science Reviews, 14, 103.

Tennent, R.M., (1967), Proc. Phys. Soc., 92, 622.

Waddoup, D.W., (1977), Ph.D. Thesis. University of Durham. To be published.

Watson, A.A., (1974), Proc. Nato Advanced Study Institute, Ed. by Osborne, J.L. and Wolfendale, A.W.

Wild, P., (1975), Ph.D. Thesis. University of Leeds.

Wilson, C.T.R., (1901), Proc. Roy. Soc., 68, 151.

Wilson, J.G., Allan, H.R., Lillicrap, S.C., Reid, R.J.O. and Turver, K.E., (1963), Proc. 8th Int. Conf. on Cosmic Rays, 4, 27.

ACKNOWLEDGEMENTS

I wish to thank Dr. A.A. Watson and his colleagues at the Department of Physics, University of Leeds, for the use of the facilities at the Haverah Park air shower array, and for the provision of the air shower analyses used in this thesis.

Professor A.W. Wolfendale is also thanked, for the use of the facilities in the Department of Physics, University of Durham.

The help of my supervisor, Dr. K.E. Turver, is acknowledged.

I would also like to express thanks to my colleagues in the Extensive Air Shower group. In particular, I am very grateful for the assistance with the data analysis given by Mr. R.T. Hammond. Mr. J.A.L. Shearer is thanked, too, for his help with measuring the film records, and Mr. R.J. Protheroe for many useful discussions.

The provision of a Research Studentship by the Science Research Council is acknowledged.